



**UTILITY OF CARDIOVASCULAR MAGNETIC  
RESONANCE IN THE ASSESSMENT OF MYOCARDIAL  
DYSFUNCTION IN PULMONARY ARTERIAL  
HYPERTENSION**

By

**Karthiges Sree Raman**  
MBChB, FRACP

*Thesis  
Submitted to Flinders University  
for the degree of*

**Doctor of Philosophy**

College of Medicine and Public Health  
11<sup>th</sup> March 2022

---

## TABLE OF CONTENTS

<b>CHAPTER 1 : INTRODUCTION.....</b>	<b>17</b>
1.1 PULMONARY ARTERY HYPERTENSION .....	17
1.2 DISEASE BURDEN AND PROGNOSIS IN PAH .....	19
1.3 MYOCARDIAL DYSFUNCTION IN PAH.....	21
1.3.1 Myocardial ischemia of the right ventricle in PAH .....	23
1.3.2 Myocardial ischemia of the left ventricle in PAH.....	24
1.4 CARDIOVASCULAR MAGNETIC RESONANCE (CMR).....	25
1.4.1 Oxygen-sensitive cardiovascular magnetic resonance (OS-CMR).....	26
1.4.2 T1-mapping .....	27
1.4.3 Cardiovascular Magnetic Resonance Feature Tracking (CMR-FT).....	29
<b>CHAPTER 2 : METHODS .....</b>	<b>31</b>
2.1 STUDY PROTOCOL.....	32
2.1.1 Ethics.....	32
2.1.2 Participant Selection and Preparation .....	32
2.2 CMR IMAGE ACQUISITION.....	35
2.2.1 Multi Plane Localisers and Scout Images .....	35
2.2.2 Cine Imaging.....	37
2.2.3 Oxygen Sensitive Cardiovascular Magnetic Resonance (OS-CMR) Imaging.....	42
2.2.4 T1 mapping .....	44
2.3 CMR ANALYSIS .....	45
2.3.1 Ventricular Volumes, Function and Mass .....	45
2.3.2 OS-CMR Analysis .....	46
2.3.3 T1 Map Analysis .....	47

2.3.4 CMR feature tracking analysis .....47

**CHAPTER 3 : FEASIBILITY OF OXYGEN SENSITIVE CARDIOVASCULAR  
MAGNETIC RESONANCE OF THE RIGHT VENTRICLE IN PULMONARY**

**ARTERY HYPERTENSION.....49**

3.1 INTRODUCTION.....50

3.2 METHODS .....51

3.2.1 Ethics.....51

3.2.2 Participant Selection.....51

3.2.3 Participant preparation .....52

3.2.4 CMR protocol.....52

3.2.5 CMR analysis .....52

3.2.6 Statistical analysis .....53

3.3 RESULTS .....54

3.3.1 Participant characteristics.....54

3.3.2 CMR Characteristics .....56

3.3.3 Right Ventricular Myocardial Oxygenation Response (OS-CMR).....58

3.3.4 LV Myocardial Oxygenation response (OS-CMR) .....61

3.3.5 Relationship between RV Myocardial Oxygenation, LV Myocardial Oxygenation  
and CMR volumetric and functional indices .....63

3.4 DISCUSSION .....65

3.4.1 Pathological mechanisms of RV ischemia in PAH .....65

3.4.2 Feasibility of OS-CMR in the RV.....66

3.4.3 Study Limitations .....68

3.5 CONCLUSION .....69

<b>CHAPTER 4 : RIGHT VENTRICULAR MYOCARDIAL DEOXYGENATION IN PATIENTS WITH PULMONARY ARTERY HYPERTENSION.....</b>	<b>70</b>
4.1 INTRODUCTION.....	71
4.3 METHODS.....	73
4.3.1 Ethics.....	73
4.3.2 Participant Selection.....	73
4.3.3 Participant preparation.....	73
4.3.4 CMR protocol.....	73
4.3.5 CMR analysis.....	74
4.3.6 Statistical analysis.....	74
4.4 RESULTS.....	75
4.4.1 Participant Characteristics.....	75
4.4.2 CMR characteristics.....	78
4.4.3 Myocardial Oxygenation Response (OS-CMR) in PAH patients.....	81
4.4.4 Right Ventricular Native T1-values in PAH patients.....	83
4.4.5 Comparing RV myocardial oxygenation and RV T1 values between iPAH and SScPAH.....	83
4.4.6 Correlations between RV myocardial oxygenation, RV T1 values, CMR RV volumetric/functional and RHC haemodynamic indices.....	85
4.5 DISCUSSION.....	87
4.5.1 Right ventricular myocardial deoxygenation in PAH.....	87
4.5.2 Native T1-values in the right ventricle.....	89
4.5.3 Study Limitations.....	91
4.6 CONCLUSION.....	92

**CHAPTER 5 : LEFT VENTRICULAR ISCHEMIA IN PRE-CAPILLARY PULMONARY HYPERTENSION: A CARDIOVASCULAR MAGNETIC RESONANCE STUDY .....93**

5.1 INTRODUCTION..... 94

5.2 METHODS ..... 96

    5.2.1 *Ethics*..... 96

    5.2.2 *Participant Selection*..... 96

    5.2.3 *Participant preparation* ..... 97

    5.2.4 *CMR protocol*..... 97

    5.2.5 *CMR analysis* ..... 97

    5.2.6 *Statistical analysis* ..... 98

5.3 RESULTS ..... 99

    5.3.1 *Participant Characteristics*..... 99

    5.3.2 *CMR characteristics* ..... 103

    5.3.3 *LV Myocardial Oxygenation Response (OS-CMR)* ..... 103

    5.3.4 *Myocardial Stress/Rest T1 Reactivity* ..... 105

    5.3.5 *Comparing LV myocardial ischemia in iPAH and SSc-PAH* ..... 105

    5.3.6 *Correlations between myocardial oxygenation,  $\Delta T1$  reactivity and CMR volumetric/functional and hemodynamic indices in PH patients.* ..... 106

5.4 DISCUSSION ..... 110

    5.4.1 *Coronary microvascular disease of the LV in pre-capillary PH*..... 110

    5.4.2 *Myocardial Oxygenation and T1 Reactivity in response to vasodilator stress* .... 111

    5.4.3 *Study Limitations* ..... 113

    5.4.4 *Clinical implication and future directions* ..... 113

5.5 CONCLUSION ..... 115

**CHAPTER 6 : CARDIOVASCULAR MAGNETIC RESONANCE FEATURE  
TRACKING EVALUATION OF MYOCARDIAL STRAIN IN PULMONARY**

**HYPERTENSION.....116**

6.1 INTRODUCTION..... 117

6.2 METHODS ..... 119

    6.2.1 *Ethics*..... 119

    6.2.2 *Participant Selection*..... 119

    6.2.3 *Participant preparation* ..... 119

    6.2.4 *CMR protocol*..... 119

    6.2.5 *CMR analysis* ..... 119

    6.2.6 *Statistical analysis* ..... 120

6.3 RESULTS ..... 121

    6.3.1 *Participants Characteristics* ..... 121

    6.3.2 *CMR Characteristics* ..... 121

    6.3.3 *CMR Myocardial Deformation* ..... 122

    6.3.4 *Comparing LV GLS and RVFWS values between iPAH and SScPAH* ..... 122

    6.3.5 *Correlations between CMR LV GLS, CMR RVFWS, myocardial oxygenation, CMR volumetric/functional and haemodynamic indices in PAH patients* ..... 122

6.4 DISCUSSION ..... 124

    6.4.1 *Limitations* ..... 125

6.5 CONCLUSION..... 126

**CHAPTER 7 : RIGHT VENTRICULAR FREE WALL SYSTOLIC STRAIN  
CORRELATES TO PRESSURE FLOW RELATIONSHIP DURING DOBUTAMINE  
STRESS ECHOCARDIOGRAPHY .....127**

7.1 INTRODUCTION..... 128

7.2 METHODS.....	130
7.2.1 Ethics.....	130
7.2.2 Participant Selection.....	130
7.2.3 Participant preparation .....	130
7.2.4 Dobutamine stress echocardiography protocol.....	130
7.2.5 CMR protocol.....	131
7.2.6 CMR analysis .....	131
7.2.7 Echocardiography analysis .....	131
7.2.8 Statistical analysis .....	133
7.3 RESULTS .....	134
7.3.1 Participant Characteristics.....	134
7.3.2 Echocardiography Characteristics .....	136
7.3.3 mPAP/CO vs echocardiographic parameters.....	138
7.3.4 mPAP/CO vs CMR parameters.....	139
7.4 DISCUSSION .....	142
7.4.1 Study limitations.....	143
7.5 CONCLUSION.....	144
<b>CHAPTER 8 : CONCLUSIONS .....</b>	<b>145</b>
8.1 MYOCARDIAL OXYGENATION IN PAH.....	145
8.2 MYOCARDIAL EXTRACELLULAR MATRIX (ECM) AND CORONARY MICROVASCULAR FUNCTION IN PAH.....	146
8.3 MYOCARDIAL DEFORMATION IN PAH .....	146
<b>CHAPTER 9 : FUTURE DIRECTIONS.....</b>	<b>147</b>
<b>CHAPTER 10 : REFERENCES.....</b>	<b>148</b>

## **THESIS SUMMARY**

Pulmonary arterial hypertension (PAH) is a pulmonary vasculature disease that predominantly involves the small pulmonary arteries and arterioles. PAH is a rare but serious disease that affects both the pulmonary vasculature and the heart. In PAH, the insult to the pulmonary vascular system causes pulmonary vascular remodelling leading to increased haemodynamic load. This leads to compensatory mechanisms of the cardiac function in response to increased right ventricle (RV) afterload. In particular, the RV adapts by increasing its force generating capacity to overcome the increase in RV afterload. As the disease progresses, the RV progresses from an adaptive to a maladaptive stage, with subsequent RV failure and death. It has been well documented that RV size and function are strong predictors of prognosis in PAH. However, in PAH the RV can negatively remodel in a clinically silent progression leading to RV failure and ultimately death. At this stage, the pathophysiological mechanisms driving this progression of the RV from adaptation to maladaptation remain unclear. Cardiovascular Magnetic Resonance (CMR) with its recent advancement of novel parametric mapping techniques have made non-invasive assessment of myocardial tissue characterisation more feasible. While these novel techniques have been comprehensively studied for various conditions in the left ventricle (LV); its use in the RV is limited.

The aims of this thesis are 1) To utilise the oxygen-sensitive CMR (OS-CMR) technique to assess the feasibility, prevalence and extent of myocardial oxygenation in response to stress and 2) to characterise the changes on myocardial extracellular matrix changes in the PAH population.

In Chapter 3, we demonstrate the feasibility of the OS-CMR technique in the RV of PAH patients, a technique previously only used for the LV myocardium. This study was followed with Chapter 4, which demonstrates the extent of myocardial oxygenation in the RV of PAH, providing new mechanistic insights into the pathophysiology of myocardial ischaemia in PAH. In Chapter 5, we demonstrate myocardial deoxygenation in the LV of PAH and with the utility of Stress/Rest T1 mapping, demonstrate concurrent myocardial perfusion abnormalities highlighting the presence of coronary microvascular dysfunction.

Furthermore, in Chapters 4 and 5, by utilising CMR parametric mapping techniques, we demonstrate changes to the myocardial extracellular matrix in PAH. However, these changes were not associated with myocardial oxygenation.

Chapters 6 and 7 examine the myocardial deformation strain changes in PAH. It demonstrates both CMR (Chapter 6), and echocardiographic (Chapter 7) strain abnormalities are associated with myocardial oxygenation and RV hypertrophy.

This thesis has advanced the mechanistic understanding into the pathophysiology of myocardial dysfunction in PAH. Further work of this nature could lead to new diagnostic, prognostic, and therapeutic possibilities for PAH patients.

## **DECLARATION**

I certify that this work of the thesis does not incorporate without acknowledgment any material previously submitted for a degree or diploma in any university. To the best of my knowledge and belief, the thesis does not contain any material previously published or written by another person except where due reference is made in the text.

Karthiges Sree Raman

March 2022

## **ACKNOWLEDGEMENTS**

I have been profoundly grateful and fortunate to receive support from many people during the course of my PhD.

Firstly, to my wife, children, family and friends for the support and encouragement in the move from New Zealand and Adelaide for my PhD. To my wife Gowri, who supported me, been there during the tough moments, provided a listening ear and laughs during these challenging years. To my children Siddarth and Arya who brought endless amounts of joy and laughter, in addition to teaching me to enjoy and appreciate the simple things in life. My family who have supported and encouraged me in my endeavours. Lastly to my friends who have been extremely supportive of me.

To my supervisors, I extend my sincerest gratitude for their guidance and support. My principle supervisor, Prof. Joseph Selvanayagam has been a great mentor and provided ample support and guidance over the course of my PhD. Associate Prof. Carmine De Pasquale and Dr Rebecca Perry have always been supportive, provided motivation and encouragement during the stressful course of the PhD years. Associate Prof. Gaetano Nucifora who has also provided guidance in this period of time.

I have been privileged to work with Prof. Richard Woodman, Dr Michael Stokes, Dr Christine Burdeniuk and Dr Susanna Proudman during my thesis; their time, assistance and support was invaluable. A special mention to Dr Ranjit Shah, who has been a friend and colleague over the journey of this PhD. In addition, a special thank you to Ms Avril Derwent, Ms Maura Hopkins and Ms Lee-Anne Horsfall for their time and assistance in recruiting participants for my PhD.

Thank you to Angela Walls, Andrew Hodges, Craig Bradbrook, Ali Sutton, Emma Smith, Cherie Raven from the MRI department, without their patience and dedication this work would not be possible. I would also like to thank Dr Majo Joseph, Lynn Brown, Tracey Hecker and Amy Swan from the echocardiography department for their help and support.

There are friends and colleagues who I am thankful for the experiences that I have been able to share with you, without your support this would not be possible. A heartfelt thank you Dr Rajiv Ananthakrishna, Dr Anthony Chung, Dr Varun Malik, Dr Amera Halabi, Serene Wong, Jonathon Foote, Janice Roesler, Jane Mackinnon, Sau Lee and Tonia Bromley for their friendship and counsel.

This research project was supported by a grant from National Health and Medical Research Council of Australia and Janssen (formerly Actelion) Australia. I would like to thank the Australian Government Research Training Programme scholarship from Flinders University, for my personal financial support which has enabled me to complete this research work.

## **PEER REVIEWED JOURNAL PUBLICATIONS**

### **Chapter 1**

Sree Raman K, Nucifora G, Selvanayagam JB. Novel cardiovascular magnetic resonance oxygenation approaches in understanding pathophysiology of cardiac diseases. Clinical and experimental pharmacology & physiology. 2018

### **Chapter 3**

Sree Raman K, Stokes M, Walls A, Perry R, Steele PM, Burdeniuk C, et al. Feasibility of oxygen sensitive cardiac magnetic resonance of the right ventricle in pulmonary artery hypertension. Cardiovascular diagnosis and therapy. 2019;9(5):502-12.

### **Chapter 4**

Sree Raman K, Shah R, Stokes M, Walls A, Woodman RJ, Perry R, et al. Right ventricular myocardial deoxygenation in patients with Pulmonary Artery Hypertension. Journal of Cardiovascular Magnetic Resonance. 2021;23(1):22.

### **Chapter 5**

Sree Raman K, Shah R, Stokes M, Walls A, Woodman RJ, Ananthakrishna R, et al. Left ventricular ischemia in pre-capillary pulmonary hypertension: a cardiovascular magnetic resonance study. Cardiovasc Diagn Ther. 2020;10(5):1280-92.

## **Abstracts**

**Sree Raman K**, Stokes M, Shah R, Walls A, Steele P, Burdeniuk C, DePasquale C, Celermajer D, Selvanayagam JB. Oxygen sensitive cardiac magnetic resonance in demonstrating myocardial ischaemia of the right ventricle in patients with pulmonary artery hypertension – European Cardiac Society Meeting (Paris) 2019.

**Sree Raman K**, Stokes M, Shah R, Walls A, Steele P, Burdeniuk C, DePasquale C, Celermajer D, Selvanayagam JB. Feasibility of Oxygen Sensitive Cardiac Magnetic Resonance in Demonstrating Right Ventricular Myocardial Ischaemia in Patients with Pulmonary Arterial Hypertension – Annual Scientific Meeting of Cardiac Society Australia and New Zealand (Adelaide) 2019.

**Sree Raman K**, Shah R, Stokes M, Walls A, Minson R, Burdeniuk C, DePasquale C, Celermajer D, Selvanayagam JB. Presence of Left Ventricular microvascular dysfunction in patients with Pulmonary Artery Hypertension. American Heart Association Scientific Sessions (Philadelphia) 2019.

## **ABBREVIATIONS**

AV – Atrio-ventricular

BOLD – Blood Oxygen Level Dependent

BSA – Body surface area

CTEPH – Chronic thromboembolic pulmonary hypertension

CI – Cardiac Index

CMR – Cardiovascular magnetic resonance

CMR-FT – Cardiovascular magnetic resonance feature tracking

ECG – Electrocardiogram

ECM – Extracellular matrix

ECV – Extracellular volume fraction

EDVi – End-diastolic volume index

ESVi – End-systolic volume index

FC – Functional class

FOV – Field of view

HLA – Horizontal Long-Axis

IV – Intravenous

iPAH – Idiopathic pulmonary artery hypertension

LV – Left ventricle

LVEF – Left ventricular ejection fraction

LVOT – Left ventricular outflow tract

LVOT XC – Left ventricular outflow tract cross cut

MBV – Myocardial blood volume

MMPs – Matric metalloproteinases

MOLLI – Modified Look-Locker Inversion recovery

mPAP – Mean pulmonary artery pressure

MRI – Magnetic Resonance Imaging

OS – Oxygenation-sensitive

PAH – Pulmonary Artery Hypertension

PCWP – Pulmonary capillary wedge pressure

PH – Pulmonary Hypertension

RHC – Right Heart Catheter

RV – Right ventricle

RVEF – Right ventricular ejection fraction

RVH – Right Ventricular Hypertrophy

ROI – Region of interest

SASHA – Saturation Recovery Single-Shot Acquisition

SD – Standard deviation

ShMOLLI – Shortened Modified Look-Locker Inversion recovery

SI – Signal Intensity

SScPAH – Systemic sclerosis associated pulmonary artery hypertension

SSFP – Steady-state-free-precession

SV – Stroke volume

TE – Echo time

TIMPs – Tissue inhibitors of metalloproteinases

TR – Repetition time

VLA – Vertical Long-Axis

WHO – World Health Organization

WSPH – World Symposium on Pulmonary Hypertension

## **Chapter 1 : Introduction**

### **1.1 Pulmonary Artery Hypertension**

The normal pulmonary vascular system is a low pressure system with a flow pressure of less than one tenth compared to systemic vascular bed (1). Pulmonary Hypertension (PH) is a haemodynamic state whereby the pressure in the pulmonary vascular system is elevated. At the first World Symposium on Pulmonary Hypertension (WSPH) in 1973, PH was defined as a mean pulmonary artery pressure (mPAP) of more than 25mmHg on right heart catheter (RHC) (2). At that stage, PH was broadly classified into primary pulmonary hypertension and secondary pulmonary hypertension (2). With the advancements in the understanding of the disease, the WSPH developed a clinical classification for PH, categorising PH into groups that share similar pathophysiological mechanisms, clinical presentations, haemodynamic features and clinical management (3). Recently at the Sixth World Symposium on PH, the definition and clinical classification of PH was updated (Table 1) (3). In the revised definition, RHC mPAP of more than 20mmHg is now considered diagnostic of PH. Pulmonary arterial hypertension (PAH) relates to the changes that mostly affects the arterial component of the pulmonary vasculature. In PAH, the pathological changes to the pulmonary vascular pressures were thought to originate from a predisposing state interacting with a provoking stimulus (4, 5). This interaction triggers various mechanisms that lead to vascular constriction, cellular proliferation and prothrombic state resulting in the clinical sequelae of PAH (4).

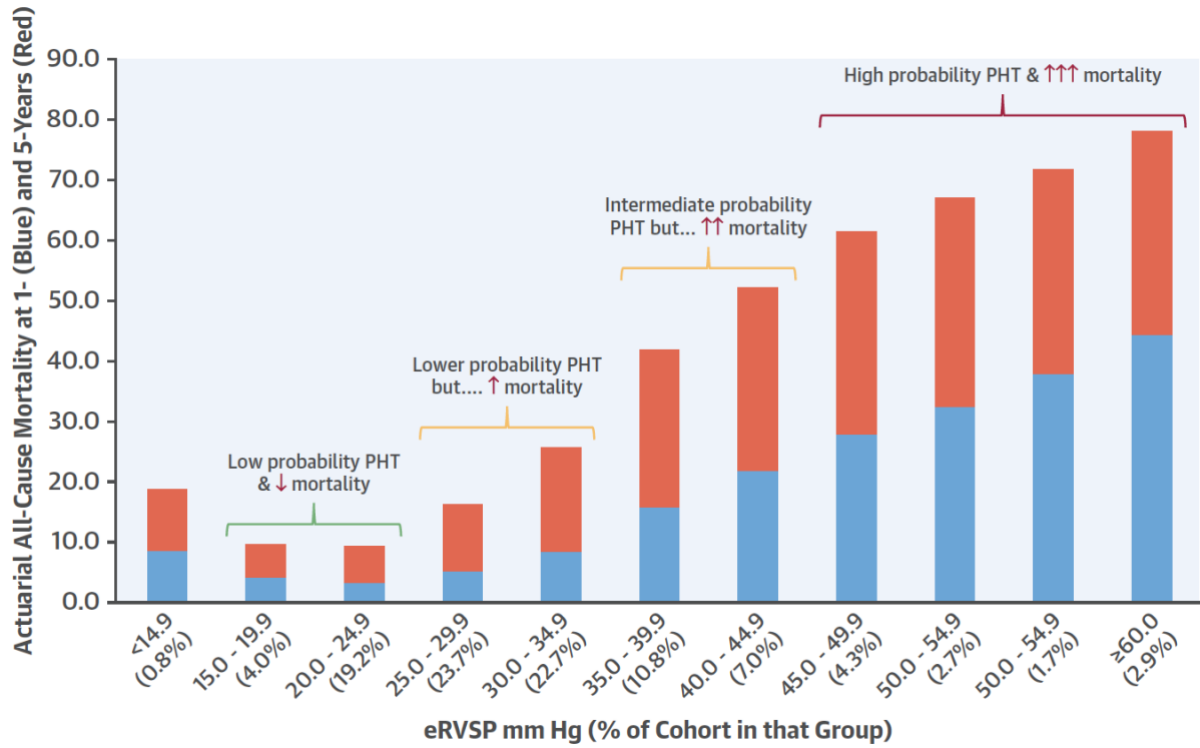
**Table 1.1: Clinical classification of Pulmonary Hypertension (PH) (3)**

<p>Group 1: Pulmonary Arterial Hypertension (PAH)</p> <ul style="list-style-type: none"><li>• Idiopathic PAH</li><li>• Heritable PAH</li><li>• Drug- and toxin-induced PAH</li><li>• PAH associated with:<ul style="list-style-type: none"><li>○ Connective tissue disease</li><li>○ HIV infection</li><li>○ Portal hypertension</li><li>○ Congenital heart disease</li><li>○ Schistosomiasis</li></ul></li><li>• PAH long-term responders to calcium channel blockers</li><li>• PAH with overt features of venous/capillaries pulmonary veno-occlusive disease/pulmonary capillary haemangiomatosis (PVOD/PCH) involvement</li><li>• Persistent PH of the newborn syndrome</li></ul>
<p>Group 2: PH due to left heart disease</p> <ul style="list-style-type: none"><li>• PH due to heart failure with preserved left ventricular ejection fraction (LVEF)</li><li>• PH due to heart failure with reduced LVEF</li><li>• Valvular heart disease</li><li>• Congenital/acquired cardiovascular conditions leading to post-capillary PH</li></ul>
<p>Group 3: PH due to lung diseases and/or hypoxia</p> <ul style="list-style-type: none"><li>• Obstructive lung disease</li><li>• Restrictive lung disease</li><li>• Other lung disease with mixed restrictive/obstructive pattern</li><li>• Hypoxia without lung disease</li><li>• Developmental lung disorders</li></ul>
<p>Group 4: PH due to pulmonary artery obstructions</p> <ul style="list-style-type: none"><li>• Chronic thromboembolic PH</li><li>• Other pulmonary artery obstructions</li></ul>
<p>Group 5: PH with unclear and/or multifactorial mechanisms</p> <ul style="list-style-type: none"><li>• Haematological disorders</li><li>• Systemic and metabolic disorders</li><li>• Others</li><li>• Complex congenital heart disease</li></ul>

## **1.2 Disease Burden and Prognosis in PAH**

Pulmonary arterial hypertension (PAH) is a progressive disorder that affects both the pulmonary vasculature and the heart (1). It is a rare but severe disease, affecting up to 50 per million population (6). Initial management of PAH was based on anecdotes followed by case reports and case series; unfortunately, these treatments did not change prognosis and were mostly ineffective. In the last two decades, a better understanding of PAH pathological process has led to more effective therapies which have improved the quality of life and prognosis (7-9). The current treatment guidelines are aimed at reducing clinical deterioration/progression and mortality by assessing a multi-parameter risk which includes World Health Organization (WHO) functional class (FC), exercise capacity, haemodynamic parameters and right ventricular (RV) function (10). While this has improved outcomes, PAH is frequently a fatal disease with no cure (11). This was demonstrated in the French registry, whereby near 20% of PAH patients with baseline WHO FC II experienced disease progression and early death (12). In addition, it has been demonstrated that despite stable medical therapy with no change in WHO FC, exercise capacity or haemodynamic parameters; PAH patients can experience silent progressive RV failure leading to death (13, 14). To add further strength, a recent Australian national database involving a large cohort of over 150,000 patients demonstrated increased cardiovascular related mortality in patients with mild PH (Figure 1.1) (15).

**Figure 1.1 : Increased 1-year and 5 year mortality at every increment of the estimated right ventricular systolic pressure (15).**



### **1.3 Myocardial Dysfunction in PAH**

Although the initial insult in PAH involves the pulmonary vasculature, the prognosis of patients with PAH is most dependent on cardiac function. In particular, the RV size and function are the most powerful determinant of prognosis in PAH (12, 16, 17). The sustained pressure overload that occurs in PAH leads to adaptive changes to the cardiomyocyte and interstitium in the RV.

In the normal myocardium, a healthy extracellular matrix (ECM) network surrounds and interconnects cardiac myocyte, myofibrils, coronary microcirculation and is crucial in maintaining function (18). The ECM network plays a role in:

1. Maintaining cardiac myocyte alignment thereby maintaining ventricular shape.
2. Maintaining the length of sarcomeres, preventing overstretch as well as re-lengthening of the myocardium during ventricular diastole.
3. Maintaining an appropriate distribution of force during ventricular systole.

Within the ECM, the interstitium provides a network of mechanical support, regulatory growth hormones, cytokines, and other signaling molecules. The interstitium forms a relationship together with cardiac myocytes in maintaining optimal cardiac function. Cardiac fibroblasts are the predominant cells located in the interstitium and are responsible for producing collagen, which is integral to elasticity and tensile strength of the myocardium. The equilibrium of collagen formation and breakdown is maintained by matrix metalloproteinases (MMPs) and tissue inhibitors of metalloproteinases (TIMPs).

In cardiac diseases, there is usually a disruption of healthy ECM due to the formation of myocardial fibrosis. However, different forms and patterns of fibrosis develop depending on the aetiology, triggers and circumstance of the cardiac disease. A direct insult to the

cardiomyocyte will lead to cell death and apoptosis with subsequent formation of replacement fibrosis of scar tissue (19). In cardiac diseases where there are triggers without direct insult to the cardiomyocyte, reactive fibrosis develops (20). Reactive fibrosis is a process of increased collagen fibres production within the interstitium surrounding the cardiomyocyte. This is followed by plexiform fibrosis which is characterised by large collagen foci's that cause disarray of myocardial fibres (21). In response to pressure overloaded conditions such as aortic stenosis or PH, there is enhanced collagen formation driven by MMPs and TIMPs which is initially adaptive by supporting the ECM to maintain ventricular shape and withstand the high pressures (22, 23). However, prolonged periods of pressure overload cause excess collagen formation and breakdown. In addition, this cycle of high collagen turnover and subsequent formation of new ECM structure differs from the healthy ECM and in the long term will lead to maladaptive alterations of the collagen network in the interstitium. Maladaptive alteration of the collagen network will cause the loss of ECM integrity, formation of fibrosis and subsequent ventricular dilatation, ventricular dysfunction and disease progression (23).

In PAH, the RV is affected more than the left ventricle (LV) and whilst there are similarities in cardiac structure, there are some key points of difference:

1. Embryologically the RV originates from the anterior heart field, whereas the LV derives from the linear heart tube (24).
2. The contrast of embryological origin is possibly the cause of different MMPs distribution between RV and LV (25).
3. Increase relative atrophy of the RV cardiomyocyte compared to the LV after birth (26), leads to higher collagen content in the RV (7.4%) compared to the LV (5.5%) (27).

These aforementioned points of difference between the LV and RV, suggest the pathophysiological mechanisms that affect the more extensively studied LV cannot be directly extrapolated to the RV. Compared to the LV, the RV not only differs embryologically, it has differing coupling between flow and contraction (28). Additionally, the RV has been demonstrated to have lower resting coronary blood flow, increased systolic coronary flow, lower oxygen requirement at both rest and exertion and greater effect of flow and pressure on oxygen consumption compared to the LV (28). Furthermore; studies have demonstrated  $\alpha$ -adrenergic stimuli selectively causes right coronary constriction (29) and nitric oxide regulates right coronary flow at rest and during transient PH but not left coronary flow (30) further highlighting the differences between LV and RV.

### **1.3.1 Myocardial ischemia of the right ventricle in PAH**

In PAH, there are many potential mechanisms of RV remodelling and subsequent dysfunction (31). A number of these mechanisms precipitate ischemia, which is thought to be a significant contributor (32) to progressive RV failure. This can occur in one of many forms 1) The increasing pulmonary vascular pressure decreases the pressure gradient between the aorta and the RV thereby reducing myocardial blood flow in the right coronary artery leading to myocardial ischemia (33, 34). In addition, RV myocardial ischemia is further exacerbated by an inadequate compensatory increase in the myocardial vasculature owing to progressive RV hypertrophy (RVH) (35-37). Furthermore; in the advanced stages of PAH, the right coronary perfusion pressure can drop below 50 mmHg leading to a decline of RV contractile function (33). 2) Occlusive microvascular damage and impairment in angiogenesis (known as capillary rarefaction) has been demonstrated in animal models, this mechanism of microvascular ischaemia is believed to be dominant in systemic sclerosis associated pulmonary artery hypertension (SScPAH) (33, 38). 3) Dysfunctional mitochondrial metabolism has been another

pathologically relevant mechanism of myocardial ischemia demonstrated in the hypertrophied RV of PAH. In animal models of PAH with RVH, there is a shift from fatty acid oxidation to glycolysis as a preference of energy substrates (39). This shift to glycolysis has been demonstrated by increased uptake of fluorodeoxyglucose on positron emission tomography (PET) in PAH patients with RVH (40). This metabolic shift to aerobic glycolysis has been associated with decreased cardiac output and RV contractility (39, 41).

### **1.3.2 Myocardial ischemia of the left ventricle in PAH**

The pathophysiology of LV dysfunction in PAH is not clearly appreciated. A number of putative mechanisms, in isolation, or in combination, have been proposed. Changes in the RV can affect the right-to-left interventricular interaction by leftward septal bowing, which leads to impaired LV diastolic filling (42, 43), and possibly to myocardial ischemia. Other studies have also demonstrated this impairment in LV diastolic function (44, 45) as well as a reduction in LV free wall mass, in association with RV dysfunction, in PAH patients (46). In a more recent study; using biopsy from explanted hearts of PAH patients, atrophy and severe contractility impairment of the LV cardiomyocyte has been demonstrated (47).

Although LV myocardial ischaemia has been described in pulmonary hypertension, it is mostly seen in association with congenital and left heart disease with limited studies in PAH. In SScPAH, the LV myocardial perfusion abnormalities have been attributed to decreased coronary flow reserve (48) and coronary microvascular dysfunction (49). Extrinsic compression of the left main coronary artery due to dilatation of the pulmonary artery has been elegantly reported by Galiè *et al.* (50). This study demonstrated the high prevalence (40%) of extrinsic compression of left main coronary arteries in patients with PAH. However, only patients with PAH and angina-like symptoms were studied, and left main coronary artery

compression due to dilated pulmonary artery has been reported in other forms of pulmonary hypertension, including patients with normal pulmonary pressures (51). Furthermore, although these patients were selected based on the presence of PAH and angina-like symptoms and not specifically based on the severity of PAH, the majority had severe PAH with systolic pulmonary pressure  $60\pm 20$ mmHg (45). It is increasingly recognised, however, that the microvascular damage seen in the pulmonary vasculature of PAH has links to coronary artery disease. A recent study by Meloche *et al.* demonstrated that the inflammation and epigenetic readers seen in PAH pulmonary vasculature were also overexpressed in the coronary arteries. The authors suggested that inflammatory and epigenetic readers may trigger coronary vascular remodeling in both the LV and RV, leading to coronary microvascular dysfunction and coronary artery disease (52). The potential role of LV ischemia, as a contributor to progressive LV dysfunction, has not been systematically studied in PAH.

#### **1.4 Cardiovascular Magnetic Resonance (CMR)**

Cardiovascular Magnetic Resonance (CMR) has high spatial resolution, excellent signal-to-noise ratio and the ability to image the heart in a three-dimensional manner. It is seen as the gold standard in the evaluation of volumes, mass and systolic function of the heart, both of the left and right ventricles (53). In multiple studies the high accuracy and reproducibility of CMR has been demonstrated in the assessment of cardiac volume and function. The accuracy of CMR derived ventricular volumes was determined from studies using in-vitro phantoms, animal models and human subjects (54-56). In the RV, both Koch *et al* and Beygui *et al* were able to demonstrate good accuracy when comparing between in-vivo RV volume and mass assessment by CMR with ex-vivo measurements (56, 57). Further studies have also demonstrated excellent reproducibility of RV measurements by CMR in normal volunteers (58, 59) as well as in various disease states (60) including in congenital heart disease (61, 62).

In PAH, CMR has been a valuable tool, especially in the assessment of the RV whereby the RV volume and function metrics can predict mortality (13, 37, 63). Furthermore, CMR is sensitive enough to demonstrate progressive RV deterioration in clinically stable PAH patients (14); although there is a varied RV volumetric and functional response to PAH therapies (64-67). This would suggest that there are other pathophysiological mechanisms in PAH that continue to drive progressive RV remodelling and subsequent dysfunction in otherwise clinically stable PAH patients.

Recent advancement in CMR parametric mapping techniques have made non-invasive assessment of tissue characterization of the myocardium clinically feasible (53). While these techniques have been extensively studied for various conditions in the LV; there is now emerging preliminary evidence of its use in the RV (68, 69). However the evidence is limited with further evaluation required, which this thesis hopes to explore.

#### **1.4.1 Oxygen-sensitive cardiovascular magnetic resonance (OS-CMR)**

The oxygenation-sensitive cardiovascular magnetic resonance (OS-CMR), otherwise known as Blood Oxygen Level Dependent (BOLD) effect, enables the *in vivo* assessment of myocardial oxygenation at the tissue level. This technique is based on the changes of paramagnetic properties of haemoglobin due to the effects of oxygenation initially described by Linus Pauling (70). The change from oxygenated to de-oxygenated haemoglobin causes significant spin-spin interactions which shortens spin-spin relaxation time and determines a change of transverse magnetization  $T_2/T_2^*$  times. De-oxygenation therefore increases the volume of magnetic susceptibility, leading to a change in magnetic resonance signal intensity (71). Thus, an increased myocardial de-oxygenation would be represented by the relative increased presence of de-oxygenated haemoglobin in the capillary blood; which is reflected as

a drop-in signal intensity in the 'T2/T2\* weighted' CMR images and vice-versa. In-vivo myocardial oxygenation is altered via the use of coronary vasodilators which increase myocardial perfusion, and this consecutively will increase oxygenation concentration and reduce myocardial venous blood deoxygenation leading to incremental changes on T2\* value on OS-CMR. (72, 73).

There have been several advances that have improved the quality of the acquired OS-CMR images over the past years. Firstly the move to acquiring images at 3 Tesla (3T). Preliminary OS-CMR studies at 1.5 Tesla (1.5T) were essentially limited by the relatively small signal difference between normal and de-oxygenated myocardial regions. The move to 3 Tesla (3T) improved the ability to detect changes in myocardial oxygenation by a factor of 2.5 (74). This however came at the cost of artefacts from the inhomogeneities of the magnetic field. Secondly, initial OS-CMR studies were limited by low signal to noise ratio (SNR), which was impaired by imaging artefacts along the heart-lung interface and long acquisition times (75, 76). The recent steady-state-free-precession (SSFP) based sequence has overcome many of these limitations (77, 78). The OS-CMR technique has been widely used to advance our understanding of the role of myocardial oxygenation in cardiomyopathy and coronary artery disease states (79).

#### **1.4.2 T1-mapping**

Human tissues have a specific T1 relaxation time based on their composition. This occurs in the direction of the magnetic field after a radio frequency pulse has disrupted the nuclei from an equilibrium state. CMR T1 mapping measures the longitudinal or spin-lattice relaxation time of these nuclei. This is achieved using different inversion times or by using saturation recovery techniques to derive a T1 recovery curve by a voxel-by-voxel measurement;

parametric maps are finally generated to represent T1 values in milliseconds. Advances in CMR imaging techniques and mapping sequences have enabled quantitative T1 assessment of myocardial composition.

Several mapping sequences have been proposed to obtain T1 mapping data. In 1970 Look and Locker implemented a method that acquired multiple data after a radio frequency pulse was delivered (80). Subsequent refinements of this approach have led to faster acquisition times. The Modified Look-Locker Inversion recovery (MOLLI) sequence significantly improved the original Look-Locker approach; (81) in a single breath hold of 17 seconds, 11 images are acquired at the same cardiac phase allowing mapping. The Shortened MOLLI (ShMOLLI) is a refinement of the MOLLI sequence; (82) ShMOLLI uses an inversion recovery that does not require full recovery of longitudinal magnetization because of the conditional data analysis algorithm. Hence, T1 mapping is acquired over a single breath hold of 9 heart beats. However, the downside of ShMOLLI is that there is increased variability due to the reduced number of acquired images to generate the T1 curves. Saturation recovery (SR) methods, such as Saturation Recovery Single-Shot Acquisition (SASHA), which involve a non-selective saturation of the longitudinal magnetization to zero, have also been developed to acquire T1 maps (83). This approach avoids the need for a recovery phase, as recovery always begins from a saturated state. In clinical practice, T1 mapping data can be acquired with (contrast enhanced) or without (native) the use of Gadolinium contrast agents. Contrast enhanced T1 mapping is used mainly for calculating the extracellular volume fraction (ECV), which represents the interstitium and extracellular matrix. The gadolinium contrast agent, which is an extra-cellular and extra-vascular agent, shortens the tissue T1 relaxation time; with conditions resulting in diffuse myocardial fibrosis leading to an expansion of ECV which are characterized by lower post-contrast T1 times (84). There are however some issues that need to be considered

when analyzing post-contrast T1 times and ECV. These include injected dose, heart rate, gadolinium chelate clearance, time of measurement post injection and hematocrit (85-87). Conversely, native T1 mapping reflects the composite of both intracellular and extracellular components (88). Native T1 values increase in edematous conditions (e.g. acute myocardial infarction and inflammation) and conditions that increase the interstitial space (e.g. cardiomyopathies). On the other side, infiltrative conditions that lead to lipid deposition (e.g. Anderson-Fabry disease) or iron overload (e.g. hemochromatosis) are characterized by reduced native T1 values.

#### **1.4.2.1 Rest/Stress T1 mapping**

CMR stress/rest T1 mapping has emerged as a novel promising technique to distinguish normal, ischemic and infarcted myocardium in patients with coronary artery disease (CAD) (89). This technique measures changes in T1-values between native (rest) T1 mapping and vasodilator induced stress T1 mapping. CMR T1 mapping is highly sensitive to changes in myocardial water content, including myocardial blood volume (MBV) (82, 90). Vasodilator stress induction causes coronary vasodilatation which leads to increased myocardial water (82) and MBV (91, 92); hence altering T1-values which will enable assessment of microvascular and MBV changes during ischemia (93). Stress/rest T1 mapping is validated to distinguish between epicardial and microvascular CAD (94-97).

#### **1.4.3 Cardiovascular Magnetic Resonance Feature Tracking (CMR-FT)**

Cardiovascular magnetic resonance myocardial feature tracking (CMR-FT) is a recent novel method introduced for high-resolution assessment of global and regional myocardial deformation by tracking the actual myocardial borders and following them over time. CMR-FT involves the use of specific software to measure global and regional myocardial

deformation from SSFP CMR images which will automatically track the myocardial changes to determine velocities, displacement, myocardial strain (circumferential, radial and longitudinal) and strain rate (98). CMR-FT has been applied to a wide range of cardiovascular condition such as ischemia (99), cardiomyopathies (98, 100) and pulmonary hypertension (101); whereby CMR-FT has been demonstrated to have a superior prediction of mortality compared to CMR functional indices.

**Table 1.2: CMR-FT applications in cardiovascular conditions**

Study	Study Characteristics	Findings
Eitel et al	Retrospective Study. Patient's with myocardial infraction (n=1235): STEMI (n=795), NSTEMI (n=440)	Deformation imaging with CMR-FT (particularly GLS) was associated with increased MACE rates after myocardial infarction.
Schuster et al	Review paper. Utility of CMR-FT in congenital heart disease.	CMR-FT has clinical value in monitoring response to therapy and predicting future events
Claus et al	Review paper. Utility of CMR-FT in DCM, HCM and infiltrative cardiomyopathy	In DCM and HCM, CMR-FT has clinical value in monitoring response to therapy, predicting future events and/or response to device therapy. In infiltrative cardiomyopathy, CMR-FT is used to track the progression of disease.
Padervinskienė et al	Prospective study. Patients with pre-capillary PH (n=43).	Deformation imaging with CMR-FT (particularly LV GLS) correlated with RV dysfunction and was associated with poor clinical outcomes.

## **Chapter 2 : Methods**

This chapter describes in general, the methodologies used in this thesis. The subsequent chapters further elaborate on the specific methodologies used in each study population.

## **2.1 Study Protocol**

### **2.1.1 Ethics**

This study was approved by the Southern Adelaide Clinical Human Research Ethics Committee (HREC/15/SAC/397). All participants provided written informed consent to participate in the study.

### **2.1.2 Participant Selection and Preparation**

All cardiovascular magnetic resonance (CMR) scans require adequate preparation. At the time when the research participant is providing consent for the study; they were given a thorough explanation of the CMR procedure. All participants were screened to ensure their MRI safety using a standard MRI safety form (Figure 2.1).

**Figure 2.1 : Example of MRI safety form**

## MRI SAFETY CHECKLIST

This form must be completed and signed by the patient.

Patient's Name: .....

Date of Birth: ...../...../.....

Weight: .....kgs Height:.....m

Please complete the questions by circling YES or NO.  
If you have any queries please ask the staff.

STAFF USE ONLY - VISUAL CHECK					
	Referral			Screen	
	Y	N		Y	N
Correct Name	Y	N		Y	N
Correct DOB	Y	N		Y	N
Correct Address	Y	N			
Clinical details read	Y	N		Y	N
Correct Modality	Y	N		Y	N
Correct Site	Y	N		Y	N
Correct Side	R	L	N/A	R	L
Correct Annotation				Y	N
Checked by					

**If you have a pacemaker or intra-cerebral aneurysm clip, or any other implanted device, please inform the MRI staff immediately.**

<b>Have you ever had:</b> Heart Surgery Y / N Brain Surgery Y / N Ear Surgery Y / N Metal in your eyes e.g. from metal grinding Y / N	<b>Female Patients:</b> Could you be pregnant? Y / N Are you breastfeeding? Y / N Do you have an intrauterine device? Y / N <small>Please note there are no known risks to the developing foetus from MRI. However, complete safety has yet to be fully established.</small>	Please list all your allergies: ..... ..... Have you had any surgery on the area we are going to scan? If YES, what & when? ..... .....
---	--	--

Do you (or have ever had) any of the following?		
Heart Attack	Y / N	Ocular (eye) prosthesis Y / N
Stroke	Y / N	Implanted pain relief pump Y / N
Peripheral Vascular Disease	Y / N	Any other form of implant Y / N
Pacemaker	Y / N	A reaction to MRI Contrast? Y / N
Pacing Wires/Defibrillator	Y / N	Hypertension Y / N
Artificial Heart Valve	Y / N	Any history of Kidney disease? Y / N
Brain aneurysm clip	Y / N	Recent blood test to look at Kidney function? If YES, where ..... Y / N
Cochlear implant	Y / N	.....
Stapes (ear) implant	Y / N	Diabetes Y / N
Neurostimulator / Biostimulator	Y / N	Any form of cancer? If YES, please describe the area affected. Y / N
IVC filter	Y / N	.....
Intravascular coils, filters or stents	Y / N	.....
Vascular clips or wires	Y / N	.....
Brain shunt tube	Y / N	.....
Metal pins, plates, rods, screws, prosthesis	Y / N	.....

Do you have any of the following?		
Hearing aid	Y / N	Shrapnel or bullet wounds Y / N
Currently have transdermal (skin) patches? e.g. nicotine patches	Y / N	Dentures, braces including magnetically activated dentures Y / N
A tattoo (or tattooed makeup)	Y / N	Any type of body piercing Y / N
Have you had an operation in the last 6 weeks? If YES, what?	.....	Y / N

As part of the MRI examination, you may need to have an injection of a contrast agent (dye) known as Gadolinium. This medication is administered intravenously (injection into a vein) through a fine needle.

Overall MRI contrast injection is a safe procedure. Occasionally patients feel a little nauseous but this only lasts momentarily.

More serious allergic type reactions, although possible, are extremely rare. The staff in the MRI department are fully trained to deal with such a reaction should it occur.

I acknowledge to the best of my understanding, the answers are true.

Date ...../...../..... Signature .....

Date ...../...../..... Signature of MRI Technologist .....

**PLEASE REMOVE ALL JEWELLERY (WATCHES, CHAINS, EARRINGS ETC) IN PREPARATION FOR YOUR EXAMINATION.**

The participants were specifically asked regarding claustrophobia and only approached if they felt they could undergo the CMR examination. Other typical CMR exclusion criteria are implantable devices such as pacemakers or defibrillators, epicardial pacing wires, orbital metallic fragments, hydrocephalus shunts or cerebral aneurysm clips. Participants were allowed to take all regular medications prior to imaging.

The subjects were required to remove metal-containing objects, removable dentures, hair clips/hair bands, earrings and all upper body clothing and change into a patient gown with the opening down the front to aid in the positioning of the electrocardiogram (ECG) leads. An IV catheter was inserted for CMR contrast agent administration. Before entering the MRI scan room, an explanation of breath-holding commands was given at the start of the examination. In addition, the potential symptomatic effects of stress adenosine were explained to all research participants.

The participants were placed in a supine position on the scan table and for additional comfort, a foam wedge was placed under the patient's knees. The vector cardiogram leads were placed on the anterior chest wall and a proper gating signal was received and checked on the scanner display. A baseline ECG, heart rate and blood pressure were performed before, during and after the stress imaging. The flex array coil was then placed over the patient's anterior chest wall. The participant was then positioned in the scanner bore by centring the laser's cross-hairs on the landmark indicated on the flex array coil so that the participant was in the centre of the magnet prior to running the CMR sequences.

## 2.2 CMR Image Acquisition

### 2.2.1 Multi Plane Localisers and Scout Images

Firstly, a set of multi-slice, multi-planar localizer images are performed in a single breath-hold, on every heartbeat, acquired at the diastolic phase of the cardiac cycle. Axial, coronal and sagittal images were acquired with the field of view (FOV) adjusted in the antero-posterior direction.

#### 2.2.1.1 Vertical Long-Axis (VLA) Scout

On the axial image, the imaging plane that bisects the LV was selected, i.e. middle mitral valve to LV apex (Figure 2.2). This imaging plane is called vertical long-axis (VLA scout).

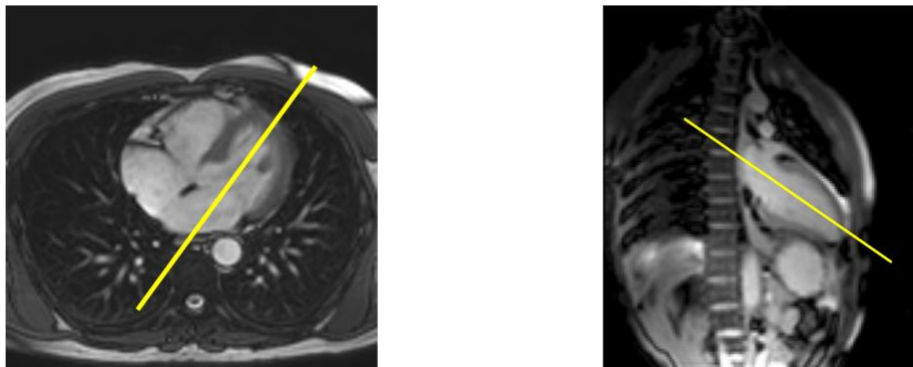


**Figure 2.2 : Example of VLA Scout image**

#### 2.2.1.2 Horizontal Long-Axis (HLA) Scout

The horizontal long-axis (HLA) plane is determined by using the VLA scout image. At end diastole of the VLA scout, an imaging plane was chosen that transects the middle of the mitral valve and LV apex (Figure 2.3). A single slice breath-hold trufi image was performed in this imaging plane. This was designated HLA scout.

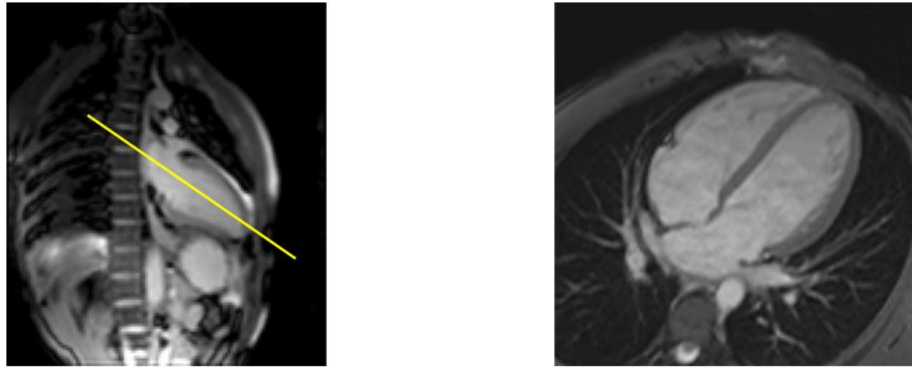


**Figure 2.3 : Example of HLA Scout image**

### 2.2.1.3 Short-Axis Scout

Utilizing the HLA and VLA scout images, three short axis scout images were acquired with the basal slice parallel to the atrioventricular (AV) groove. The three slices were acquired perpendicular to the long axis of the left ventricle. The distance between the slices were chosen such that they encompassed the basal, mid and apical regions of the LV (Figure 2.4).

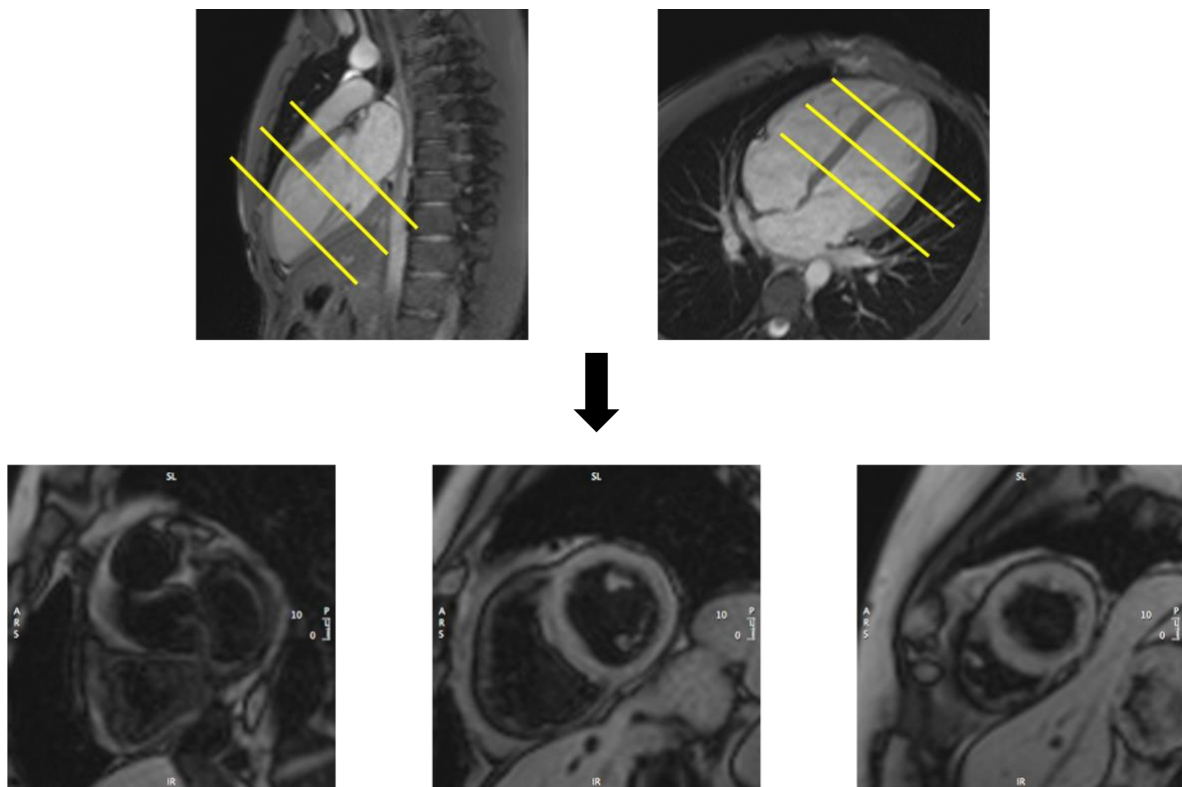


**Figure 2.4 : Example of Short-Axis Scout image**

## 2.2.2 Cine Imaging

Cine images were acquired in the VLA, HLA and ten short-axis images covering the entirety of the right and left ventricles, using a retrospective ECG gating SSFP sequence (repetition time (TR) 3ms, echo time (TE) 1.5ms, matrix 173 x 256, field of view 370 x 370 mm, bandwidth 1302, spatial resolution 1.81 x 1.45 x 6, slice thickness 6 mm, flip angle 55°).

### 2.2.2.1 VLA (Two Chamber) Cine

To acquire the VLA cine, a planned parallel line was placed in a 'vertical orientation' on a short axis scout image (Figure 2.5). The planned line transects the anterior and posterior insertion points of the RV into the inter-ventricular septum.

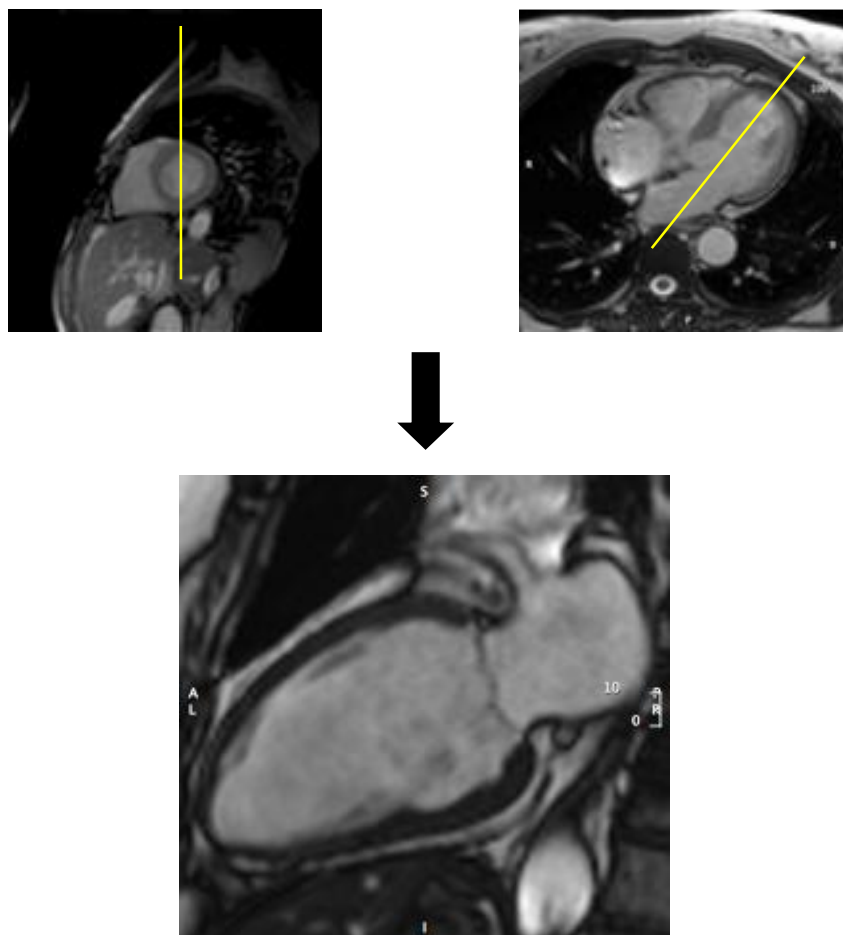


**Figure 2.5 : Example of VLA Cine**

### 2.2.2.2 HLA (Four Chamber) Cine

The HLA cine was acquired by positioning a planned parallel line in a ‘horizontal orientation’ on a short axis scout image (Figure 2.6). On this mid-ventricular SA scout image, the planned parallel line was carefully manipulated to go through (or as close as possible to) the major axis of the RV free wall, the mid IV septum, the mid LV cavity and the lateral LV wall.

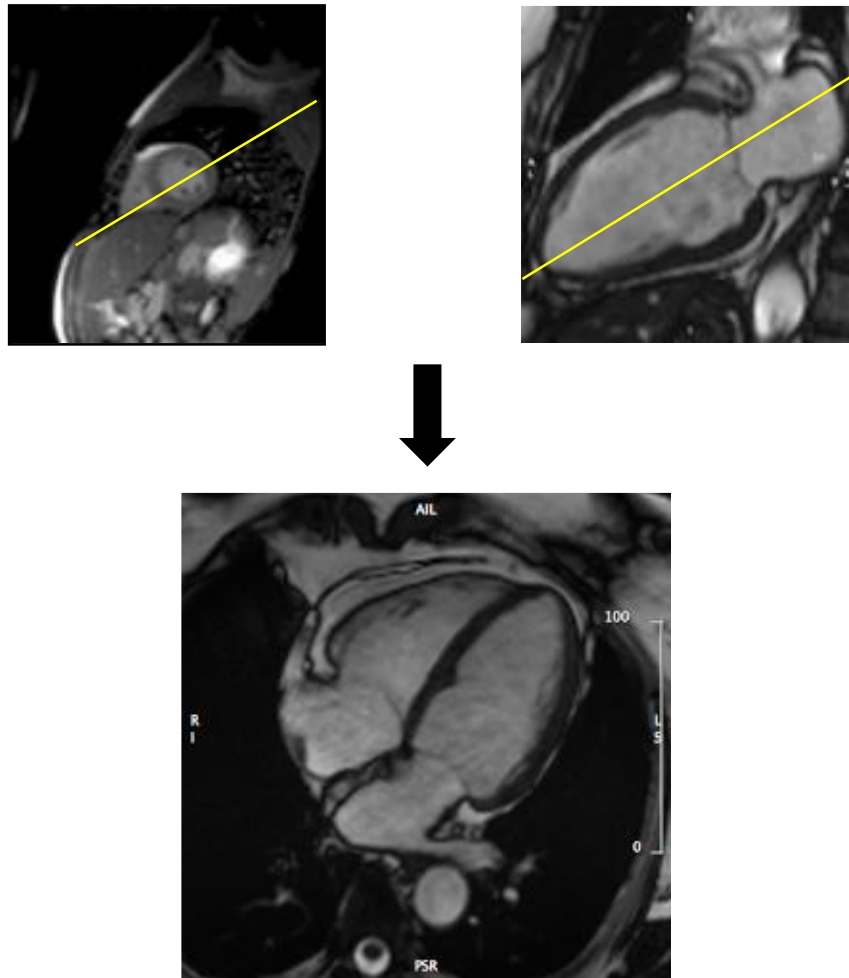
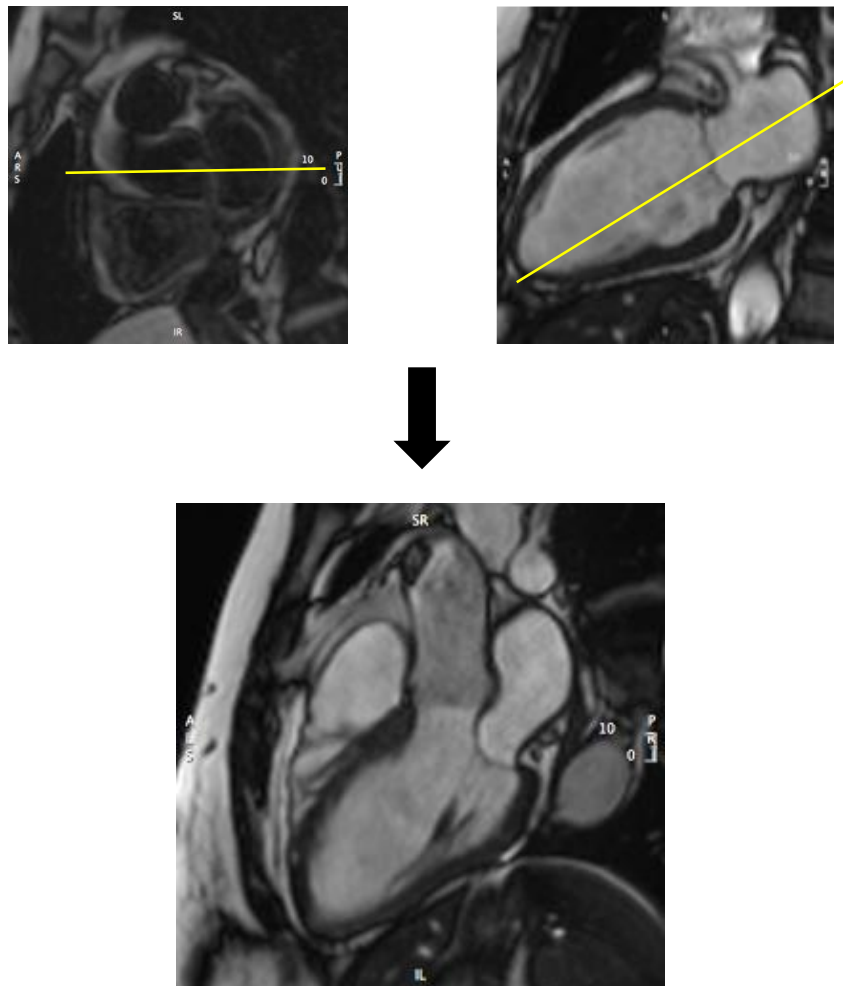


Figure 2.6 : Example of HLA Cine

### 2.2.2.3 Left Ventricular Outflow Tract (LVOT) Cine

The LVOT cine was acquired by positioning a planned parallel line that passed across the centre of the aortic and mitral valves on the basal short axis scout image and rotating the slice on the VLA view through the apex of the heart (Figure 2.7).



**Figure 2.7 : Example of LVOT Cine**

#### **2.2.2.4 Left Ventricular Outflow Tract Cross Cut (LVOT XC) Cine**

The LVOT XC cine was acquired by positioning a planned parallel line through and perpendicular to the aortic valve in the LVOT cine view (Figure 2.8).

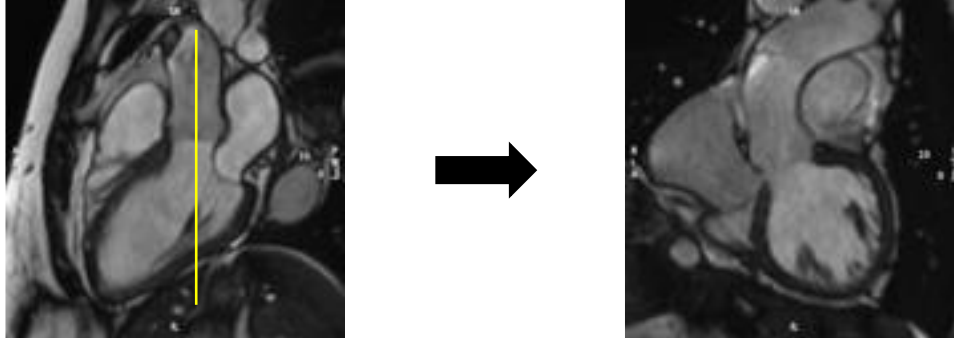


**Figure 2.8 : Example of LVOT XC Cine**

#### **2.2.2.5 Short Axis Cine**

The short-axis cine was a set of consecutive image slices encompassing the entire LV from base to apex. Short Axis Cine was a series of multi-slice studies covering the entire LV in short axis direction (perpendicular to the VLA image) which forms what was called a short axis cine stack. (Figure 2.9). Depending on the size of the left ventricle, approximately 10 to 14 short-axis slices were obtained.

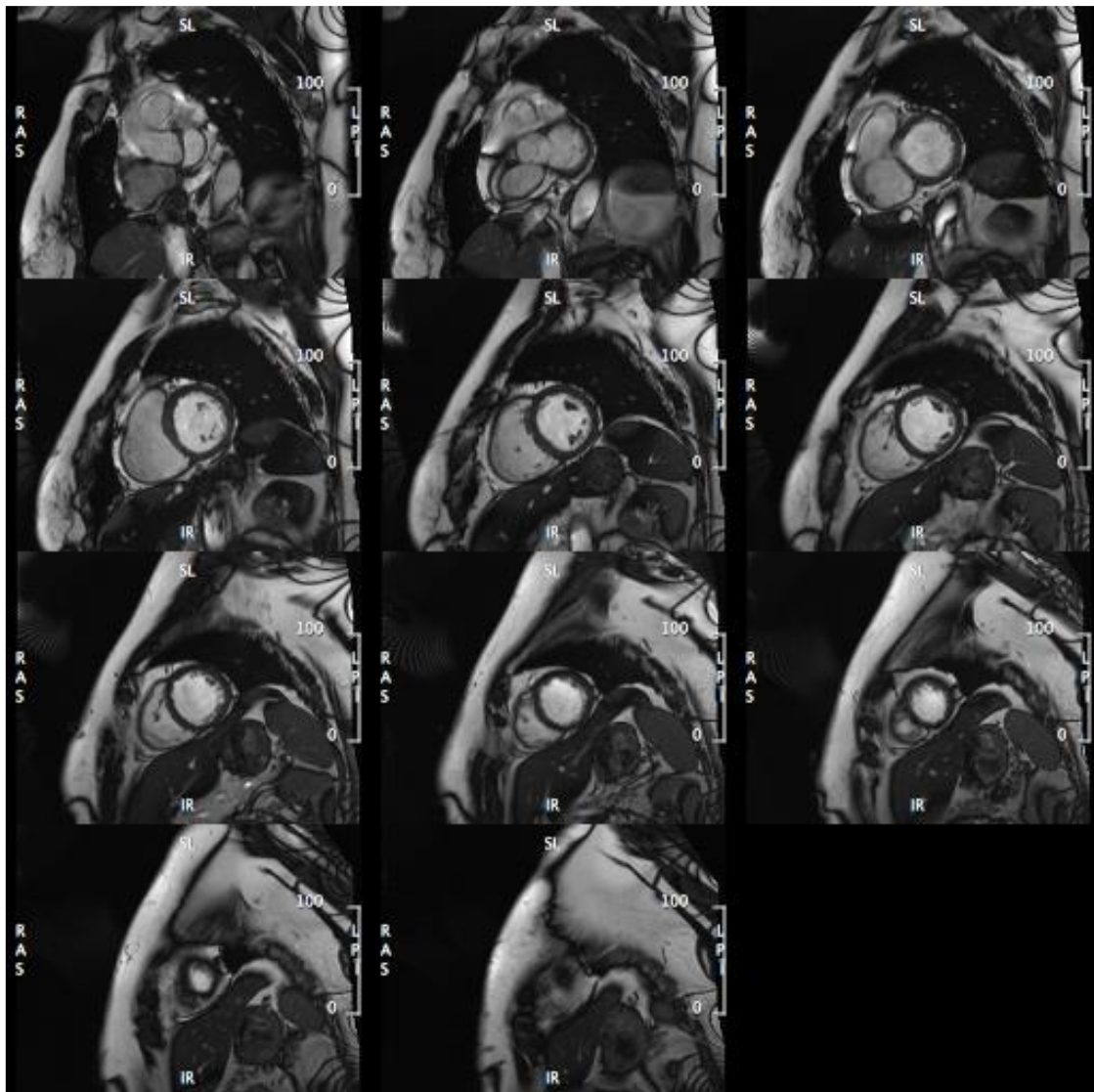
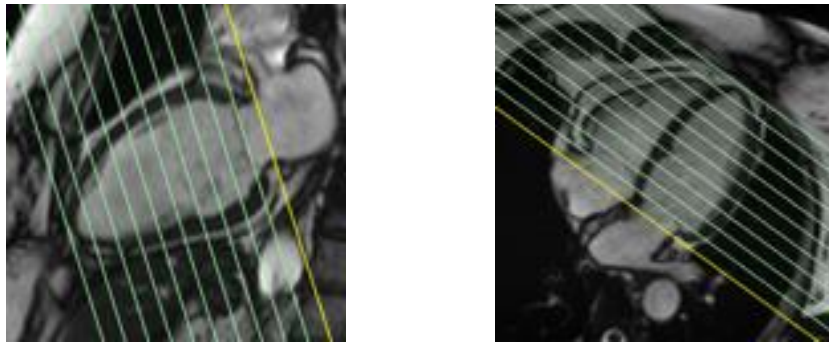
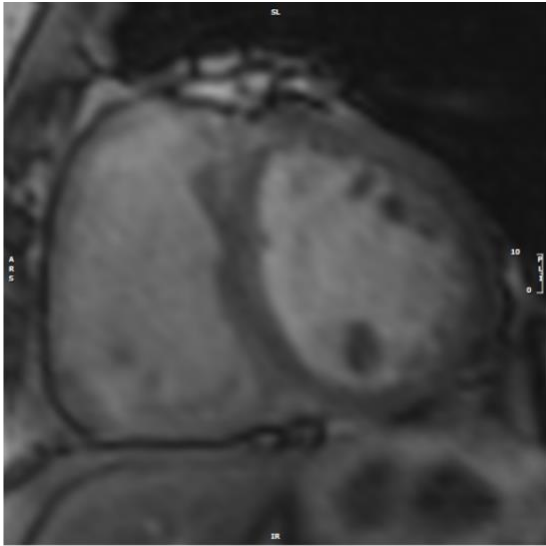


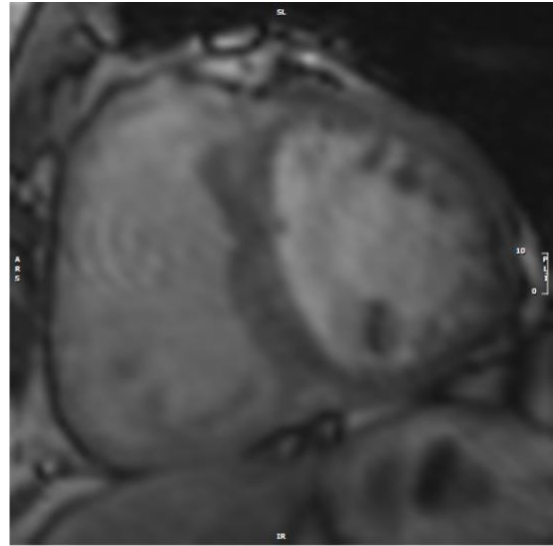
Figure 2.9 : Example of Short Axis Cine Stack

### **2.2.3 Oxygen Sensitive Cardiovascular Magnetic Resonance (OS-CMR) Imaging**

All participants were scanned using a 3 Tesla clinical MR scanner (Siemens, 3T MAGNETOM Skyra, 18 channel torso phased array coil in conjunction with a spinal coil posteriorly) and refrained from caffeine 24 hours prior to the scan. A single mid-ventricular slice was acquired at mid-diastole using a single-shot T2-prepared ECG-gated SSFP sequence (TR 256ms, TE 1.21ms, T2 preparation time 40ms, matrix 168 x 192, field of view 340 x 340 mm, slice thickness 6 mm, flip angle 44°). Volume shimming and frequency adjustments were performed as required before the oxygenation imaging to minimise off-resonance artefacts. Each OS-CMR image was acquired during a single breath-hold over six heart beats. Four resting OS-CMR images were acquired at rest prior to commencement of adenosine infusion (Figure 2.10A). Acquisition of the OS-CMR stress images commenced at 2 minutes of adenosine infusion. Each acquisition lasted 8-10 seconds on average (was heart rate dependent); we obtained four to six OS-CMR acquisitions over the stress period with an average of 30 seconds interval between acquisitions (Figure 2.10B). Hence, a typical duration of stress OS-CMR image acquisition was 3 minutes with the total duration of adenosine infusion was about 5 minutes. Stress heart rate and blood pressure were obtained every minute of adenosine infusion. Patients were monitored by ECG, sphygmomanometry and pulse oximetry throughout the study.



A



B

**Figure 2.10 : Example of Rest (A) and Stress (B) OS-CMR image**

### 2.2.4 T1 mapping

T1 mapping was acquired using Shortened Modified Look-Locker Inversion recovery (ShMOLLI) in three short-axis slice positions (basal, mid-ventricular and apical) as previously described (89). The ShMOLLI sequence was performed with prospective ECG triggering until optimal image quality was obtained. This sequence has a FOV of 360 x 360 cm, matrix 192 x 144 m, slice thickness 8 mm, producing a voxel size 1.88 mmx1.88 mm. The repetition time TR is 379.40 and echo time TE of 1.07. Typically, the flip angle is set to 35 degrees and IPAT (GRAPPA) factor of 2, TI (inversion time) of 260 ms. The native (resting) T1 maps were acquired after the resting OS-CMR images (Figure 2.11). The mid-ventricular slice location selected was matched to the selected mid-ventricular resting OS-CMR images.

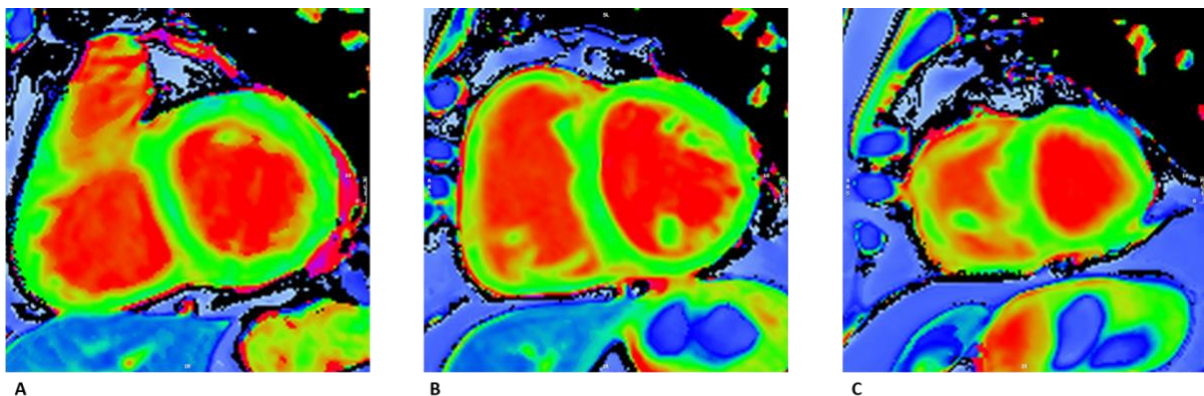


**Figure 2.11 : Example of Native (Rest) T1 maps at basal (A), mid (B) and apex (C)**

#### 2.2.4.1 Rest/Stress T1 mapping

Similar to the native (resting) T1 mapping, Rest/Stress T1 mapping was acquired using the ShMOLLI sequence as described above. The mid-ventricular slice location was matched to the mid-ventricular resting OS-CMR images, and the basal slice was carefully selected to avoid the LV outflow tract. Stress T1 maps were acquired after the stress OS-CMR images (starting 5 mins after the commencement of the adenosine infusion) in 3 short-axis slices matching the resting T1 maps.

## 2.3 CMR Analysis

### 2.3.1 Ventricular Volumes, Function and Mass

The LV and RV volumes, function and mass were analyzed using dedicated software (CVI<sup>42</sup>, Circle Cardiovascular Imaging, Calgary) using the acquired Short Axis Cine Stack. The analysis starts at the end-diastolic phase, with the most basal slice, which is defined as the slice with at least 50% of the myocardium. Using a mid-ventricular slice, the phases were advanced until the end-systolic phase when the smallest cavity was reached (102). The CVI<sup>42</sup> software automatically calculated the volumes, function and mass (Figure 2.12). These contours were manually checked, and any errors were corrected. The ventricular volumes and mass were indexed to body surface area (BSA).

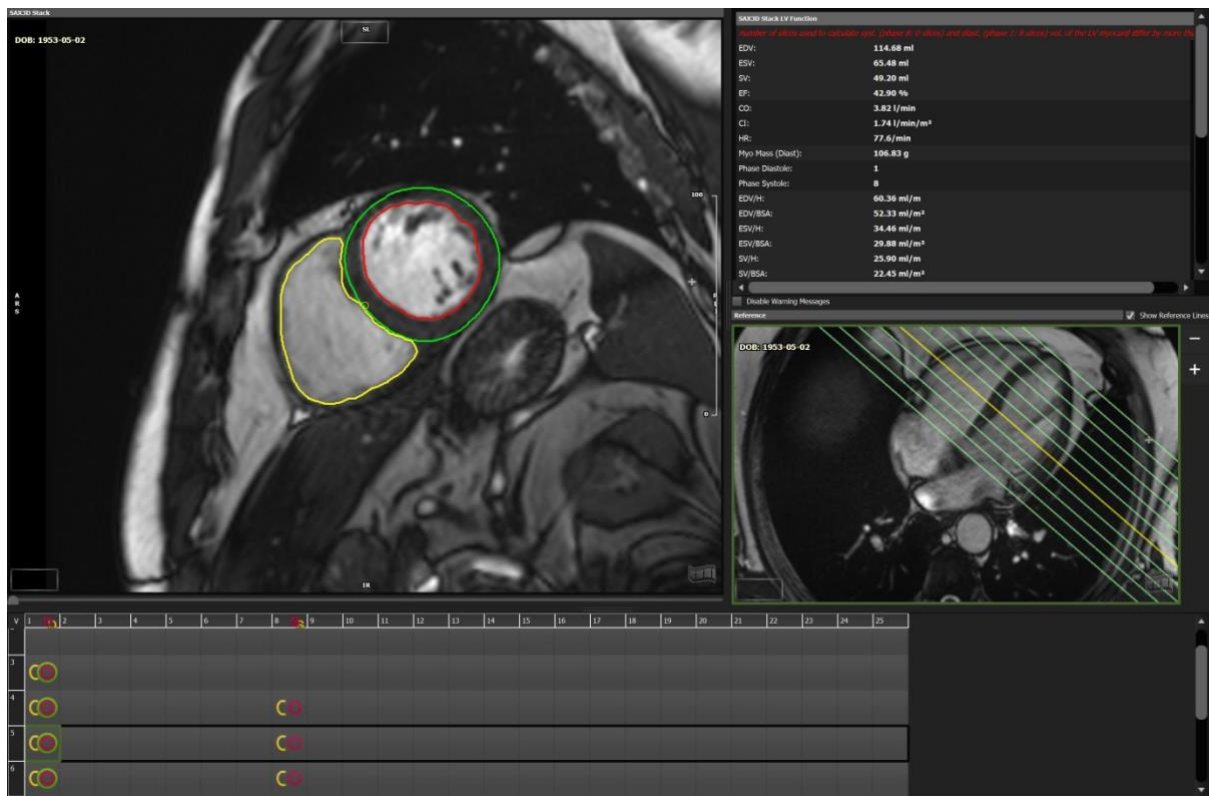


Figure 2.9 : CVI<sup>42</sup> analysis of ventricular Volumes, Function and Mass

### 2.3.2 OS-CMR Analysis

OS-CMR Image analysis was performed using CVI<sup>42</sup>. Assessment of the LV was performed whereby epicardium and endocardium borders were manually traced and sub-divided into 6 equiangular segments based on a standard American Heart Association segmentation of the mid-ventricular slice (103). The RV was segmented to into RV anterior (RV Ant), RV free-wall (RV FW) and RV inferior (RV Inf) and a region of interest (ROI) contour was traced manually. The mean resting myocardial signal intensity (SI) within each segment was obtained by averaging signal measurements from all the acquired rest OS-CMR images. Similarly, mean stress SI was calculated by averaging the signal measurements from all the stress OS-CMR images acquired during adenosine infusion. As it was a cardiac gated sequence, corrections were made to the mean signal intensity due to the variations of heart rate and its effects on T1 relaxation (104). These corrections were applied to previous OS-CMR studies involving the LV, and a similar correction was applied to the OS-CMR RV SI. The following equation was used for correction for measured signal intensity for heart rate:

$$S = S_0/[1-\beta e^{(-TR/T1)}]$$

where S is the corrected SI and S<sub>0</sub> is the measured SI. TR is the image dependent time between acquisitions of sections of *k*-space, governed by the heart rate. An empirical value of T1=1220ms<sup>22</sup> and β=0.59 from previously described work was appropriate for this sequence (105). The relative SI change was calculated as:

$$\Delta SI (\%) = (SI \text{ stress} - SI \text{ rest})/SI \text{ rest} \times 100.$$

As PAH is a global process, the LV OS-CMR assessment was evaluated globally by averaging the ΔSI (%) from all the 6 LV segments.

### **2.3.3 T1 Map Analysis**

The T1-values of the LV and RV were assessed using CVI<sup>42</sup>. For the LV the endocardial and epicardial contours were manually traced for all the 3 short-axis T1 map images (basal, mid-ventricular and apical) and were divided into 16 segments according to the American Heart Association 17-segment model (103). As for the RV, a ROI contour was traced manually on the T1 maps of RV Ant, RV FW and RV Inf regions. A mean myocardial T1 value was obtained within each segment.

#### **2.3.3.1 Rest/Stress T1 Analysis**

Rest/Stress T1 analysis was performed on the LV T1 maps acquired during rest and stress. The endocardial and epicardial contours were manually traced for all the 3 short-axis T1 map images (basal, mid-ventricular and apical) and were divided into 16 segments according to the American Heart Association 17-segment model (103). The mean myocardial T1 within each segment was obtained, both at rest and stress. The T1 reactivity ( $\Delta T1$ ) was then calculated from the T1-values at rest ( $T1_{Rest}$ ) and during adenosine stress ( $T1_{Stress}$ ) as:

$$\Delta T1 = (T1_{Stress} - T1_{Rest}) / T1_{Rest} \times 100\%$$

### **2.3.4 CMR feature tracking analysis**

The myocardial mechanics assessment was performed using CVI<sup>42</sup> by utilizing cine short axis and long axis (VLA, HLA and LVOT) images. First, at the end diastolic phase, the contrast and brightness were manually optimized to ensure optimal endocardial/blood pool discrimination; following which the mitral valve annular plane and the position of LV apex were identified. The LV endocardial and epicardial borders (excluding papillary muscles and trabeculae) were then manually traced on the end-diastolic frame of the cine images. The CVI<sup>42</sup> software automatically propagated the contours and followed its features throughout the

remainder of the cardiac cycle. LV myocardial architecture consists of longitudinally and circumferentially orientated fibres located predominately in the epicardium/endocardium and mid-wall. This is reflected by longitudinal, circumferential, and radial strain which demonstrate subendocardial, mid-wall, and transmural myocardial functions. Global peak systolic longitudinal strain (GLS) was derived from the long-axis cine images analysis while global peak systolic circumferential (GCS) and radial (GRS) strains were derived from the short-axis cine images analysis.

### **Chapter 3 : Feasibility of oxygen sensitive cardiovascular magnetic resonance of the right ventricle in pulmonary artery hypertension**

Prior to using oxygen-sensitive cardiovascular magnetic resonance clinically the feasibility must be tested. This chapter describes the feasibility of right and left ventricular oxygen-sensitive cardiovascular magnetic resonance in both patients with pulmonary arterial hypertension and normal controls.

### 3.1 Introduction

Pulmonary arterial hypertension (PAH) is a progressive disorder that affects both the pulmonary vasculature and the heart (1). The natural progression of PAH involves gradual development of right ventricle (RV) dysfunction which is often silent until advanced (16, 106). Whilst the exact cause of RV remodelling and subsequent dysfunction remains unclear; an ischemic precipitant is thought to be a significant contributor (32). Oxygen-sensitive (OS) cardiovascular magnetic resonance (CMR) technique has been used to investigate myocardial oxygenation and ischemia in the LV (71, 79). This technique has been based on the effects of oxygenation on the paramagnetic properties of haemoglobin (70). Deoxygenated haemoglobin acts as an endogenous contrast agent with  $T_2/T_2^*$ -dependent signal effects. The signal intensity (SI) changes in OS-CMR images are inversely correlated with the concentration of deoxygenated haemoglobin. Hence with the relative increase of deoxygenated haemoglobin there will be a decrease in OS-CMR SI. Although OS-CMR has been used to advance the understanding of myocardial ischemia and a number of LV myocardial (107-110) and coronary artery disease states (79, 105, 111), the utility in the RV has not yet been determined. Additionally, the need for other markers of early recognition and diagnosis of PAH is paramount, particularly for individuals at higher risk for development of RV failure. It is possible that the novel imaging technique of RV targeted OS-CMR may provide an earlier diagnosis of RV abnormality in these patients. However, before the utility of these techniques can be implemented as a screening tool for RV ischemia and/or dysfunction, the feasibility of this technique must first be established. The aim of the present work therefore was to examine the feasibility of RV targeted OS-CMR to detect ischemia in a population with known PAH.

## **3.2 Methods**

### **3.2.1 Ethics**

This study was approved by the Southern Adelaide Clinical Human Research Ethics Committee (HREC/15/SAC/397). All participants provided written informed consent to participate in the study.

### **3.2.2 Participant Selection**

Patients undergoing treatment in the PAH clinics at two South Australian hospitals were invited to participate in this study. Patients were considered for inclusion if they had right heart catheter proven PAH and resting echocardiographic mean PA pressure between 25-50mmHg (as measured by the peak pulmonary regurgitant signal on echocardiography and added to estimated right atrial pressure) and/or systolic PA pressure between 40-90mmHg (as measured by the peak tricuspid regurgitant velocity gradient on echocardiography and added to estimated right atrial pressure). Exclusion criteria included severe RV dysfunction on echocardiography, diagnosis of significant left heart cardiomyopathy and/or coronary artery disease (defined as >70% luminal stenosis in an epicardial coronary artery at angiography or prior myocardial infarction) as well as contraindications to CMR and/or adenosine (second or third degree heart block, obstructive pulmonary disease or dipyridamole use). Nine healthy volunteers also underwent the same imaging procedures to act as a control group. The healthy volunteers had no known cardiac disease or symptoms and were free of any cardiac risk factors, including hypertension, smoking or diabetes.

### **3.2.3 Participant preparation**

As per section 2.1.2

### **3.2.4 CMR protocol**

The CMR protocol was performed as outlined in sections 2.2.1, 2.2.2 and 2.2.3. To optimise the OS-CMR for the RV, a frequency with the fewest banding artefacts and best homogeneity was selected and applied to the OS sequence. In addition, the volume, size and shape of the shim was set to tightly cover the heart in the mid short axis slice, with the thickness reduced to shim the slice area only. This enables further reduction of both banding frequency artefact and susceptibility artefacts.

### **3.2.5 CMR analysis**

The CMR analysis was performed as outlined in sections 2.3.1 and 2.3.2. All OS-CMR analysis was undertaken by experienced (SCMR Level 3) observers blinded to the clinical information of the participant. To evaluate inter-reproducibility, the OS-CMR images were independently assessed by 2 experienced (SCMR Level 3) observers. To evaluate intra-observer reproducibility, one observer measured OS-CMR SI twice on 2 separate days with a washout period of at least 2 weeks.

### **3.2.6 Statistical analysis**

Baseline and follow up data will be summarised using appropriate descriptive statistics and graphical representations. Discrete variables are summarised using the frequencies and percentages, whereas continuous variables will be presented by mean, standard deviation, median, Q1, Q3 as appropriate. Percentages will be calculated according to the number of patients for whom the data are available. These data will be presented for all patients and p-value reported for the difference between the groups using the appropriate statistical tests for categorical or continuous variables. Statistical tests were two-tailed and  $p < 0.05$  was considered statistically significant. Reproducibility of OS-CMR SI measurements was assessed by using the coefficient variability method. Associations between the test parameters were assessed using the Pearson r correlation coefficient.

### **3.3 Results**

#### **3.3.1 Participant characteristics**

The baseline characteristics of both groups are detailed in Table 3.1. Both groups were well matched for age and gender, but the control group had a lower body mass index (BMI, 27.0kg/m<sup>2</sup> vs 30.9kg/m<sup>2</sup>, p = 0.004). Amongst the PAH patients, 11 (55%) had idiopathic pulmonary hypertension (iPAH), 6 (30%) patients had systemic sclerosis (SSc)-associated PAH and 3 (15%) patients had chronic thromboembolic PAH (CTEPH). All patients had right heart catheter proven diagnosis of PAH with a mean pulmonary artery pressure of 35 (30 – 41) mmHg and mean pulmonary capillary wedge pressure of 12 (10 – 14) mmHg. The 6 minute walk data was retrospectively obtained from patient records. Mean 6 minute walk distance was 421 (368 – 474) meters. World Health Organisation functional class was between class II (n = 16, 80%) and III (n = 4, 20%). On echocardiography seven patients (35%) had RV dilatation but none had systolic RV dysfunction. The PAH patients had an echocardiography-estimated mean pulmonary artery pressure of 47 (38 – 57) mmHg. All PAH patients were treated with pulmonary vasodilators such as bosentan, macitentan, sildenafil, riociguat or a combination macitentan and sildenafil. The PAH patients were stable on treatment and continued their pulmonary vasodilators therapy during the OS-CMR research scan.

**Table 3.1: Patient demographics and baseline clinical data**

<b>Variables</b>	<b>PAH (n = 20)</b>	<b>Control (n = 9)</b>	<b>p-value</b>
Age (years), n (range)	67 (62 – 73)	63 (57 – 70)	0.293
Females sex, n (%)	15 (75%)	4 (44%)	0.117
BMI (kg/m <sup>2</sup> ), n (range)	30.9 (28.7 – 33.0)	27.0 (25.6 – 28.4)	0.004
Comorbidities			
• Hypertension, n (%)	6 (30%)	0	
• Diabetes, n (%)	3 (15%)	0	
• Obstructive Sleep Apnoea, n (%)	6 (30%)	0	
Medication			
• Beta-blockers, n (%)	4 (20%)	0	
• ACEi/ARB, n (%)	3 (15%)	0	
• Endothelin receptor blockers, n (%)	16 (80%)	0	
• PDE5 inhibitor, n (%)	11 (55%)	0	
• Soluble guanylate cyclase, n (%)	1 (10%)	0	

BMI – Body Mass Index, ACEi = angiotensin-converting enzyme inhibitors, ARB = angiotensin II receptor blockers, PDE5 = phosphodiesterase type 5 inhibitor

### 3.3.2 CMR Characteristics

Table 3.2 shows a comparison of CMR variables between PAH patients and controls. The only statistically significant difference in CMR volumetric and functional indices between PAH and controls were the RV mass index ( $20 \pm 12$  vs  $14 \pm 9\text{g/m}^2$ ,  $p = 0.014$ ) and RV inferior wall thickness ( $5 \pm 1$  vs  $4 \pm 1\text{mm}$ ,  $p = 0.019$ ). The RV inferior wall thickness was measured on the short axis cine slice location similar to the mid ventricular slice location chosen for the OS imaging.

**Table 3.2: CMR Ventricular Function**

<b>Variables</b>	<b>PAH (n = 20), mean ± SD</b>	<b>Control (n = 9), mean ± SD</b>	<b>p-value</b>
CMR LVEF (%)	66 ± 10	69 ± 7	0.409
CMR LV EDVi (ml/m <sup>2</sup> )	62 ± 24	66 ± 11	0.505
CMR LV ESVi (ml/m <sup>2</sup> )	21 ± 11	19 ± 4	0.496
CMR LV ED Mass Index (g/m <sup>2</sup> )	48 ± 18	51 ± 10	0.593
CMR LV SV Index (ml/m <sup>2</sup> )	40 ± 16	47 ± 8	0.167
CMR RVEF (%)	58 ± 11	64 ± 9	0.165
CMR RV EDVi (ml/m <sup>2</sup> )	66 ± 23	65 ± 14	0.846
CMR RV ESVi (ml/m <sup>2</sup> )	28 ± 17	24 ± 9	0.321
CMR RV SV Index (ml/m <sup>2</sup> )	38 ± 12	41 ± 10	0.412
CMR RV ED Mass Index (g/m <sup>2</sup> )	20 ± 12	14 ± 9	0.014
RV inferior wall thickness* (mm)	5 ± 1	4 ± 1	0.019

\* RV inferior wall was measured at the short axis cine slice location similar to the OS-CMR mid ventricular slice location.

CMR = cardiovascular magnetic resonance, LV = left ventricle, RV = right ventricle, EF = ejection fraction, EDVi = end-diastolic volume index, ESVi = end-systolic volume index, ED = end-diastolic, SV = stroke volume

### **3.3.3 Right Ventricular Myocardial Oxygenation Response (OS-CMR)**

#### **3.3.3.1 Safety and tolerability**

All participants tolerated and completed the adenosine induced stress component of the OS-CMR. Both the patients and controls had a good hemodynamic stress response, increase in heart rate (>10 beats/min) and at least one adenosine-related symptom (chest tightness, shortness of breath, flushing, transient headache or nausea). There was a drop of systolic blood pressure (>10 mmHg) in 10 patients (50%). All side effects dissipated within a minute of stopping the adenosine infusion.

#### **3.3.3.2 OS-CMR acquisition and optimization of the RV signal**

The feasibility of detecting the RV OS-CMR signal differed according to the RV myocardial segments. In both PAH and controls, reliable OS signal was only obtained in the inferior RV myocardial segment. Overall OS-CMR analysis was possible in 89% (396/444) of the RV (OS-CMR rest and stress) myocardial segments in the pulmonary hypertension patients and 80% (189/237) of the RV (OS-CMR rest and stress) myocardial segments in the control group. In the PAH group, 84% of the RV Ant (124/148) and RV FW (125/148) myocardial segments were analysed and 99% of RV Inf (147/148) myocardial segments were analysed. In the control group 73% of the RV Ant (58/79) and 75% of RV FW (59/79) myocardial segments were analysed with all the RV Inf myocardial segments were analysed. Segments were excluded from analysis because of thinned myocardium, off-resonance artefacts and image artefacts (Figure 3.1). We had attempted to reduce the limitation of thinned RV myocardium by reviewing all the short axis (SA) cine acquisitions and selecting the best mid ventricle SA cine slice with the maximal RV myocardial thickness. The OS sequence was then applied to this mid ventricle SA slice location.

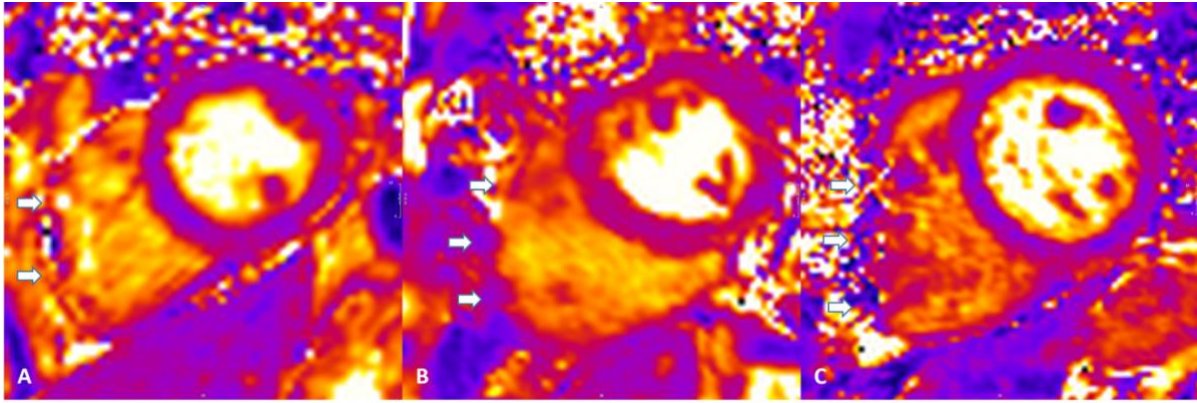


**Figure 3.1 – OS-CMR images in patients with pulmonary hypertension demonstrating poor image quality and segmental (RV Ant and RV FW) exclusions. Myocardial segments are excluded (arrow) from analysis primarily due to thin myocardium (A), off-resonance artefacts (B) and image artefacts (C).**

To limit the effects of off-resonance artefacts, a frequency shift scout series was applied to the selected mid ventricle SA cine slice location. A frequency range between -150Hz to 150Hz was acquired and reviewed to select the optimal frequency. The delta frequency of the OS-CMR sequence was adjusted according to the optimal frequency chosen from the frequency shift scout. Image artefacts of the RV myocardium, in particular the RV FW segments were due to artefacts from air, heart-lung borders, sternal wires. This was overcome by modifying the adjustment volumes to match to selected mid ventricle SA slice location (Figure 4 – green box). To begin with the thickness of the adjusted volume was modified to focus only on the selected mid ventricle SA slice thickness (Figure 3.2A). Then the area of the adjustment volume was reduced inplane to the myocardium and to exclude unwanted air and sternal wires (Figure 3.2B). No adjustments were made to the matrix, field of view or slice thickness between rest and stress OS-CMR imaging in both groups. All the OS-CMR images were acquired in the same part of the cardiac cycle. A constant OS-CMR sequence voxel size of 2.02mm x 1.77mm was maintained in both PAH and controls.

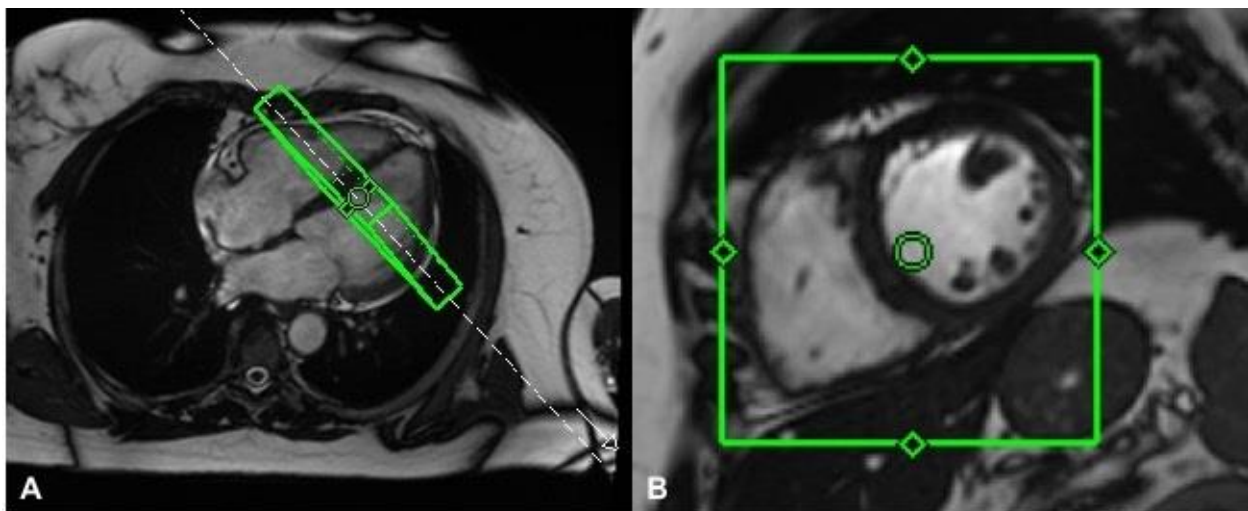


**Figure 3.2 – Adjustments volumes made to OS-CMR cardiac shim images to mitigate the effects of artefacts. Adjusted volume modified to focus on the selected mid ventricle SA slice thickness (A). Adjustment volume reduced inplane to the myocardium and to exclude unwanted air and sternal wires (B).**

### **3.3.3.3 Oxygenation response (OS-CMR signal)**

The RV OS SI response in the three RV segments in PAH patients were: RV Ant  $10 \pm 12\%$ , RV FW  $3 \pm 15\%$  and RV Inf  $11 \pm 9\%$ . In controls, reliable OS SI response was obtained in the RV Inf segment. The RV Inf OS SI changes between PAH patients and controls was  $11 \pm 9\%$  vs  $17 \pm 5\%$  ( $p = 0.045$ ). Figure 3.3A further highlights the distribution of OS signal response in PAH vs control group to stress in the inferior RV segments. There was less variability of the OS SI between PAH patients and controls. In the RV Inf, the PAH patients have a median OS SI change of 11% (interquartile range: 5 to 18%) versus control median OS SI change of 17% (interquartile range: 12 to 21%). The inter-observer coefficient variability was 0.812 and the intra-observer coefficient variability was 0.945.

### **3.3.4 LV Myocardial Oxygenation response (OS-CMR)**

The global LV  $\Delta$ OS-CMR SI change was significantly lower in the PAH group compared to the controls ( $11.1 \pm 7.3\%$  vs  $21.1 \pm 9.1\%$ ,  $p=0.019$ ) (Figure 3.3B).

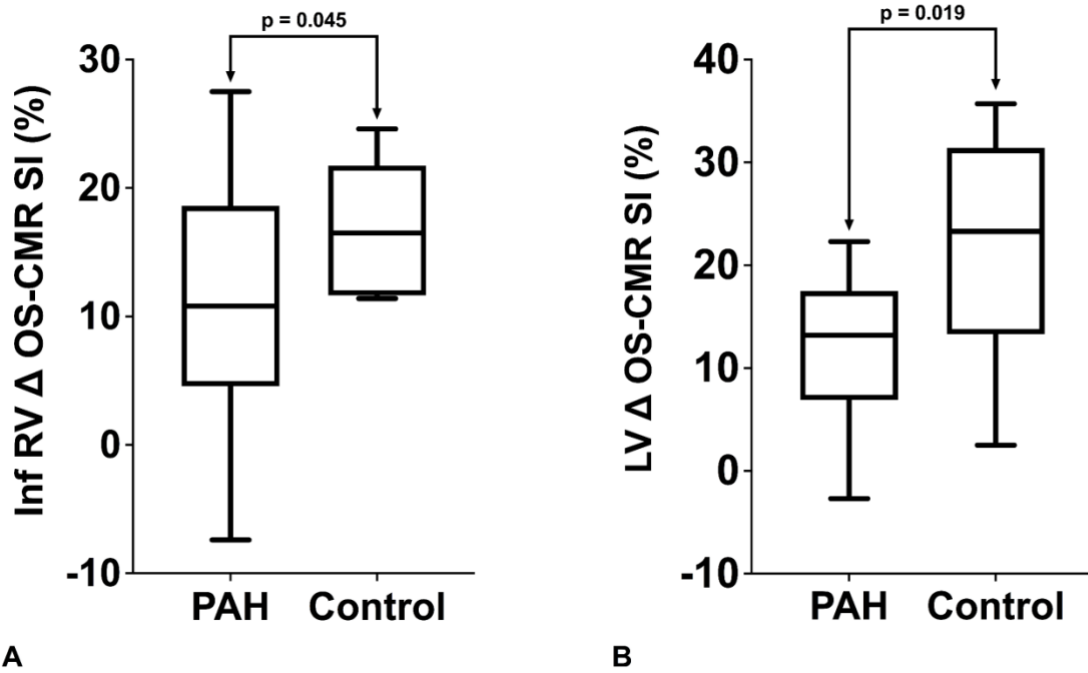
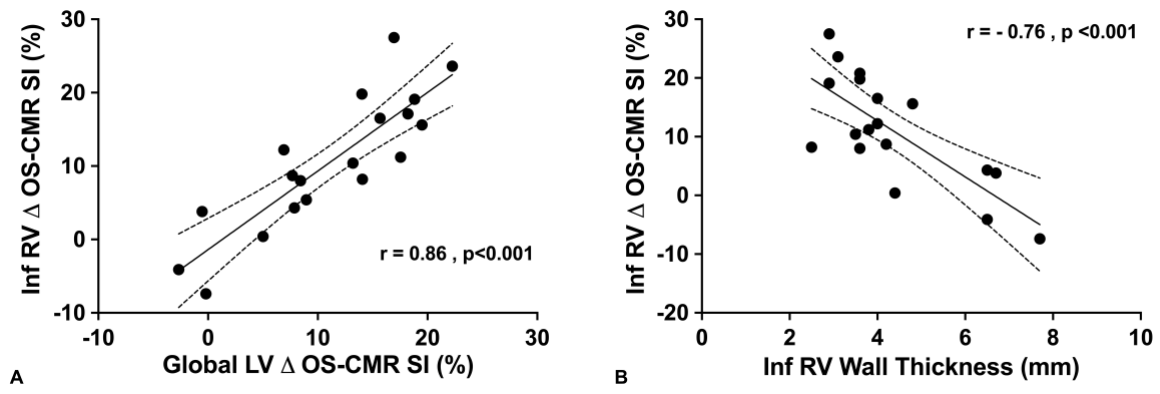


Figure 3.3 – Distribution of OS Signal Response to Stress between PAH and control in the inferior RV segment (A) and LV (B).

### **3.3.5 Relationship between RV Myocardial Oxygenation, LV Myocardial Oxygenation and CMR volumetric and functional indices**

There was a strong correlation between RV OS-CMR SI and LV OS-CMR SI ( $r = 0.86$ ,  $p < 0.001$ ) (Figure 3.4A). Furthermore, there was an inverse relation whereby the RV Inf OS SI change was increasingly blunted with increasing RV wall thickness ( $r = -0.76$ ,  $p < 0.001$ ) (Figure 3.4B). However, there was no correlation between RV Inf OS SI and CMR RVEF ( $r = 0.24$ ,  $p = 0.346$ ), CMR RV EDVi ( $r = -0.21$ ,  $p = 0.377$ ) or RV mass index ( $r = -0.44$ ,  $p = 0.079$ ).



**Figure 3.4 – Correlation between Inf RV OS-CMR SI (%) to global LV OS-CMR SI (%) and Inf RV wall thickness (mm).**

### **3.4 Discussion**

The main finding of this proof of concept study is that the use of OS-CMR with vasodilator stress is safe and feasible in PAH patients. We found that compared with age-matched healthy volunteers, OS-CMR shows myocardial deoxygenation most reliably in the inferior RV of patients with PAH. Furthermore, the RV myocardial deoxygenation correlates with the LV myocardial deoxygenation in PAH patients. This technique therefore holds promise as a non-invasive tool to assess early RV myocardial ischemia in patients with PAH.

#### **3.4.1 Pathological mechanisms of RV ischemia in PAH**

It has long been recognised that an ischaemic insult is the most likely precipitant in the remodelling and subsequent development of RV dysfunction in PAH (32). This occurs in one of many forms. 1) Increasing pulmonary vascular and thence RV pressure decreases the pressure gradient between the aorta and the RV and might thereby reduce myocardial blood flow in the right ventricular branch of the right coronary artery, which may lead to ischemia (38, 112). Progressive RV hypertrophy (RVH) without a sufficient compensatory increase in the myocardial vasculature and flow would likely exacerbate ischemia of the RV (35-37). It has been demonstrated in the advanced stages of PAH that right coronary perfusion pressure can drop below 50 mmHg leading to a decline of RV contractile function (33). 2) Microvascular ischemia may also occur, due to occlusive microvascular damage and impairment in angiogenesis (known as capillary rarefaction); this has been demonstrated in animal models and SSc associated PAH (33, 38). There is also decreased expression of genes such as insulin growth factor 1, VEGF, apelin and angiopoietin-1 in the RV in PAH, which can lead to further microvascular damage, rendering the myocardial fibres more vulnerable to ischemia (106). 3) Dysfunctional mitochondrial metabolism has been another pathologically relevant feature of myocardial ischemia demonstrated in hypertrophied RV of PAH. In animal models of PAH

with RVH, there is a shift from fatty acid oxidation to glycolysis as a preference of energy substrates (39). This shift in glycolysis has been demonstrated by increased uptake of fluorodeoxyglucose on positron emission tomography (PET) in PAH patients with RVH (40). This metabolic shift to aerobic glycolysis has been associated with decreased cardiac output and RV contractility (39, 41). The complex interplay between reduced right coronary perfusion pressure, microvascular ischemia and worsening RV contractility can lead to a decrease in myocardial oxygenation. Even in the absence of epicardial coronary artery disease, these mechanisms could form a vicious cycle leading to progressive RV dysfunction, resulting in RV hibernation (113).

#### **3.4.2 Feasibility of OS-CMR in the RV**

The use of OS-CMR has been established as a direct assessment of myocardial oxygenation in the LV (79). The OS signal intensity changes reflect the changes in haemoglobin oxygenation; hence it can be used to study the state of myocardial oxygenation in the capillary bed. OS-CMR is a novel non-invasive technique that can provide insights into the balance (or the lack of) between myocardial oxygen supply and demand. As it is a direct measure of oxygenation changes within the myocardium, it has been utilized to demonstrate ischemia in diseases in the absence of significant epicardial coronary artery disease (79). The OS-CMR technique has increased understanding of in-vivo myocardial oxygenation in epicardial coronary artery disease and cardiomyopathies involving the LV; however, its utility in the assessment of myocardial ischemia of RV has not yet been examined.

Our study has demonstrated that OS-CMR of the RV with stress induced via pharmacological adenosine infusion is a safe and feasible technique in patients with PAH. Nevertheless, in some patients the RV Ant and RV FW segments had to be excluded from analysis due to thin

myocardium (causing partial volume effects), off-resonance artefacts and image artefacts. Whilst every effort was taken to limit these effects, there are a known limitation of the OS-CMR technique. Other OS-CMR studies involving the LV have excluded segments with thinned myocardium and artefacts (from partial volumes) as it affects the accuracy of OS-CMR SI (114). In our study the measured Inf RV wall thickness and consistent voxel-size during OS-CMR imaging provided sufficient coverage to avert partial volume effects. Off-resonance artefacts seen in OS-CMR by nature arise from the inhomogeneities of using a higher magnetic field (74). However the advantages of using a higher field strength are improved ability to detect OS-CMR SI changes, increased contrast to noise ratio and signal to noise ratio (74). Despite these limitations, the feasibility of OS-CMR in the RV offers a potentially novel non-invasive, contrast and tracer independent technique that may offer new insights to myocardial oxygenation in the RV. Furthermore the OS SI in the RV has a good correlation with the LV, an area of the myocardium in which the OS-CMR technique has been extensively validated and studied (71, 79). Coincidentally we have demonstrated LV myocardial deoxygenation in PAH patients. While the focus of this study has been the feasibility of OS-CMR of the RV, the presence of LV deoxygenation in PAH needs further study. In summary, establishing a means of studying the in-vivo state of myocardial oxygenation of the RV in PAH patients may help in the pathophysiological understanding of RV dysfunction in this high risk group.

### **3.4.3 Study Limitations**

This study has a small sample size which may increase the margin of error. Further, larger studies would help further optimize as well as determine the clinical utility of OS-CMR of the RV in PAH and its association with clinical outcomes. Additionally, there was incomplete coverage of the full RV myocardium due to the CMR acquisition being performed on a single mid-ventricular slice however this is unlikely to be of major relevance in RV assessment of PAH which is a global process. Indeed, the mid RV wall is the most vulnerable to ischemia anatomically because of its precarious blood supply. The presence of thin myocardium, off-resonance artefacts and image artefacts led to poor image quality and segment exclusion. However, the feasibility and safety of pharmacological induced OS-CMR of the RV should provide novel insights into the mechanisms of RV dysfunction in PAH patients. Moreover, a novel marker of early or impending RV failure might become a clinically useful guide for therapy augmentation. These findings should be considered as hypothesis-generating for future studies.

### **3.5 Conclusion**

This is the first study to show that pharmacological induced OS-CMR is a feasible and safe technique to identify and study myocardial oxygenation in the RV of PAH patients. With a larger study this technique has potential implications in the understanding of myocardial ischemia of the RV in patients with PAH, or other pathologic conditions affecting the RV myocardium.

## **Chapter 4 : Right ventricular myocardial deoxygenation in patients with Pulmonary Artery Hypertension**

Now that the feasibility of oxygen-sensitive cardiovascular magnetic resonance has been established it needs to be determined if it correlates with functional and haemodynamic indices of pulmonary hypertension. This chapter describes the prevalence of RV myocardial ischaemia and its relationship with changes in the myocardial interstitium and correlation with functional and haemodynamic indices of patients with known PAH.

## 4.1 Introduction

Pulmonary arterial hypertension (PAH) is a progressive disorder that affects both the pulmonary vasculature and the heart (1). It is a rare but serious disease, affecting up to 50 per million population (6). Although the initial insult in PAH involves the pulmonary vasculature, prognosis of patients with PAH is most dependent on right ventricular (RV) size and function (12). While there are several putative causes, RV ischemia is thought to be a significant driver (32). The increasing pulmonary pressure decreases the pressure gradient between the aorta and the RV thereby reducing myocardial blood flow in the right coronary artery which, leads to myocardial ischemia (33, 34). In addition, the RV adapts to the increased afterload by increasing wall thickness and contractility. However, RV hypertrophy without a corresponding increase in the cross-sectional area of the right coronary artery can exacerbate ischemia of the RV (37). RV adaptive changes due to the elevated pulmonary pressures affects the integrity of the collagen network of the cardiomyocyte and interstitium leading to RV fibrosis (31). Whether the adaptive changes in the myocardial interstitium has any causal relationship to myocardial ischaemia in PAH patients remains unknown.

Oxygen-sensitive (OS) cardiovascular magnetic resonance (OS-CMR), also known as blood oxygen level dependent (BOLD) cardiovascular magnetic resonance (CMR) enables the in-vivo assessment myocardial oxygenation at the tissue level (79, 105, 107, 108, 111). OS-CMR utilises the natural paramagnetic properties of haemoglobin (70). Following vasodilator stress, the alterations to the deoxygenated haemoglobin concentration act as an endogenous contrast agent leading to signal intensity (SI) changes in OS-CMR sequence. CMR T1 mapping can be used to characterise changes in the interstitial myocardium of the left ventricle (115). T1 mapping quantifies the T1 relaxation time of each voxel of an image being quantified. Different tissues each have distinctive T1 relaxation times and this can vary with a change in tissue

composition. CMR T1 mapping has been used for inflammation/oedema imaging and serves as a surrogate for diffuse interstitial fibrosis in the absence of an alternative cause of interstitial expansion (oedema, infiltrations/fibre disarray) (116). Previous studies have demonstrated higher T1 values in the RV of patients with PAH (117), however to our knowledge no study has looked at the relationship between interstitial myocardial changes in PAH and myocardial ischaemia. Furthermore, in a recent small proof of concept study, we have demonstrated the feasibility of OS-CMR technique in detecting myocardial oxygenation abnormalities in the RV of 20 patients with PAH (118). However, the sample size was too small to look at the relationship between myocardial oxygenation and functional or haemodynamic indices. Hence the aim of the present study was to assess the prevalence of RV myocardial ischaemia and its relationship with changes in the myocardial interstitium of patients with known PAH and with non-obstructive coronaries using OS-CMR and T1 mapping.

## **4.3 Methods**

### **4.3.1 Ethics**

This study was approved by the Southern Adelaide Clinical Human Research Ethics Committee (HREC/15/SAC/397). All participants provided written informed consent to participate in the study.

### **4.3.2 Participant Selection**

As per 3.2.2. Inclusion criteria included right heart catheter (RHC) proven PAH (defined as pulmonary capillary wedge pressure (PCWP)  $\leq 15$  mmHg, and mean pulmonary artery pressure (mPAP)  $\geq 25$  mmHg). Exclusion criteria included severe RV dysfunction on echocardiography (determined by tricuspid annular plane systolic excursion  $< 1.7$ ), echocardiographic LV ejection fraction  $< 50\%$  and/or coronary artery disease (defined as  $> 70\%$  luminal stenosis in an epicardial coronary artery at angiography or prior myocardial infarction) as well as contraindications to CMR and/or adenosine (second or third degree heart block, obstructive pulmonary disease or dipyridamole use). Eleven healthy volunteers also underwent the same imaging procedures to act as a control group. The healthy volunteers had no known cardiac/respiratory disease or symptoms and were free of any cardiac risk factors, including hypertension, smoking and diabetes.

### **4.3.3 Participant preparation**

As per section 2.1.2.

### **4.3.4 CMR protocol**

The CMR protocol was performed as outlined in sections 2.2.1, 2.2.2, 2.2.3 and 2.2.4.

#### **4.3.5 CMR analysis**

The CMR analysis was performed as outlined in sections 2.3.1, 2.3.2 and 2.3.3.

#### **4.3.6 Statistical analysis**

All analyses were performed using the Stata statistical software version 15.1 (StataCorp., USA). Categorical data are described using frequencies and percentages and continuous data using median and range. Differences between groups in the mean change in myocardial oxygenation response and native T1-values were assessed using Mann-Whitney test. Changes in these same outcomes within patient groups were assessed using the Sign-rank test. Reproducibility of measurements for inter and intra-observers was assessed by using the coefficient of variation and by assessing the absolute and proportional bias. Absolute bias was assessed using a t-test of the differences in the 2 measures versus zero and proportional bias by regressing the differences in the 2 measures on the mean for the 2 measurements. Associations between test parameters were assessed using the Spearman's rho ( $\rho$ ) correlation coefficient. A 2-sided Type 1 error rate of  $\alpha=0.05$  was used for assessing statistical significance.

## **4.4 Results**

### **4.4.1 Participant Characteristics**

The subject characteristics are summarised in Table 4.1. Both PAH and control groups were well matched for age and gender. The aetiology within PAH were idiopathic pulmonary artery hypertension (iPAH) (n = 20, 48%), systemic sclerosis associated PAH (SScPAH) (n = 17, 40%) and chronic thromboembolic PAH (CTEPH) (n = 5, 12%). All patients had RHC and coronary angiogram proven diagnosis of PAH with a median (range) mPAP of 33 (16 – 67) mmHg and PCWP of 12 (4 – 15) mmHg. Median duration between RHC with coronary angiogram and CMR research study was 17 months. The median 6 minute walk distance in the patient group was 384 (100 – 600) meters. World Health Organisation functional class was between class II (n = 27, 64%) and III (n = 15, 36%). The PAH patients had an echocardiography-estimated resting systolic pulmonary artery pressure of 41 (27 – 128) mmHg. Furthermore, on echocardiography 8 patients (19%) had mild RV dilatation and 5 patients (12%) had moderate RV dilation. All PAH patients were receiving treatment with pulmonary vasodilators such as Bosentan, Macitentan, Sildenafil, Riociguat or a combination of Macitentan and Sildenafil. At recruitment the PAH patients were stable, and the pulmonary vasodilators therapy was not ceased prior to the CMR research scan.

**Table 4.1: Patient demographics and baseline clinical data**

<b>Variables</b>	<b>PAH (n = 42)</b>	<b>Control (n = 11)</b>	<b>p-value</b>
Age (years), median (range)	71 (63 – 79)	66 (60 – 69)	0.123
Females sex, n (%)	27 (68%)	4 (36%)	0.061
Comorbidities			
• Hypertension, n (%)	22 (52%)	0	
• Diabetes, n (%)	7 (17%)	0	
• Dyslipidaemia	13 (31%)	0	
• Chronic Obstructive Airways Disease, n (%)	10 (24%)	0	
• Obstructive Sleep Apnoea, n (%)	11 (26%)	0	
• Atrial Fibrillation, n (%)	8 (19%)	0	
Right heart catheter haemodynamic indices			
• Mean pulmonary artery pressures (mmHg), median (range)	33 (16 – 57)	0	
• Pulmonary artery wedge pressure (mmHg ), median (range)	12 (4 – 15)	0	
• Mean right atrial pressures (mmHg ), median (range)	12 (2 – 18)	0	
• Cardiac index (L/min/m <sup>2</sup> ), median (range)	3 (2 – 4)	0	
• Pulmonary vascular resistance index (Woods unit m <sup>2</sup> ), median (range)	7 (3 – 28)	0	
Medication			
• Aspirin, n (%)	6 (14%)	0	
• Beta-blockers, n (%)	10 (24%)	0	
• ACEi/ARB, n (%)	12 (29%)	0	
• Statins, n (%)	8 (19%)	0	
• Calcium channel blockers	13 (31%)	0	
• Endothelin receptor blockers, n (%)	34 (81%)	0	
• PDE5 inhibitor, n (%)	18 (43%)	0	
• Soluble guanylate cyclase, n (%)	3 (7%)	0	
• *Combination therapy, n (%)	14 (33%)	0	

\* Combination therapy of a dual therapy comprising of either endothelin receptor blocker,

PDE5 inhibitor or soluble guanylate cyclase

ACEi = angiotensin-converting enzyme inhibitors, ARB = angiotensin II receptor blockers,  
PDE5 = phosphodiesterase type 5 inhibitor

#### 4.4.2 CMR characteristics

Table 4.2 shows a comparison of CMR variables between PAH patients and controls. The only statistically significant difference in CMR volumetric and functional indices between PAH and controls were the RV mass index (17 (9 – 42) vs 13 (9 – 19)g/m<sup>2</sup>, p=0.001), RV Mass/Volume ratio (0.30 (0.22 – 0.49) vs 0.22 (0.15 – 0.25), p<0.001) and inferior RV wall thickness (4 (3 – 9) vs 3 (2 – 5)mm, p=0.002). Table 4.3 demonstrates the CMR variables between the iPAH and SSc-PAH subgroups. The inferior RV wall thickness was measured on the short axis cine slice location similar to the mid ventricular slice location chosen for the OS imaging.

**Table 4.2 : CMR Ventricular Function**

<b>Variables</b>	<b>PAH (n = 42)</b>	<b>Control (n = 11)</b>	<b>p-value</b>
LVEF (%), median (range)	70 (46 – 86)	69 (51 – 75)	0.875
LV EDVi (ml/m <sup>2</sup> ), median (range)	70 (44 – 112)	65 (45 – 81)	0.302
LV ESVi (ml/m <sup>2</sup> ), median (range)	21 (7 – 52)	20 (13 – 28)	0.645
LV ED Mass Index (g/m <sup>2</sup> ), median (range)	51 (36 – 72)	48 (39 – 68)	0.280
LV SV Index (ml/m <sup>2</sup> ), median (range)	46 (32 – 71)	45 (29 – 58)	0.428
RVEF (%), median (range)	61 (45 – 79)	63 (50 – 79)	0.304
RV EDVi (ml/m <sup>2</sup> ), median (range)	60 (30 – 111)	60 (47 – 89)	0.972
RV ESVi (ml/m <sup>2</sup> ), median (range)	22 (12 – 61)	22 (10 – 41)	0.823
RV SV Index (ml/m <sup>2</sup> ), median (range)	37 (15 – 60)	38 (27 – 54)	0.595
RV ED Mass Index (g/m <sup>2</sup> ), median (range)	17 (9 – 42)	13 (9 – 19)	0.001
RV (ED) Mass/Volume ratio, median (range)	0.30 (0.22 – 0.49)	0.22 (0.15 – 0.25)	<0.001
RV inferior wall thickness (mm), median (range)	4 (3 – 9)	3 (2 – 5)	0.002

CMR = cardiovascular magnetic resonance, LV = left ventricle, RV = right ventricle, EF = ejection fraction, EDVi = end-diastolic volume index, ESVi = end-systolic volume index, ED = end-diastolic, SV = stroke volume

**Table 4.3 : CMR Ventricular Function between iPAH and SSc-PAH subgroups**

<b>Variables</b>	<b>iPAH (n = 20)</b>	<b>SSc-PAH (n = 17)</b>	<b>p-value</b>
LVEF (%), median (range)	70 (46 – 86)	70 (54 – 81)	0.715
LV EDVi (ml/m <sup>2</sup> ), median (range)	71 (44 – 94)	70 (54 – 112)	0.408
LV ESVi (ml/m <sup>2</sup> ), median (range)	19 (7 – 44)	23 (10 – 52)	0.805
LV ED Mass Index (g/m <sup>2</sup> ), median (range)	52 (36 – 72)	51 (44 – 68)	0.858
LV SV Index (ml/m <sup>2</sup> ), median (range)	45 (34 – 58)	49 (32 – 71)	0.080
RVEF (%), median (range)	58 (49 – 79)	63 (45 – 73)	0.518
RV EDVi (ml/m <sup>2</sup> ), median (range)	59 (30 – 102)	60 (42 – 111)	0.502
RV ESVi (ml/m <sup>2</sup> ), median (range)	22 (13 – 49)	20 (12 – 61)	0.939
RV SV Index (ml/m <sup>2</sup> ), median (range)	34 (15 – 60)	39 (27 – 54)	0.394
RV ED Mass Index (g/m <sup>2</sup> ), median (range)	17 (9 – 27)	17 (14 – 42)	0.860
RV (ED) Mass/Volume ratio, median (range)	0.30 (0.22 – 0.49)	0.29 (0.23 – 0.41)	0.758
RV inferior wall thickness (mm), median (range)	4 (3 – 7)	4 (3 – 8)	0.262

CMR = cardiovascular magnetic resonance, LV = left ventricle, RV = right ventricle, EF = ejection fraction, EDVi = end-diastolic volume index, ESVi = end-systolic volume index, ED = end-diastolic, SV = stroke volume

#### **4.4.3 Myocardial Oxygenation Response (OS-CMR) in PAH patients**

Of the total 42 PAH patients recruited, 40 (95%) patients and all the healthy controls completed the OS-CMR study protocol. The mean RV  $\Delta$ OS-CMR SI change in the inferior RV segments was significantly lower in PAH group compared to the controls (9.5 (-7.4 – 42.8) vs 12.5 (9 – 24.6)%,  $p=0.02$ ) (Figure 4.1A). The global LV  $\Delta$ OS-CMR SI change was also significantly lower in PAH group compared to the controls (11.0 (-2.7 – 33.2) vs 21.0 (2.5 – 35.7)%,  $p=0.004$ ) (Figure 4.1B). The  $\Delta$ OS-CMR SI in the inferior RV wall of PAH patients was comparable to both the LV septal wall (9.5 (-7.4 – 42.8) vs 11.3 (-2.8 – 36.5)%,  $p=0.32$ ) and LV lateral wall (9.5 (-7.4 – 42.8) vs 11.5 (-9.2 – 31.8)%,  $p=0.57$ ) of PAH patients.

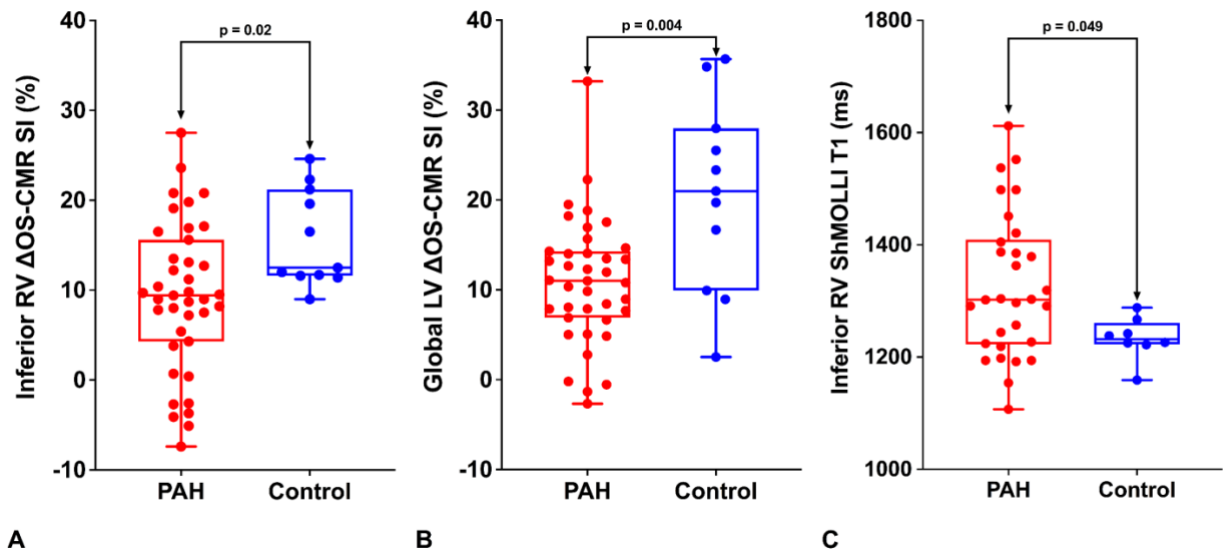


**Figure 4.1: Distribution of inferior RV  $\Delta$ OS-CMR SI, global LV  $\Delta$ OS-CMR SI and inferior RV T1-mapping for PAH and control group.**

#### **4.4.4 Right Ventricular Native T1-values in PAH patients**

Good quality and analysable RV T1 maps were obtained from 71% (30/42) PAH patients and 73% (8/11) of controls. Reasons for excluding T1 maps were image artefacts and partial volume effects. Compared to controls, patients with PAH had higher native ShMOLLI T1 values in the inferior RV wall: 1303 (1107 – 1612) vs 1232 (1159 – 1288)ms,  $p=0.049$  (Figure 3C). The LV T1-values for the control were within previously published ranges: 1151 (1106 – 1227)ms (96). In PAH patients, the native ShMOLLI T1 values in the inferior RV wall was comparable to both the LV septal (1303 (1107 – 1612) vs 1332 (1169 – 1492)ms,  $p=0.71$ ) and LV lateral wall (1303 (1107 – 1612) vs 1301 (1102 – 1500)ms,  $p=0.85$ ) of PAH patients. The inter-observer absolute bias was 2.0, 95% confidence interval (CI) (-4.95, 8.95),  $p=0.53$  and the relative bias was -0.05, 95% CI (-0.19, 0.84),  $p=0.41$ . The intra-observer absolute bias was 9.1, 95% confidence interval (CI) (-39.12, 57.32),  $p=0.68$  and the relative bias was 0.48, 95% CI (-0.28, 1.23),  $p=0.18$ .

#### **4.4.5 Comparing RV myocardial oxygenation and RV T1 values between iPAH and SScPAH**

The RV  $\Delta$ OS-CMR SI between the iPAH ( $n = 20$ ) and SScPAH ( $n = 17$ ) patients was 9.4 (-5.1 – 23.6) vs 9.0 (-7.4- 42.8)%,  $p=0.88$  (Figure 4.2A). The ShMOLLI T1 values in inferior RV wall between the iPAH ( $n = 14$ ) and SScPAH ( $n = 14$ ) patients were significantly different: 1242 (1107 – 1612) vs 1386 (1219 – 1552)ms,  $p=0.007$  (Figure 4.2B). Among the 5 CTEPH patients, 2/5 (40%) did not complete the OS-CMR protocol and 3/5 (60%) had poor quality RV T1-maps, hence no comparison was made in this group.

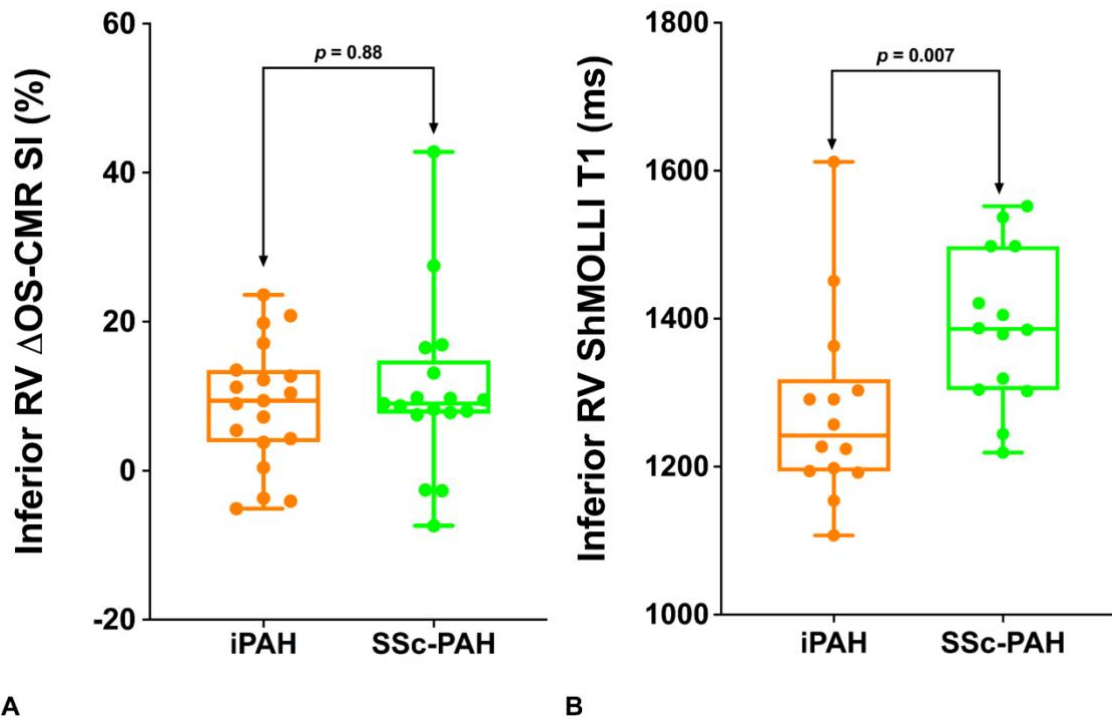


**Figure 4.2: Distribution of inferior RV  $\Delta$ OS-CMR SI and RV T1-mapping for iPAH and SSc-PAH.**

#### **4.4.6 Correlations between RV myocardial oxygenation, RV T1 values, CMR RV volumetric/functional and RHC haemodynamic indices**

There was a moderate-good correlation between the inferior RV  $\Delta$ OS-CMR SI and the global LV  $\Delta$ OS-CMR SI ( $r=0.7$ ,  $p<0.001$ ) (Figure 4.3A). Compared with the CMR volumetric/functional and haemodynamic indices, the inferior RV  $\Delta$ OS-CMR SI had a moderate-good inverse correlation to RV inferior wall thickness ( $r=-0.7$ ,  $p<0.001$ ) (Figure 4.3B) and moderate inverse correlation to RHC mPAP ( $r=-0.4$ ,  $p=0.02$ ) (Figure 4.3C). This suggests that increased RV hypertrophy is associated with increased myocardial deoxygenation. However, compared to ShMOLLI T1 values, there was no correlation between RV  $\Delta$ OS-CMR SI and RV ShMOLLI T1 values ( $r=0.02$ ,  $p=0.91$ ) (Figure 4.3D). Furthermore, no correlation between RV  $\Delta$ OS-CMR SI and RV ShMOLLI T1 values was demonstrated in iPAH and SScPAH subgroups. RV ShMOLLI T1 had a moderate inverse correlation to RV Mass/Volume ratio ( $r=-0.41$ ,  $p=0.036$ ). However, there was no other significant correlation between RV ShMOLLI T1 values and CMR volumetric/functional or haemodynamic indices.

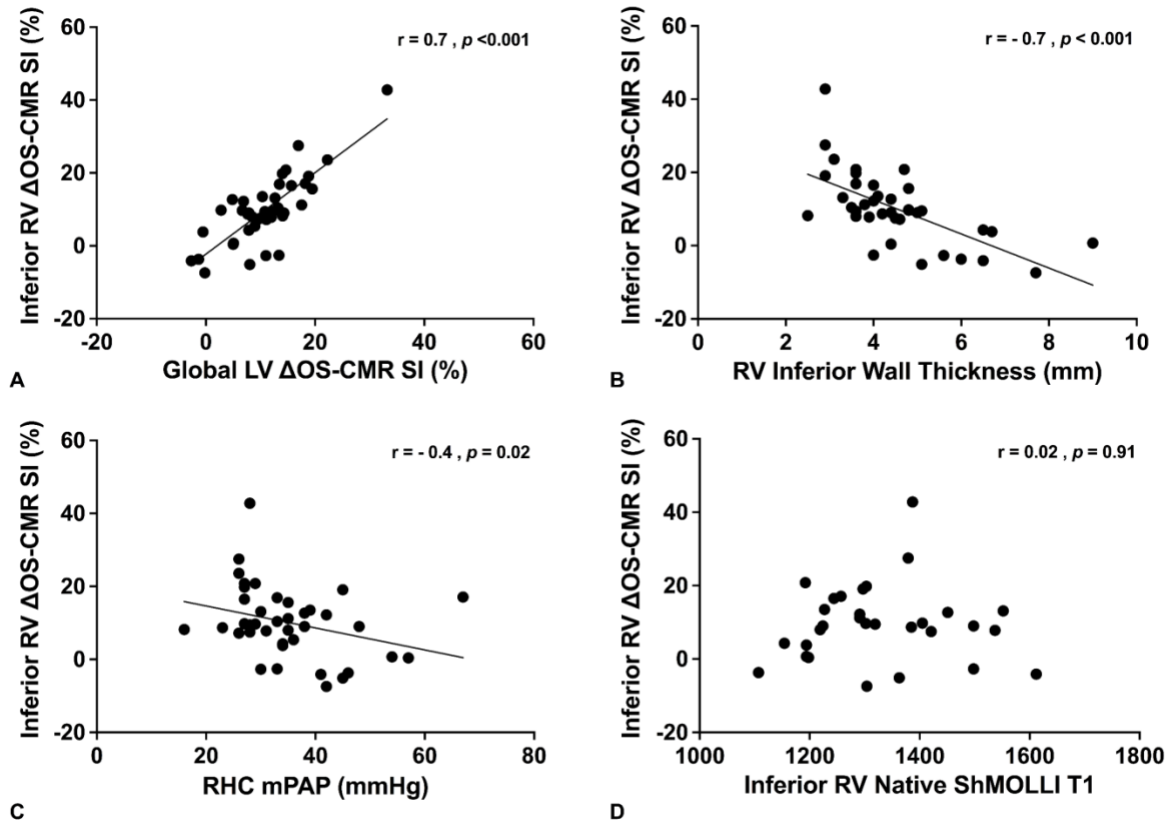


**Figure 4.3: Correlation between inferior RV  $\Delta$ OS-CMR SI to global LV  $\Delta$ OS-CMR SI, CMR volumetric/ functional indices, hemodynamic indices and inferior RV T1-mapping.**

## **4.5 Discussion**

The principal finding from this study is that myocardial oxygenation response to adenosine stress is blunted in patients with PAH compared to healthy controls. The blunted oxygenation response was demonstrated in PAH patients who were stable on pulmonary vasodilator therapy and at an adaptive stage of PAH with non-obstructive epicardial coronaries, and was correlated inversely with RV wall thickness and RHC mPAP. Although we had demonstrated changes to the myocardial interstitium, no clear interaction with myocardial oxygenation was noted. These findings highlight the potential contribution of myocardial ischemia to the pathophysiology of RV dysfunction in PAH, and could subsequently lead to new potential treatment targets, in such patients.

### **4.5.1 Right ventricular myocardial deoxygenation in PAH**

In PAH, RV myocardial ischemia is acknowledged to be a significant contributor to adverse remodelling and progressive RV dysfunction (32). Reduced right coronary perfusion pressure (49) and microvascular ischemia leads to progressive RV dysfunction causing RV failure and death. Abnormal pressure gradient between the aorta and the RV due to escalating pulmonary vascular resistance, reduces myocardial blood flow in the right ventricular branch of the right coronary artery causing ischemia (37, 119). RV myocardial ischemia is further exacerbated by inadequate compensatory increase in the myocardial vasculature owing to progressive RV hypertrophy (RVH) (35-37). Occlusive microvascular damage and impairment in angiogenesis (known as capillary rarefaction) has been demonstrated in animal models and SScPAH, is thought to cause microvascular ischemia (33, 38). Furthermore, a recent study by Meloche *et al.* proposes common pathobiology mechanisms between PAH pulmonary vasculature and coronary arteries (52). These pathobiology mechanisms trigger coronary vascular remodeling in both the LV and RV leading to microvascular ischemia.

In this study, we have demonstrated a blunted myocardial oxygenation response to vasodilator stress in the inferior RV segment on PAH patients. Specifically our study demonstrates the presence of in-vivo myocardial deoxygenation in the adaptive stage of PAH. The findings of in-vivo RV myocardial deoxygenation in PAH are novel because abnormalities in myocardial blood flow or microvascular dysfunction may not necessarily lead to myocardial deoxygenation (111). Arnold *et al.* had demonstrated that in coronary artery disease, 50% of hypoperfused segments on quantitative myocardial perfusion demonstrate no evidence of deoxygenation (111). Furthermore in dilated cardiomyopathy, Dass *et al.* had demonstrated disassociation between microvascular dysfunction and oxygenation (120). Although we had not performed any direct comparison between myocardial blood flow and myocardial oxygenation, these findings provide further mechanistic insight into pathophysiology of myocardial ischemia in the RV in PAH.

The OS-CMR SI changes in the RV had good correlation with global OS-CMR SI changes seen in the LV, an area of myocardium in which there is good validation with the OS-CMR technique. In our study, the OS-CMR technique has demonstrated significant changes in the inferior RV segment. Thinned myocardium (causing partial volume effects), off-resonance artefacts and image artefacts are known limitations of the OS-CMR technique in the RV (118). However, these limitations have previously been known to affect the accuracy of OS-CMR SI in LV myocardium (114). Consistent voxel-size was applied during OS-CMR imaging, hence the measured inferior RV wall thickness provided sufficient coverage to avert partial volume effects. Additionally, it has been shown that the inferior RV segment has the greatest end-diastolic wall thickness once the afterload, serum biomarkers and RV structural adaptation in pre- and post-capillary pulmonary hypertension have been taken into consideration (121).

Furthermore, our study has demonstrated a moderate inverse correlation between RV OS-CMR SI and mPAP. The moderate correlation highlights that there are other pathophysiological factors (such as microvascular ischemia) that affect the RV besides elevated mPAP. Patients with microvascular ischemia often present with typical effort-induced angina, but also with atypical symptoms such as dyspnea on exertion (122). Exertional limitation is the dominant symptom in PAH, however it is contributed by many factors such as respiratory mechanics/ventilation, cardiovascular response and psychological/emotional aspects (123). Even though RHC resting hemodynamic measures such as mPAP and cardiac output correlate with severity of symptoms, there are considerable inter-individual variability that is not explained by RHC hemodynamic severity (124). The findings of myocardial deoxygenation provide further mechanistic insights into the pathophysiology of myocardial ischaemia in PAH population.

#### **4.5.2 Native T1-values in the right ventricle**

In PAH, the RV adaptation extends to the cardiomyocytes and interstitium altering the cardiac structure and function (31). Although the initial adaptive changes of myocardial collagen accumulation serve as a favorable response helping the RV withstand higher pressures, over time maladaptive alteration ensues leading to fibrosis and progressive RV dysfunction (22). Native CMR T1 parametric mapping has been used as a surrogate for diffuse interstitial fibrosis in the absence of an alternative cause of interstitial expansion (oedema, infiltrations/fibre disarray) (116). Previous studies of RV T1 mapping in PAH using Modified Look-Locker Inversion recovery (MOLLI) sequence has produced varying results (68, 69, 117). One possible explanation is that each of these studies have adapted an altered version of the MOLLI sequence thus producing differing results. Utilising the ShMOLLI sequence, our study demonstrated increased native T1-values in the inferior RV wall compared to controls. The

native T1-values in the inferior RV wall were comparable to the LV septum and LV free wall in PAH patients, similar to the findings previously demonstrated by Spruijt *et al* (69). Unexpectedly in our study, we found that the RV native T1-values did not correlate with inferior RV OS-CMR SI changes. This is pertinent in PAH as the pressure overload leads to disruption of the healthy extracellular matrix in the RV due to the excess collagen formation and myocardial interstitial fibrosis. Changes in RV extracellular matrix could potentially disrupt the coronary microvasculature and hence myocardial oxygen supply. However, the lack of association between RV T1-values and RV OS-CMR SI in our study suggests that the changes in RV extracellular matrix does not directly impact myocardial oxygenation.

Interestingly our study is the first to have demonstrated a significant difference in the native T1-values between the iPAH and SScPAH. We have used the ShMOLLI sequence in contrast to other studies that have used the MOLLI sequence (69, 117, 125). The ShMOLLI sequence is heart rate independent (90) and as such is able to estimate long T1s which is important for assessing oedematous tissue (126). Previous ShMOLLI T1 mapping studies of the LV in systemic sclerosis patients suggested the presence of interstitial fibrosis and low-grade inflammation (127). Therefore, the higher T1-value SScPAH seen in our study could signify a combination of diffuse interstitial fibrosis and myocardial inflammation, a theory that fits with the pathophysiology of systemic sclerosis.

### 4.5.3 Study Limitations

Our study only performed a single mid-ventricular slice on OS-CMR imaging rather than the entire ventricle hence there was incomplete coverage of the full RV myocardium. This is unlikely to be of major relevance in RV assessment of PAH which is a global process. While our study had demonstrated in-vivo myocardial deoxygenation in the RV of PAH, we had not performed any direct comparison with myocardial blood flow, an area for future studies. Late-gadolinium enhancement or extracellular volume assessment was not performed due to concerns of patient safety and tolerability during CMR research scan. While OS-CMR sequence has been studied in many conditions (79), to our knowledge it has not been studied in PAH. The multiple breath-hold during rest/stress OS-CMR image acquisitions could potentially be challenging for PAH patients as dyspnoea is a common symptom in this cohort of patients. The numbers in the control groups were relatively small especially with female controls, compared to the PAH group. However the control group were age-matched, minimizing any significant bias. This is important, especially in T1-values whereby age is known to influence native myocardial T1-values (90). Measuring RV T1 on a curved RV myocardium can be challenging. RV T1 mapping with ShMOLLI sequence at 8mm slice thickness can be a potential substrate for partial volume effects affecting T1-values. However, every effort was taken to ensure the ROI was drawn in the myocardium. Furthermore the adequate reproducibility and the comparable RV T1-values to the LV T1-values in PAH patients suggest accurate interpretation of RV T1. Although this study was prospective, the PAH patients were stable on pulmonary vasodilator therapy, this could have mitigated against the finding of RV ischemia. A larger study would help to determine the clinical and prognostic utility of these novel CMR techniques in PAH.

#### **4.6 Conclusion**

Blunted OS-CMR SI suggest the presence of in-vivo microvascular dysfunction in the RV of PAH patients. Future studies would be essential to determine the utility of OS-CMR of the RV in predicting progressive RV dysfunction and mortality.

## **Chapter 5 : Left Ventricular Ischemia in pre-capillary Pulmonary Hypertension: A Cardiovascular Magnetic Resonance Study**

This chapter describes the presence and extent of LV myocardial ischemia in patients with pulmonary hypertension and absent epicardial coronary artery disease.

## 5.1 Introduction

Pulmonary arterial hypertension (PAH) is a serious and progressive disorder, in which the prognosis is largely dependent on right ventricular (RV) function (12). Recent studies, however, have suggested the presence of left ventricular (LV) dysfunction in PAH patients. Studies from explanted hearts of PAH patients, for example, have demonstrated atrophy and severe contractility impairment of the LV cardiomyocyte (47). The potential contribution of left ventricular (LV) ischemia, to progressive LV dysfunction has not been systematically studied in PAH.

Oxygen-sensitive (OS) cardiovascular magnetic resonance (CMR), also known as blood oxygen level-dependent (BOLD) CMR imaging, enables the *in vivo* assessment of myocardial oxygenation at the tissue level. The utility of this technique is underpinned by the natural paramagnetic properties of hemoglobin (70). Following vasodilator stress, healthy vessels dilate sufficiently to increase myocardial oxygenation creating a BOLD- effect, leading to signal intensity (SI) changes in OS-CMR sequence. In segments subtended by healthy vessels there is relative reduction deoxyhemoglobin concentration, leading to a rise in SI. Conversely a mismatch in oxygen supply and demand causes to a relative accumulation of deoxyhemoglobin which would blunt the SI changes. The OS-CMR sequence has been validated by direct measurement of myocardial oxygenation in various conditions involving the left ventricle (LV) (79). In addition to OS-CMR, CMR stress/rest T1 mapping has emerged as a novel promising technique to distinguish normal, ischemic and infarcted myocardium in patients with coronary artery disease (CAD) (89). This technique measures changes in T1-values between native (rest) T1 mapping and vasodilator induced native (stress) T1 mapping. CMR T1 mapping is highly sensitive to changes in myocardial water content, including myocardial blood volume (MBV) (82, 90). Vasodilator stress induction causes coronary

vasodilatation which leads to changes to myocardial water (82) and MBV (91, 92); hence altering T1-values which will enable assessment of microvascular and MBV changes during ischemia (93). Stress/rest T1 mapping is validated to distinguish between epicardial and microvascular CAD (94-96, 128).

While epicardial coronary artery disease is the most common cause of myocardial ischemia, studies have demonstrated that coronary microvascular dysfunction (CMD) leads to reduced quality of life and carries an adverse long-term prognosis (129, 130). To date, no study has used these emerging CMR techniques to advance the understanding of myocardial ischemia and/or oxygenation in the left ventricle of pre-capillary PH patients. This could potentially provide novel mechanistic insights into the pathophysiology of the complex PH clinical syndrome and subsequently lead to potential new treatment pathways. Hence, the present study sought to assess the presence and extent of LV myocardial ischemia in patients with known pre-capillary PH and absent epicardial coronary artery disease, using OS-CMR and stress/rest T1 mapping. We present the following article in accordance with the STROBE reporting checklist.

## **5.2 Methods**

### **5.2.1 Ethics**

This study was approved by the Southern Adelaide Clinical Human Research Ethics Committee (HREC/15/SAC/397). All participants provided written informed consent to participate in the study.

### **5.2.2 Participant Selection**

Participant selection was performed as per section 3.2.2. The inclusion criteria were right heart catheter-proven pre-capillary PH (defined as mean pulmonary artery pressure (mPAP)  $\geq 25$ mmHg and pulmonary artery wedge pressure (PAWP)  $< 15$ mmHg). Exclusion criteria included severe RV dysfunction on echocardiography (determined by tricuspid annular plane systolic excursion), echocardiographic LV ejection fraction  $< 50\%$  and/or coronary artery disease (defined as  $> 70\%$  luminal stenosis in an epicardial coronary artery at angiography or prior myocardial infarction) as well as contraindications to CMR and/or adenosine (second or third-degree heart block, obstructive pulmonary disease or dipyridamole use). Eight patients with known CAD (CAD controls) on coronary angiogram were recruited into the study in order to characterize the OS-CMR and T1 reactivity values in their ischemic myocardial segments for comparison with the values in the myocardium of patients with PH. The ischemic myocardial segments in the CAD controls were segments that were subtended with significant coronary stenosis. Eleven healthy volunteers (normal controls) with no known cardiac or respiratory disease or symptoms and no cardiac risk factors, including hypertension, smoking and diabetes, were invited to participate as controls.

### **5.2.3 Participant preparation**

As per section 2.1.2

### **5.2.4 CMR protocol**

The CMR protocol was performed as outlined in sections 2.2.1, 2.2.2, 2.2.3 and 2.2.4.

### **5.2.5 CMR analysis**

The CMR analysis was performed as outlined in sections 2.3.1, 2.3.2 and 2.3.3.

### **5.2.6 Statistical analysis**

All analyses were performed using the Stata statistical software version 15.1 (StataCorp., USA). Categorical data are described using frequencies and percentages and continuous data using mean and standard deviation. Differences between groups in mean resting T1, the mean changes in T1 and the mean changes in myocardial oxygenation response were assessed using independent t-tests. Group comparisons were made using ANOVA with post-hoc Dunnett's test used for multiple group corrections. Changes in these same outcomes within patient groups were assessed using paired t-tests. The overall association between OS-CMR and T1 reactivity was assessed using a mixed effects model to account for non-independence of observations due to multiple measures from different segments. We included a random intercept for the subject as well as a fixed effect for the segment. Separate associations between OS-CMR and T1 reactivity for each segment were assessed using the Pearson r correlation coefficient. A 2-sided Type 1 error rate of  $\alpha=0.05$  was used for assessing statistical significance.

## **5.3 Results**

### **5.3.1 Participant Characteristics**

The subject characteristics are summarized in Tables 5.1 and 5.2. Among the PH patients, 11 (39%) had idiopathic pulmonary artery hypertension (iPAH), 13 (46%) patients had systemic sclerosis-associated PAH (SSc-PAH), and 4 (14%) patients had chronic thromboembolic PH (CTEPH). Average mPAP was  $34 \pm 7$  mmHg and the average mean PAWP was  $12 \pm 3$  mmHg. The mean interval between right heart catheter with coronary angiogram and the CMR research study was 2 years. The mean 6-minute walk distance was  $392 \pm 114$  meters. On echocardiography, 9 (36%) patients had RV dilatation with an echocardiography-estimated resting systolic pulmonary artery pressure of  $52 \pm 25$  mmHg. All PH patients were treated with pulmonary vasodilators such as bosentan, macitentan, sildenafil, riociguat with 14 (50%) on combination therapy. The PH patients were stable and continued their pulmonary vasodilator therapy during the CMR research scan.

**Table 5.1: Patient demographics and baseline clinical data**

Variables	PH (n = 28)	CAD (n=8)	Control (n = 11)	p-value
Age, mean $\pm$ SD (years)	69 $\pm$ 10	70 $\pm$ 9	64 $\pm$ 7	0.217 <sup>§</sup>
Females sex, n (%)	19 (68%)	4 (50%)	4 (36%)	0.291 <sup>‡</sup>
Comorbidities				
• Hypertension, n (%)	15 (54%)	7 (87.5%)	0	
• Diabetes, n (%)	4 (14%)	8 (100%)	0	
• Dyslipidaemia	8 (29%)	2 (25%)	0	
• Chronic Obstructive Airways Disease, n (%)	9 (32%)	0	0	
• Obstructive Sleep Apnoea, n (%)	5 (18%)	0	0	
• Atrial Fibrillation, n (%)	6 (21%)	0	0	
Right heart catheter haemodynamic indices				
• Mean pulmonary artery pressures (mmHg)	34 $\pm$ 7	N/A	N/A	
• Pulmonary artery wedge pressure (mmHg)	12 $\pm$ 3	N/A	N/A	
• Mean right atrial pressures (mmHg)	11 $\pm$ 4	N/A	N/A	
• Cardiac index (L/min/m <sup>2</sup> )	2.8 $\pm$ 0.7	N/A	N/A	
• Pulmonary vascular resistance index (Woods unit m <sup>2</sup> )	8.3 $\pm$ 4.7	N/A	N/A	
Medication				
• Aspirin, n (%)	4 (14%)	7 (88%)	0	
• Beta-blockers, n (%)	9 (32%)	5 (63%)	0	
• ACEi/ARB, n (%)	10 (36%)	3 (38%)	0	
• Statins, n (%)	5 (18%)	8 (100%)	0	
• Calcium channel blockers	11 (39%)	2 (25%)	0	
• Endothelin receptor blockers, n (%)	26 (93%)	0	0	
• PDE5 inhibitor, n (%)	13 (46%)	0	0	
• Soluble guanylate cyclase, n (%)	2 (7%)	0	0	
• *Combination therapy, n (%)	14 (50%)	0	0	

PH = pulmonary hypertension, CAD = coronary artery disease, SD = standard deviation, ACEi = angiotensin-converting enzyme inhibitors, ARB = angiotensin II receptor blockers, PDE5 = phosphodiesterase type 5 inhibitor

\* Combination of either endothelin receptor blocker, PDE5 inhibitor or soluble guanylate cyclase

‡ Chi-square test

§ *p*-value from one-way ANOVA

**Table 5.2: CMR Ventricular Function**

<b>Variables</b>	<b>PH (n = 28)</b>	<b>CAD (n=8)</b>	<b>Control (n = 11)</b>	<b>p-value<sup>s</sup></b>
LV EF (%), mean $\pm$ SD	68 $\pm$ 8	60 $\pm$ 14	68 $\pm$ 6	0.182
LV EDV <sub>i</sub> (ml/m <sup>2</sup> ), mean $\pm$ SD	72 $\pm$ 15	88 $\pm$ 38	64 $\pm$ 11	0.194
LV ESV <sub>i</sub> (ml/m <sup>2</sup> ), mean $\pm$ SD	24 $\pm$ 10	39 $\pm$ 28	20 $\pm$ 4	0.131
LV ED Mass Index (g/m <sup>2</sup> ), mean $\pm$ SD	53 $\pm$ 9	58 $\pm$ 20	51 $\pm$ 9	0.589
LV SV Index (ml/m <sup>2</sup> ), mean $\pm$ SD	48 $\pm$ 9	49 $\pm$ 13	44 $\pm$ 10	0.546
LV CI (l/min/m <sup>2</sup> ), mean $\pm$ SD	3.2 $\pm$ 0.6	3.0 $\pm$ 0.7	2.8 $\pm$ 0.3	0.154
RV EF (%), mean $\pm$ SD	60 $\pm$ 9	74 $\pm$ 5	64 $\pm$ 8	<0.001
RV EDV <sub>i</sub> (ml/m <sup>2</sup> ), mean $\pm$ SD	66 $\pm$ 17	66 $\pm$ 20	63 $\pm$ 13	0.878
RV ESV <sub>i</sub> (ml/m <sup>2</sup> ), mean $\pm$ SD	27 $\pm$ 12	17 $\pm$ 7	23 $\pm$ 8	0.020
RV SV Index (ml/m <sup>2</sup> ), mean $\pm$ SD	39 $\pm$ 8	48 $\pm$ 14	40 $\pm$ 9	0.164

CMR = cardiovascular magnetic resonance, LV = left ventricle, RV = right ventricle, EF = ejection fraction, EDVi = end-diastolic volume index, ESVi = end-systolic volume index, ED = end-diastolic, SV = stroke volume, CI = cardiac index SD = standard deviation

§ *p*-value from one-way ANOVA

### 5.3.2 CMR characteristics

Table 5.2 shows a comparison of CMR variables between PH, CAD and controls. The only statistically significant difference in CMR volumetric and functional indices between PH, CAD and controls was the RVEF ( $p < 0.001$ ) and RV ESVi ( $p = 0.020$ ).

### 5.3.3 LV Myocardial Oxygenation Response (OS-CMR)

All 28 patients completed the OS-CMR study protocol. The mean global LV  $\Delta$ OS-CMR SI change was significantly lower in the PH group compared to the controls ( $11.1 \pm 6.7\%$  vs  $20.5 \pm 10.5\%$ ,  $p=0.016$ ). In contrast, the  $\Delta$ OS-CMR SI changes in the myocardium of the PH patients were comparable to the ischemic segments of CAD patients ( $11.1 \pm 6.7\%$  vs  $10.3 \pm 6.4\%$ ,  $p=0.773$ ) (Figure 5.1). As there is interventricular ‘septal bowing’ (D shaping) in PH we also compared the  $\Delta$ OS-CMR SI in various segments of the LV. We found in PH, the mean global LV  $\Delta$ OS-CMR SI was comparable to mean LV septal  $\Delta$ OS-CMR SI ( $11.1 \pm 6.7\%$  vs  $12.3 \pm 7.6\%$ ,  $p=0.523$ ) and mean LV free-wall  $\Delta$ OS-CMR SI ( $11.1 \pm 6.7\%$  vs  $10.3 \pm 8.2\%$ ,  $p=0.710$ ). In addition, there was comparable mean  $\Delta$ OS-CMR SI changes between LV septal and LV free-wall ( $12.3 \pm 7.6\%$  vs  $10.3 \pm 8.2\%$ ,  $p=0.352$ ) in the PH group.

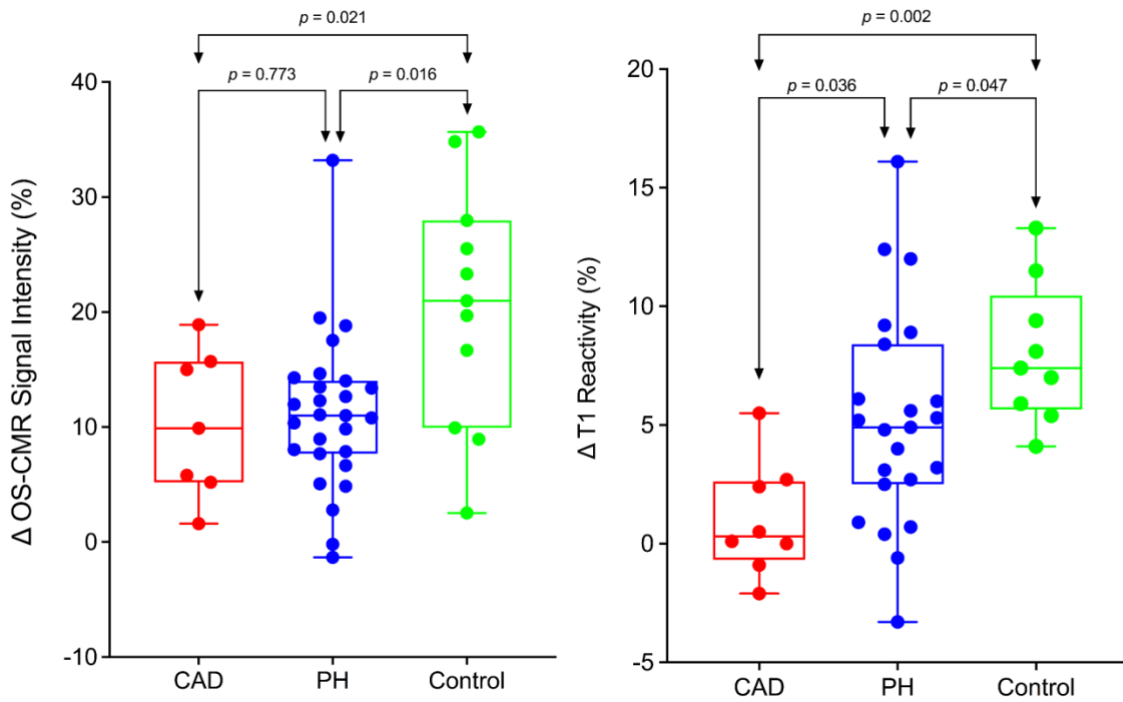


**Figure 5.1: Distribution of vasodilator stress response of OS-CMR and T1 Reactivity in coronary artery disease (CAD), pulmonary hypertension (PH) and control.**

### 5.3.4 Myocardial Stress/Rest T1 Reactivity

Of the total of 28 PH patients who underwent the Stress/Rest T1 CMR protocol, 23 (82%) patients had good quality analyzable T1 maps. Stress/Rest T1 maps were excluded due to the presence of left ventricular outflow tract on the basal T1 map slices at stress in 3 (11%) patients and the remaining 2 (7%) patients had poor T1 maps due to cardiac or respiratory motion. Resting T1-values for the control were within previously published ranges:  $1153 \pm 33$  (96). Compared to controls, patients with PH had higher resting T1-values:  $1247 \pm 74$ ,  $p < 0.0001$ . During vasodilator stress, the T1-values increased significantly in both PH patients (from  $1247 \pm 74$  to  $1311 \pm 83$ ,  $p < 0.0001$ ) and controls (from  $1153 \pm 33$  to  $1245 \pm 38$ ,  $p < 0.0001$ ). However, the global  $\Delta T1$  reactivity was significantly blunted in the PH patients compared to controls ( $5.2 \pm 4.5\%$  vs  $8.0 \pm 2.9\%$ ,  $p = 0.047$ ). The ischemic segments of CAD patients had comparable resting T1 value to controls ( $1197 \pm 78$  vs  $1153 \pm 33$ ,  $p = 0.170$ ) and PH patients ( $1197 \pm 78$  vs  $1247 \pm 74$ ,  $p = 0.138$ ). However, the  $\Delta T1$  reactivity in the ischemic segments of CAD was  $1.1 \pm 4.2\%$  and this is significantly lower when compared to the global  $\Delta T1$  reactivity in PH patients ( $5.2 \pm 4.5\%$ ,  $p = 0.036$ ) and controls ( $8.0 \pm 2.9\%$ ,  $p = 0.002$ ) (Figure 5.1). In PH, the global LV  $\Delta T1$  reactivity was comparable to mean LV septal  $\Delta T1$  reactivity ( $5.2 \pm 4.5\%$  vs  $4.4 \pm 3.7\%$ ,  $p = 0.537$ ) and mean LV free-wall  $\Delta T1$  reactivity ( $5.2 \pm 4.5\%$  vs  $5.8 \pm 4.9\%$ ,  $p = 0.625$ ). In addition, there was no significant difference between mean  $\Delta T1$  reactivity of LV septal and LV free-wall ( $4.4 \pm 3.7\%$  vs  $5.8 \pm 4.9\%$ ,  $p = 0.267$ ).

### 5.3.5 Comparing LV myocardial ischemia in iPAH and SSc-PAH

No significantly different changes in global  $\Delta OS$ -CMR SI or  $\Delta T1$  reactivity were seen between iPAH and SSc-PAH patients. The global LV  $\Delta OS$ -CMR SI in the iPAH (n=11) and SSc-PAH (n=13) patients was  $9.7 \pm 5.1\%$  vs  $11.5 \pm 7.9\%$ ,  $p = 0.516$ . The global  $\Delta T1$  reactivity between

the iPAH (n=9) and SSc-PAH (n=13) patients was  $6.5 \pm 5.3\%$  vs  $4.3 \pm 4.0\%$ ,  $p=0.319$ . The CTEPH patients were not compared due to low patient numbers.

### **5.3.6 Correlations between myocardial oxygenation, $\Delta T1$ reactivity and CMR volumetric/functional and hemodynamic indices in PH patients.**

When the changes in OS-CMR and T1 were averaged, there was a moderate correlation between global  $\Delta OS-CMR$  SI and  $\Delta T1$  reactivity ( $r=0.50$ ,  $p=0.015$ ) (Figure 5.2). However, a stratified segmental analysis between a mid-ventricular  $\Delta OS-CMR$  SI and mid-ventricular  $\Delta T1$  reactivity showed mostly weak associations with Pearson  $r$  correlation coefficients for the 6 segments of  $0.46$  ( $p=0.03$ ),  $0.50$  ( $p=0.02$ ),  $0.54$  ( $p=0.009$ ),  $0.31$  ( $p=0.16$ ),  $0.28$  ( $p=0.20$ ) and  $0.35$  ( $p=0.11$ ) (Figure 5.3). In addition, there was no overall association between mid-ventricular  $\Delta OS-CMR$  SI and mid-ventricular  $\Delta T1$  reactivity when assessed using the mixed effects model ( $\beta=-0.05$ , 95% CI= $-0.32$ ,  $0.22$ ;  $p=0.71$ ). These findings imply that while a blunted global  $\Delta OS-CMR$  SI and  $\Delta T1$  reactivity suggest presence of abnormal myocardial oxygenation and vasodilatory response, there is poor association between blunted myocardial deoxygenation and  $\Delta T1$  reactivity. Compared to CMR volumetric/functional indices  $\Delta OS-CMR$  SI had moderate correlation to CMR RV EDVi ( $r=-0.47$ ,  $p=0.016$ ) and CMR LVEF ( $r=0.41$ ,  $p=0.038$ ).  $\Delta T1$  reactivity had strong correlation to CMR RV EDVi ( $r=-0.73$ ,  $p<0.001$ ) and a moderate correlation to CMR LVEF ( $r=0.48$ ,  $p=0.023$ ). These findings suggest that increased CMR RV EDVi and decreased CMR LVEF are associated with blunted  $\Delta OS-CMR$  SI and  $\Delta T1$  reactivity (Figure 5.4). There was no significant correlation between myocardial oxygenation and  $\Delta T1$  reactivity to RV haemodynamic indices.

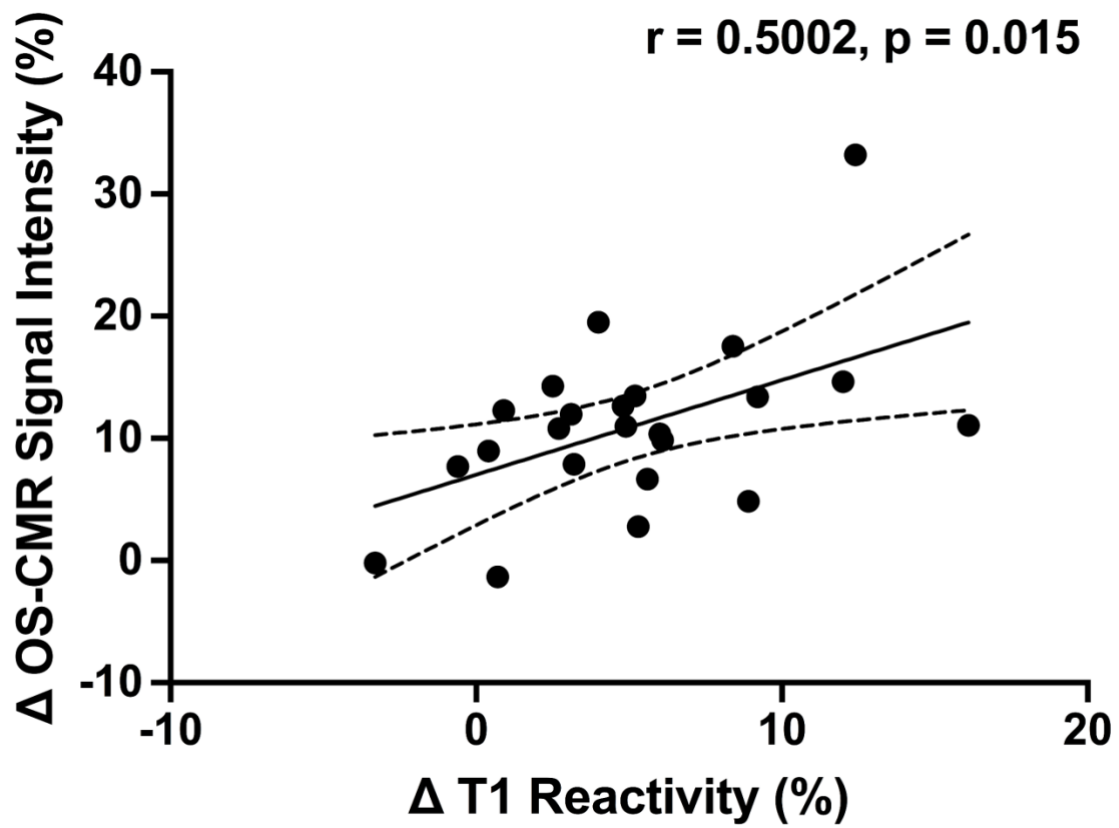
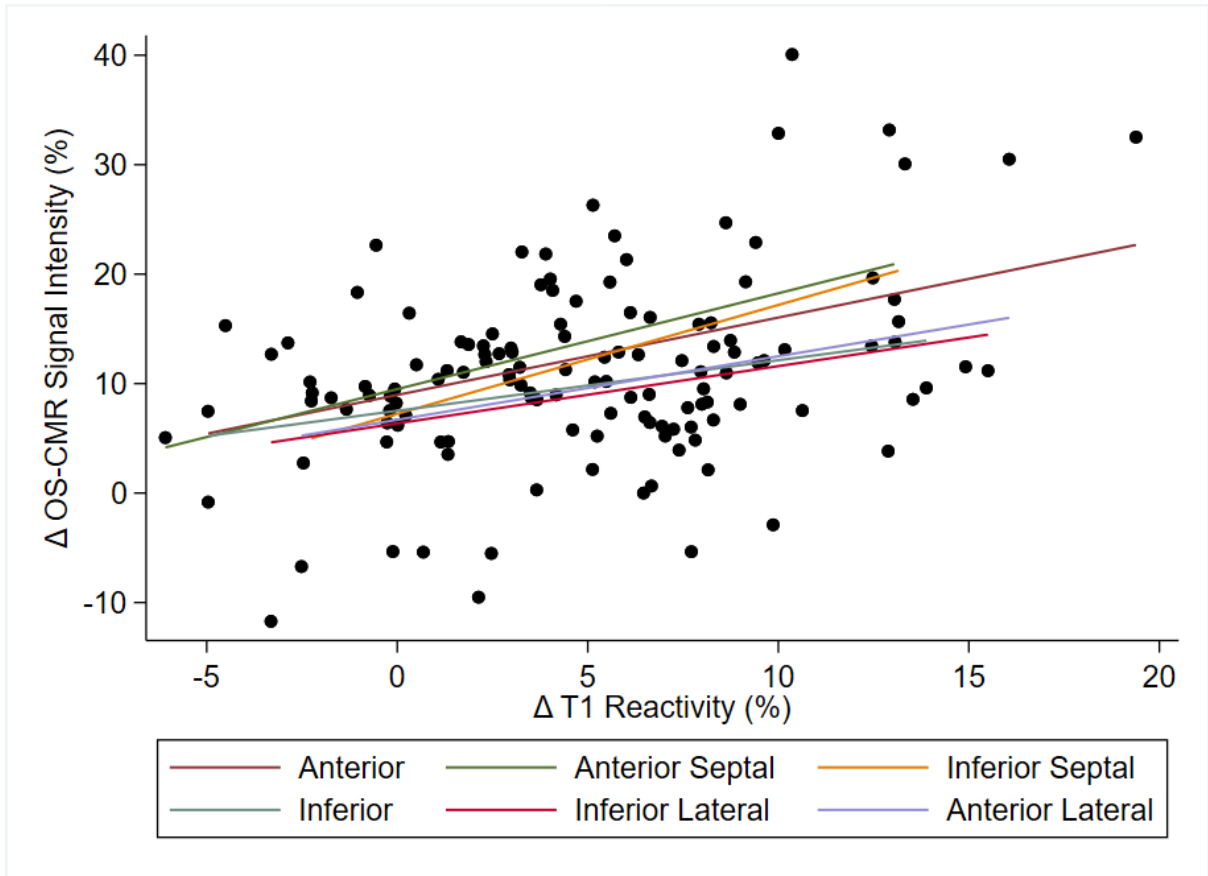
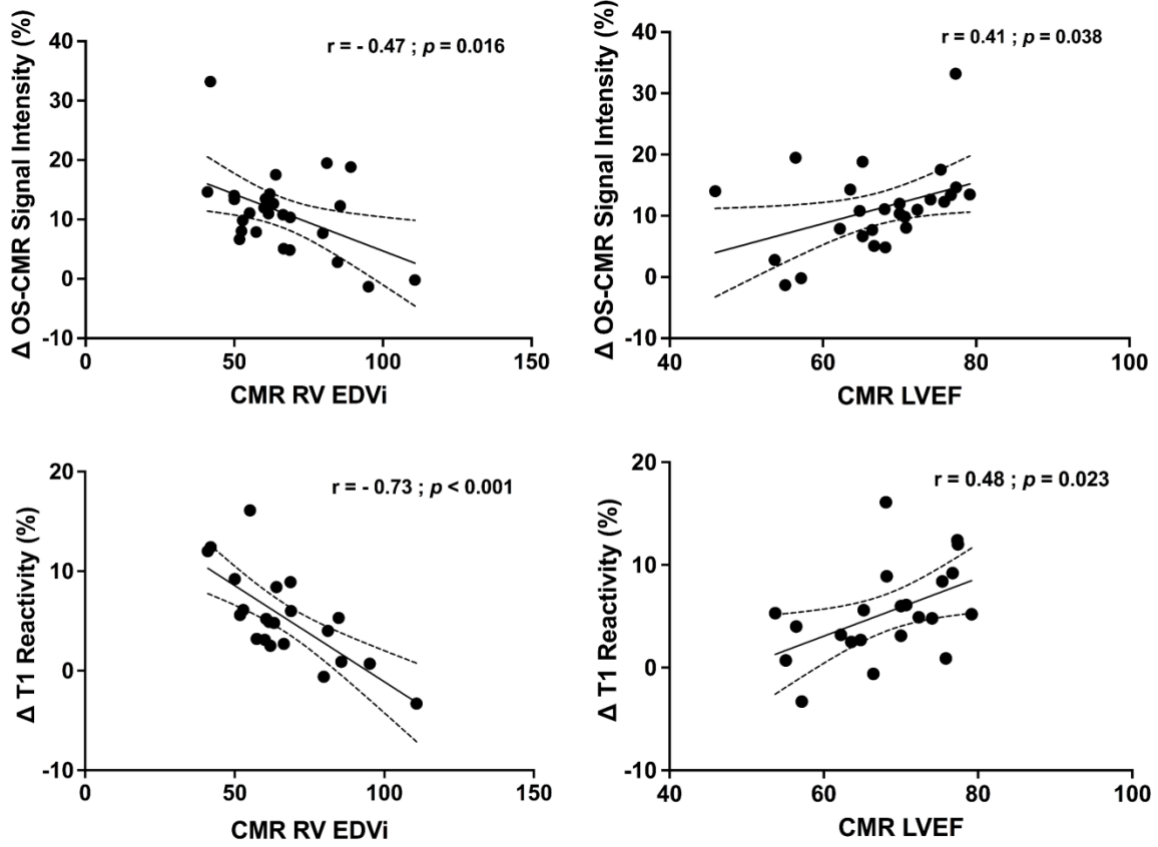


Figure 5.2: Correlation between OS-CMR and T1 Reactivity



**Figure 5.3: Segmental correlation between OS-CMR and T1 Reactivity**



**Figure 5.4: Correlation between OS-CMR, T1 Reactivity and CMR volumetric and functional indices.**

## **5.4 Discussion**

In this study, we have demonstrated the presence of blunted myocardial oxygenation and T1 reactivity in the LV of PH patients. These blunted responses to adenosine stress was demonstrated in PH patients who were stable on pulmonary vasodilator therapy and at an early ‘adaptive’ stage of PH with non-obstructive epicardial coronaries. These data strongly suggest the presence of coronary microvascular dysfunction (CMD). This provides a novel mechanistic understanding into the pathophysiology of LV dysfunction in PH, and could subsequently lead to new potential treatment targets, in such patients.

### **5.4.1 Coronary microvascular disease of the LV in pre-capillary PH**

Several studies have described different pathophysiological causes of LV dysfunction in patients with PAH (42-46, 131). Changes in RV affect the interventricular interaction by leftward septal bowing, which leads to impaired LV diastolic filling (42, 43). Other studies have also demonstrated LV diastolic dysfunction (44, 45) and reduction in LV free wall mass, in association with RV dysfunction, in PAH (46).

It has been recognized that in PAH, RV myocardial ischemia is a precipitant of adverse remodeling and progressive RV dysfunction (32). The gradual remodeling of small distal pulmonary arteries followed by elevated pulmonary vascular resistance, microvascular ischemia and mitochondrial dysfunction culminates in RV failure and death (32). Although LV myocardial ischemia has been described in congenital heart and left heart disease associated post-capillary pulmonary hypertension, there are limited studies in PAH. In SSc-PAH, the LV myocardial perfusion abnormalities have been attributed to decreased coronary flow reserve (48) and CMD (49) related to concurrent SSc involvement of the myocardium. Extrinsic compression of the left main coronary arteries (LMCA) due to a dilated pulmonary artery has

been elegantly described by Galiè *et al.* (50). It is increasingly recognized however, that the microvascular damage seen in the pulmonary vasculature of PAH has links to coronary vascular disease. A recent study by Meloche *et al.* demonstrated that the inflammation and epigenetic readers seen in PAH pulmonary vasculature were also overexpressed in the coronary arteries. The authors suggested that inflammatory and epigenetic readers may trigger coronary vascular remodeling in both the LV and RV leading to CMD and CAD (52). We have now extended these findings by demonstrating that patients with less severe PH, and no obstructive CAD, have a blunted myocardial oxygenation response and stress/rest T1 response to adenosine stress. These findings are consistent with the presence of CMD in pre-capillary PH patients.

#### **5.4.2 Myocardial Oxygenation and T1 Reactivity in response to vasodilator stress**

Elevated resting (native) T1-values with a significant rise in stress T1-values on vasodilator stress in PH has been demonstrated in aortic stenosis (94), chronic kidney disease (96), and primary cardiomyopathies (132, 133). Native CMR T1 parametric mapping has been used for inflammation/edema imaging and as a proxy for diffuse interstitial fibrosis in the absence of an alternative cause of interstitial expansion (edema, infiltrations/fiber disarray) (116). T1 mapping measures the total water content in the tissue and any changes to intravascular MBV will prolong T1 relaxation time. Vasodilator stress-induced coronary vasodilatation will lead to changes to MBV which forms the basis of stress/rest T1 mapping. Preliminary studies using stress/rest T1-mapping and CMR first-pass perfusion imaging in hypertrophic (132) and dilated (133) cardiomyopathy have demonstrated a correlation between T1 reactivity and myocardial perfusion. While this is encouraging, more in-depth validation of stress/rest T1 mapping is required. In our study, patient tolerability limited the use of CMR first-pass perfusion imaging, however other studies have demonstrated myocardial perfusion abnormalities on CMR first-

pass perfusion imaging in PAH (119). Furthermore, elevated myocardial T1-values have been demonstrated in PAH (125), which appears to be consistent with myocardial interstitial space expansion (134). While PAH associated LV underfilling is thought to be the cause of LV interstitial changes, the exact mechanism is not completely understood (135, 136). In addition, there were no differences in the elevated T1-values between iPAH, SSc-PAH or CTEPH (69, 125). Therefore, the observed blunted  $\Delta T1$  reactivity in PAH occurs as a result altered intravascular MBV during stress secondary to coronary vascular remodeling.

Previous studies have shown that myocardial oxygenation and perfusion during vasodilator stress may be dissociated (111). For example, our group has previously shown that in patients with known CAD, there was a disassociation between OS-CMR SI and quantitative perfusion myocardial blood flow with 50% of hypoperfused segments demonstrating no evidence of deoxygenation (111). In dilated cardiomyopathy, Dass *et al.* demonstrated a disassociation between microvascular dysfunction and oxygenation (120). Conversely, oxygen demand may be increased in the absence of perfusion abnormalities as demonstrated in hypertrophic cardiomyopathy gene carriers (137) despite the absence of LV hypertrophy (107). In this study, we have demonstrated a blunted global  $\Delta OS-CMR$  SI and global  $\Delta T1$  reactivity in response to vasodilator stress suggesting the presence of CMD. Furthermore the  $\Delta OS-CMR$  SI and  $\Delta T1$  reactivity affects the LV globally with comparable findings in the LV septal and free wall segments. However, on segmental analysis there is poor correlation between myocardial deoxygenation and changes to intravascular MBV (i.e.  $\Delta T1$  reactivity), suggesting that myocardial oxygenation and perfusion may be dissociated in PH patients also. This interplay between myocardial deoxygenation and changes in intravascular MBV during stress in pre-capillary PH has not been previously demonstrated.

### **5.4.3 Study Limitations**

Our study only performed a single mid-ventricular slice on OS-CMR imaging rather than the entire ventricle. However, we believe that in PH, the myocardium is affected globally and it is unlikely to affect the results. The OS-CMR images were acquired in mid-diastole as opposed to systole. While there are studies that have demonstrated advantages on acquiring OS-CMR images in systole (74), we have chosen mid-diastole acquisition to keep it consistent with T1 mapping acquisition. Moreover, the mid-diastole OS-CMR acquisition was also consistent with our and other studies that have demonstrated microvascular dysfunction in the LV (108, 109, 138, 139). This study has a small sample size which could increase the margin of error. A further larger study would help determine the utility of these novel techniques in PAH and its association with clinical outcomes. Moreover, compared to the PH group, the numbers in the CAD and control groups were relatively small. Nonetheless, both CAD and control groups were age-matched to the PH group, minimizing any significant bias. This is important, especially in T1-values whereby age is known to influence native myocardial T1-values (90). While this was a prospective study, we recruited PH patients who were stable on pulmonary vasodilator therapy which would have mitigated against the finding of LV ischemia. A larger study would help to determine the clinical and prognostic utility of these novel CMR techniques in PH.

### **5.4.4 Clinical implication and future directions**

The current study provides insights into the myocardial perfusion and oxygenation abnormalities in patients with non-severe PH. These findings suggest the presence of CMD, which has important clinical implications. Patients with CMD may present with typical effort-induced angina, but also with atypical symptoms such as dyspnea on exertion (122). In PAH, exertional limitation is the dominant symptom, and there are other factors (respiratory

mechanics/ventilation, cardiovascular response and psychological/emotional aspects) that can contribute to this (123). Although resting hemodynamic measures such as mPAP and cardiac output correlate with severity of symptoms, there is a substantial inter-individual variability that is not explained by hemodynamic severity (124). Although, we have not demonstrated any significant correlation between these novel CMR techniques and conventional prognostic markers of CMR RV EF and hemodynamic indices, OS-CMR and Stress/Rest T1 mapping techniques may provide additional pathophysiological insights in PH patients with ongoing exertional symptoms. In addition, characterizing CMD adds further potential for newer therapies that target myocardial ischemia and oxidative stress, such as ranolazine and trimetazidine that are currently in clinical trials (140).

## **5.5 Conclusion**

Blunted OS-CMR signal intensity and T1 reactivity with stress suggest the presence of coronary microvascular dysfunction in pre-capillary PH patients without significant epicardial coronary artery disease. This provides novel pathophysiological insights and may suggest potential future therapeutic targets, in PH.

## **Chapter 6 : Cardiovascular Magnetic Resonance Feature Tracking Evaluation of Myocardial Strain in Pulmonary Hypertension.**

This chapter describes the presence of myocardial strain abnormalities in the ventricles of in patients at the ‘early’ adaptive stage of pulmonary hypertension.

## 6.1 Introduction

Pulmonary arterial hypertension (PAH) is a serious and progressive disorder, in which the prognosis is largely dependent on cardiac function. In the right ventricle (RV), the RV size and function are the most powerful determinant of prognosis in PAH (12, 16, 17). Recent studies have demonstrated left ventricular (LV) dysfunction with several different pathophysiological causes of LV dysfunction that have been described in patients with PAH (42-47, 131). RV changes affect the interventricular interaction by leftward septal bowing, which leads to impaired LV diastolic filling (42, 43). Other studies have also reported LV diastolic dysfunction (44, 45) and reduction in LV free wall mass, in association with RV dysfunction, in PAH (46). Additionally, in vitro studies have demonstrated atrophy and severe contractile impairment of the LV cardiomyocyte (47).

Cardiovascular magnetic resonance myocardial feature tracking (CMR-FT) is a novel method introduced for high-resolution assessment of global and regional myocardial deformation by tracking the myocardial borders and following them over time. CMR-FT has been studied in a wide range of cardiovascular conditions such as ischemia (99) and cardiomyopathies (98, 100). Moreover, CMR-FT has been used to demonstrate myocardial strain abnormalities in the RV and LV of PAH patients (141, 142); which are associated with adverse prognosis (141, 143). However, these abnormalities were only demonstrated in a cohort of PAH patients with altered CMR volumetric and/or functional indices. It is therefore unclear if there are myocardial strain abnormalities in PAH patients with preserved cardiac function. Furthermore, in the previous chapters, we have demonstrated the presence of coronary microvascular dysfunction in both the RV and LV in PAH patients with otherwise preserved cardiac function (118, 144). It is possible that this coronary microvascular dysfunction may affect myocardial deformation in the 'early' adaptive stage of PAH. Hence this study aimed to assess the prevalence of

myocardial strain abnormalities in the 'early' adaptive stage of PAH and its relationship with coronary microvascular dysfunction.

## **6.2 Methods**

### **6.2.1 Ethics**

This study was approved by the Southern Adelaide Clinical Human Research Ethics Committee (HREC/15/SAC/397). All participants provided written informed consent to participate in the study.

### **6.2.2 Participant Selection**

Participant selection was performed as per section 4.3.2.

### **6.2.3 Participant preparation**

As per section 2.1.2

### **6.2.4 CMR protocol**

The CMR protocol was performed as outlined in sections 2.2.1, 2.2.2, 2.2.3 and 2.2.5.

### **6.2.5 CMR analysis**

The CMR analysis was performed as outlined in sections 2.3.1, 2.3.2 and 2.3.4.

### **6.2.6 Statistical analysis**

All analyses were performed using the Stata statistical software version 15.1 (StataCorp., USA). Categorical data are described using frequencies and percentages and continuous data using median and range. Differences between groups in the mean change in myocardial oxygenation response and native T1-values were assessed using Mann-Whitney test. Changes in these same outcomes within patient groups were assessed using the Sign-rank test. Associations between test parameters were assessed using the Spearman's rho ( $\rho$ ) correlation coefficient. A 2-sided Type 1 error rate of  $\alpha=0.05$  was used for assessing statistical significance.

## **6.3 Results**

### **6.3.1 Participants Characteristics**

The subject characteristics are as previously described in sections 4.4.1 (summarised on Table 4.1). Both PAH and control groups were well matched for age and gender. The aetiology within PAH were idiopathic pulmonary artery hypertension (iPAH) (n = 20, 48%), systemic sclerosis associated PAH (SScPAH) (n = 17, 40%) and chronic thromboembolic PAH (CTEPH) (n = 5, 12%). All patients had RHC and coronary angiogram proven diagnosis of PAH with a median (range) mPAP of 33 (16 – 67) mmHg and PCWP of 12 (4 – 15) mmHg. Median duration between RHC with coronary angiogram and CMR research study was 17 months. The median 6 minute walk distance in the patient group was 384 (100 – 600) meters. World Health Organisation functional class was between class II (n = 27, 64%) and III (n = 15, 36%). The PAH patients had an echocardiography derived resting systolic pulmonary artery pressure of 41 (27 – 128) mmHg. Furthermore, on echocardiography 8 patients (19%) had mild RV dilatation and 5 patients (12%) had moderate RV dilation. All PAH patients were receiving treatment with pulmonary vasodilators such as Bosentan, Macitentan, Sildenafil, Riociguat or a combination of Macitentan and Sildenafil. At recruitment the PAH patients were stable, and the pulmonary vasodilators therapy was not ceased prior to the CMR research scan.

### **6.3.2 CMR Characteristics**

The CMR characteristics are as previously described in sections 4.4.2 (summarised on Table 4.2). The only statistically significant difference in CMR volumetric and functional indices between PAH and controls were the RV mass index (17 (9 – 42) vs 13 (9 – 19)g/m<sup>2</sup>, p=0.001), RV Mass/Volume ratio (0.30 (0.22 – 0.49) vs 0.22 (0.15 – 0.25), p<0.001) and inferior RV wall thickness (4 (3 – 9) vs 3 (2 – 5)mm, p=0.002).

### **6.3.3 CMR Myocardial Deformation**

There was no significant difference in the LV global longitudinal strain (LV GLS) in the PAH group compared to the controls (-17.0 (-27.7 – 10.8) vs -17.2 (-21.7 – -15.5)%,  $p=0.37$ ). Similarly, there was no significant difference in the RV free wall strain (RVFWS) between the PAH group and controls (-20.0 (-29.7 – 7.9) vs -22.2 (-26.3 – -15.6)%,  $p=0.34$ ).

### **6.3.4 Comparing LV GLS and RVFWS values between iPAH and SScPAH**

The LV GLS between iPAH and SScPAH was -17.1 (-27.7 – -10.8) vs -16.7 (-21.2 – -13.3),  $p=0.839$  with the RVFWS between iPAH and SScPAH was -19.3 (-26.0 – -12.9) vs -20.1 (-29.7 – -7.9).

### **6.3.5 Correlations between CMR LV GLS, CMR RVFWS, myocardial oxygenation, CMR volumetric/functional and haemodynamic indices in PAH patients**

There were no significant correlations demonstrated between LV GLS and myocardial oxygenation, CMR volumetric/functional or haemodynamic indices. However, when compared to myocardial oxygenation, CMR RVFWS had a moderate correlation to LV OS-CMR SI ( $r=-0.50$ ,  $p=0.009$ ) (Figure 6.1A) and RV OS-CMR SI ( $r=-0.40$ ,  $p=0.045$ ) (Figure 6.1B). These findings suggest that abnormal LV and RV myocardial oxygenation are both associated with abnormal RV myocardial strain abnormalities. Compared to CMR volumetric/functional indices, CMR RVFWS had a strong correlation to RV inferior wall thickness ( $r=0.70$ ,  $p<0.001$ ) (Figure 6.1D) with moderate correlation to RV mass index ( $r=0.44$ ,  $p=0.023$ ) (Figure 6.1C) and RHC mPAP ( $r=0.43$ ,  $p=0.030$ ) (Figure 6.1E).

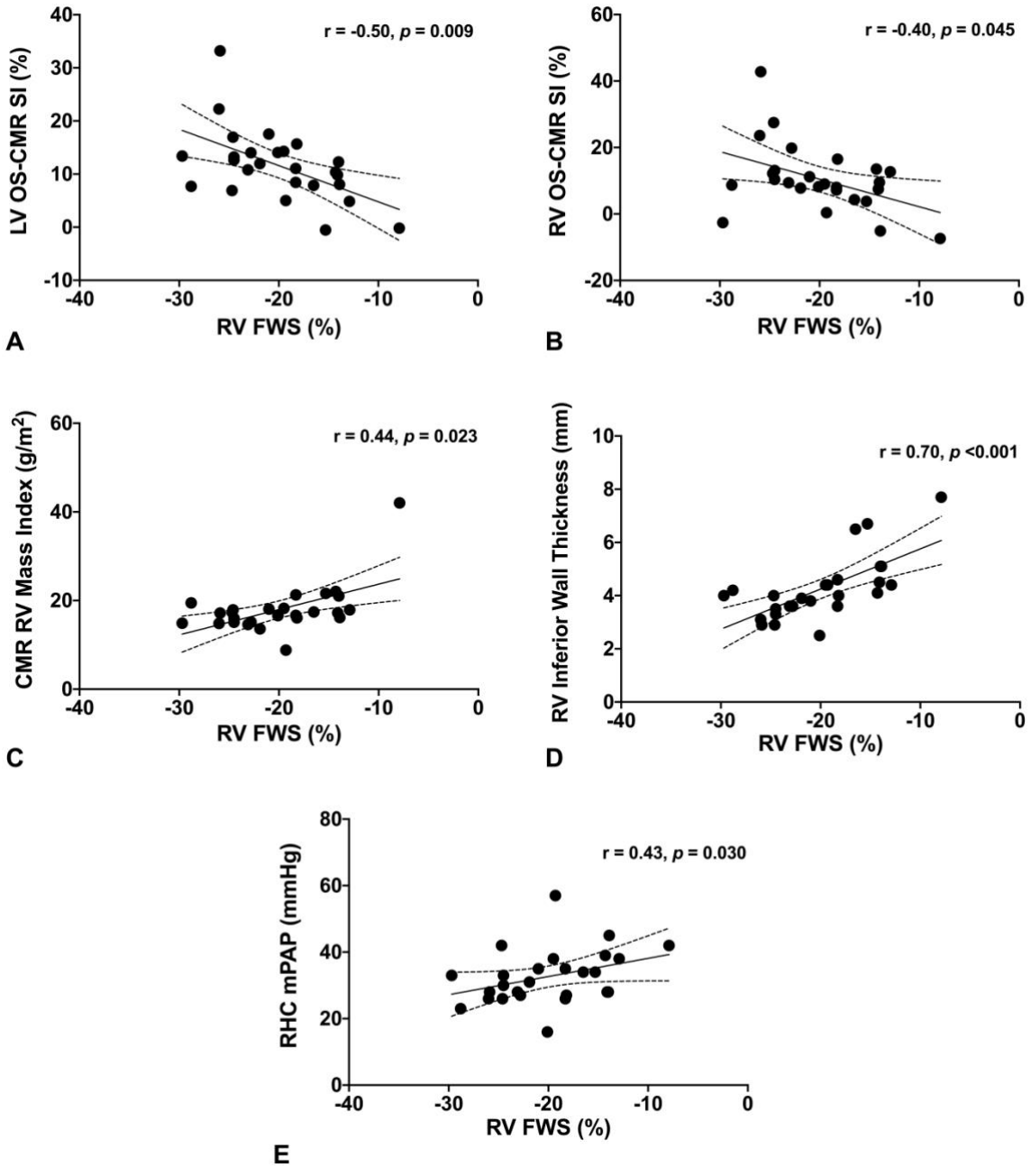


**Figure 6.1: Correlation between RV FWS to LV OS-CMR SI, RV OS-CMR SI, RV Mass Index, RV inferior wall thickness, RHC mPAP.**

## 6.4 Discussion

This study demonstrates CMR derived RVFWS correlates with LV and RV myocardial oxygenation, RV inferior wall thickness, RV mass index and RHC mPAP. However, there were no significant difference in the median LV GLS and RVFWS between PAH and control. These findings would suggest limited myocardial deformation changes in the ‘early’ adaptive stage of PAH, at a stage when the RV function and volume is mostly preserved. Despite this, RV free wall strain abnormalities were associated with myocardial oxygenation abnormalities and increasing RV hypertrophy – a sign of RV remodelling.

In PAH, there are several potential mechanisms of RV remodelling such as neurohormonal activation, growth factors, profibrotic cytokines, inflammation, capillary rarefaction, mitochondrial dysfunction, oxidative stress and ischemia (31). A number of these above mechanisms in addition to the increased haemodynamic load, precipitates RV hypertrophy (RVH) and subsequent RV dysfunction. In response to increased haemodynamic stress, RVH is a necessary adaptive mechanism in order to increase the force generating capacity by fivefold (145). In this circumstance, RVH is represented by an increase in cardiomyocyte size which is reflected by increased wall thickness and cardiac mass (146). This adaptation of RVH compensates for the increased RV wall stress (147) and oxygen consumption (148) to preserve RV-arterial coupling (149). In conjunction with RVH there are associated increases in RV angiogenesis which initially complements RVH (150). However, progressive RV hypertrophy without any further compensatory increase in the myocardial vasculature leads to RV myocardial ischaemia (35-37). In the previous chapters, we have demonstrated the presence of myocardial deoxygenation in the RV of PAH (118).

Although we found no significant difference in myocardial deformation compared to healthy volunteers in the ‘early’ adaptive stage of PAH, it is interesting to note its correlation with both LV and RV myocardial oxygenation and RVH. It has been previously demonstrated that RVH and RV myocardial strain abnormalities are associated with adverse prognostic outcomes (141, 151). However, it is unclear if the presence of myocardial deformation abnormalities in ‘early’ adaptive stage of PAH portends to the progressive transition of the RV from adaptive to a maladaptive stage of PAH with subsequent RV failure and death. Moreover, it is well known that PAH patients can experience silent progressive RV failure leading to death (13, 14). Hence, further studies are required to determine the role of RV free wall strain in subclinical RV dysfunction and its progression.

#### **6.4.1 Limitations**

Our study has several limitations. This study has a small sample size which could increase the margin of error. The predominantly correlative finding of the study should be interpreted as hypothesis generating rather than conclusive. The numbers in the control groups were relatively small compared to the PAH group. However, the control group were age-matched, minimizing any significant bias. The PAH patients were stable on pulmonary vasodilator therapy, which may have reduced myocardial deformation abnormalities. A larger study would help to determine the clinical and prognostic utility of this novel CMR techniques in PAH.

## **6.5 Conclusion**

Presence of right ventricular hypertrophy and myocardial deoxygenation is associated with abnormalities in the right ventricular mechanics in PAH patient with preserved right ventricular volume and function. Further studies are required to determine the role of RV free wall strain in subclinical RV dysfunction and its progression.

## **Chapter 7 : Right ventricular free wall systolic strain correlates to pressure flow relationship during dobutamine stress echocardiography**

This study describes the CMR-FT and echocardiographic right ventricular free wall systolic strain association with pressure flow relationship during dobutamine stress echocardiography.

## 7.1 Introduction

In a person without pulmonary vascular disease the pulmonary circulation has low pressure and low vascular resistance. Under exercise there is flow mediated dilatation of the pulmonary vasculature as well as recruitment of pulmonary microcirculation allowing accommodation of increased cardiac output (CO) with minimal increase in mean pulmonary arterial pressure (mPAP) (152-154). The pressure-flow relationship, in the form of the ratio between mPAP and cardiac output (CO) or index, may unmask abnormal response to exercise in the pulmonary vasculature prior to abnormalities in the resting mPAP (155). Up until 2008 exercise measurements formed part of the definition of PAH with a mPAP>30mmHg during exercise considered abnormal (10). As the CO increases an abnormally elevated increase in the mPAP/CO ratio may reflect increased left atrial pressure (LAP), increased pulmonary vascular resistance (PVR), reduced RV contractive function or a combination of these (156). Furthermore, elevated mPAP under stress has been shown to be associated with symptoms (157) and functional status (158).

Recently low dose dobutamine stress echocardiography (DSE) has been shown to be useful in determination of mPAP/CO ratio and therefore helpful in the non-invasive assessment of the functional status of the pulmonary circulation and RV contractile function (158). However, DSE in these patients is time consuming, not without risk, and the plotting and calculation of mPAP/CO graphs difficult in a clinical setting. Ideally a single resting parameter that is predictive of an elevation in the pressure-flow relationship of the pulmonary vasculature would be suited to daily clinical assessment of patients with established PAH and at risk of PAH development.

Speckle-tracking echocardiography (STE) and cardiovascular magnetic resonance imaging feature tracking (CMR-FT) are angle-independent techniques for quantifying myocardial motion. Right ventricular (RV) free wall systolic strain (RVFWS) has been shown to predict clinical deterioration and mortality in established PAH (159), independent of and incremental to clinical and left ventricular (LV) deformation parameters (160). In systemic sclerosis (SSc) patients of whom 71% had pulmonary hypertension on echocardiography, RV strain declined with poorer functional class, shorter 6-minute walk distances, higher NT-proBNP levels, and the presence of right heart failure. RV strain predicted survival across pulmonary pressures and according to strain quartile with a 1.46 higher risk of death per 6.7% decline in RV strain (161).

It is unclear if RVFWS is linked to the flow-pressure relationship and if it can be substituted as a simple resting measurement forgoing the need for low dose DSE in patients with PAH. We hypothesised that RVFWS at rest, either by cardiovascular magnetic resonance imaging (CMR) or echocardiography may predict this pressure-flow relationship and be superior to conventional measures of PAH.

## **7.2 Methods**

### **7.2.1 Ethics**

This study was approved by the Southern Adelaide Clinical Human Research Ethics Committee (HREC/15/SAC/397). All participants provided written informed consent to participate in the study.

### **7.2.2 Participant Selection**

Ten consecutive patients with right heart catheter (RHC) proven PAH (defined as pulmonary capillary wedge pressure (PCWP)  $\leq 15$  mmHg, and mean pulmonary artery pressure (mPAP)  $\geq 25$  mmHg), who consented to both OS-CMR and DSE were selected as per criteria outlined in 3.2.2.

### **7.2.3 Participant preparation**

As per section 2.1.2

### **7.2.4 Dobutamine stress echocardiography protocol**

Echocardiography was performed using a commercially available machine (GE E95, GE Healthcare, USA) by an experienced, senior cardiac sonographer. Dobutamine was given as a continuous infusion at incremental doses of 5, 10, 15 and a maximum of 20  $\mu$ g/kg/min. Each infusion stage was for 3 minutes and during the final minute of each stage the following echocardiographic images were taken, with at least 3 beats taken for each moving image: parasternal long axis view, zoom view of aortic valve and LV outflow tract (LVOT), parasternal short axis view, apical 4 chamber view with RV focus, the same view with a right atrial focus, m-mode through the tricuspid free wall annulus, colour Doppler through the tricuspid valve, continuous wave (CW) Doppler of the tricuspid regurgitation, apical 4

chamber, 2 chamber and long axis views with a focus on the LV, the same with the focus on the LA, mitral valve inflow, tissue pulsed wave (PW) Doppler of both the septal and lateral annulus and PW Doppler of the LVOT from an apical 5 chamber view. The heart rate (HR) was noted at each infusion level. The pre-specified infusion end points were reaching the maximum dobutamine dose or HR >120 beats/min (to avoid inducing very high HR in patients with PAH for safety reasons).

### **7.2.5 CMR protocol**

The CMR protocol was performed as outlined in sections 2.2.1, 2.2.2, 2.2.3, 2.2.4 and 2.2.5.

### **7.2.6 CMR analysis**

The CMR analysis was performed as outlined in sections 2.3.1, 2.3.2, 2.3.3 and 2.3.4.

### **7.2.7 Echocardiography analysis**

Analysis was performed using dedicated software (EchoPAC v204, GE Healthcare, USA) by a senior Echocardiographer with over 20 years' experience in cardiac sonography. Measurements were made according to the American Society of Echocardiography guidelines (162). These included the measurement of LVOT diameter and the LVOT velocity time integral which were multiplied together and then multiplied by the HR to calculate CO. Early mitral inflow velocity (E), atrial contraction flow velocity (A) and mitral deceleration time was measured from the mitral valve inflow. Early mitral annular septal and lateral (E') velocities were measured to give an average E' value which was used to calculate the E:E' ratio. Right atrial area and left atrial volume were measured from appropriate views. Right ventricular size was measured from linear measurements of the end diastolic and end systolic area and fractional area change (FAC) was calculated. The maximum velocity of the tricuspid

regurgitant CW Doppler signal was measured and RA pressure estimated from the inferior vena cava diameter and collapsibility to determine systolic PAP (sPAP). The mPAP was calculated as  $0.6 \times \text{sPAP} + 2$  (163). Speckle-tracking strain analysis was performed on the LV focused views from an apical 4 chamber, 2 chamber and long axis view and the RV focused apical 4 chamber view. Studies were deemed inadequate for analysis when 2 or more LV segments or 1 RV free wall segment were unable to be visualised. A region of interest was applied to the endocardial and epicardial borders of either the LV or the RV with the tracking adjusted to cover the entire myocardium. Global longitudinal strain (GLS) was calculated as the average of all peak regional strain values in the 16 segments of the LV.

The left atrium was imaged from the apical 4 chamber and 2 chamber views with care to ensure the left atrium was within the imaging sector over the whole cardiac cycle. The right atrium was imaged from a modified right heart focused apical 4 chamber view with care to ensure the right atrium was within the imaging sector over the whole cardiac cycle. For both left and right atrial acquisitions, the frame rate was between 50 and 80 frames per second. Speckle-tracking strain analysis was performed on the left and right atrium from the appropriate views using Automated Function analysis of the atrium (AFI LA, EchoPac Version 204, GE Vingmed Ultrasound). A region of interest was placed on the endocardial border of the left and right atrium and the tracking adjusted to cover the entire atrium throughout the cardiac cycle. Studies were deemed inadequate for analysis when any part of the tracking was unable to follow the atrial wall adequately. Reservoir strain is the lengthening of the atrial wall during the reservoir phase of the atrial filling where the mitral and tricuspid valves are closed (ventricular systole).

### **7.2.8 Statistical analysis**

All analyses were performed using IBM SPSS Statistics version 26 (IBM Corp., USA). Categorical data are described using frequencies and percentages and continuous data using median and range. Differences between rest and dobutamine peak stress parameters were determined using Wilcoxon Signed Ranks test. Correlations between mPAP/CO and imaging parameters were determined using Spearman's Rank Order correlation. A 2-sided Type 1 error rate of  $\alpha=0.05$  was used for assessing statistical significance.

## **7.3 Results**

### **7.3.1 Participant Characteristics**

The subject characteristics are summarized in Table 7.1. Among the 10 PAH patients, 2 (20%) had idiopathic pulmonary artery hypertension (iPAH), 5 (50%) patients had systemic sclerosis-associated PAH (SSc-PAH), and 3 (30%) patients had chronic thromboembolic PH (CTEPH). All patients had right heart catheter (RHC) and coronary angiogram proven diagnosis of PAH with a median mPAP of 35 (26 – 67) mmHg and the median PAWP of 10 (6 - 15) mmHg. Median duration between RHC with coronary angiogram and OS-CMR/DSE research study was 3 years. The median 6-minute walk distance was 419 (100 – 600) meters. On echocardiography, 5 (50%) patients had RV dilatation with an echocardiography-estimated resting systolic pulmonary artery pressure of 45 (31 – 96) mmHg. All PAH patients were treated with pulmonary vasodilators such as bosentan, macitentan, sildenafil, riociguat with 5 (50%) on combination therapy. The PAH patients were stable and continued their pulmonary vasodilator therapy during both the CMR and DSE research scans. The median duration between the CMR and DSE research scans was 18 days.

**Table 7.1 Participant demographics and baseline clinical data**

<b>Variable</b>	<b>PAH (n=10)</b>
Age (years), median (range)	71 (34 – 81)
Females sex, n (%)	8 (80%)
Comorbidities <ul style="list-style-type: none"> <li>• Hypertension, n (%)</li> <li>• Diabetes, n (%)</li> <li>• Dyslipidaemia</li> <li>• Chronic Obstructive Airways Disease, n (%)</li> <li>• Obstructive Sleep Apnoea, n (%)</li> </ul>	5 (50%) 2 (20%) 1 (10%) 2 (20%) 3 (30%)
Right heart catheter haemodynamic indices <ul style="list-style-type: none"> <li>• Mean pulmonary artery pressures (mmHg), median (range)</li> <li>• Pulmonary artery wedge pressure (mmHg ), median (range)</li> <li>• Mean right atrial pressures (mmHg), median (range)</li> <li>• Cardiac index (L/min/m<sup>2</sup> ), median (range)</li> <li>• Pulmonary vascular resistance index (Woods unit m<sup>2</sup> ), median (range)</li> </ul>	35 (26 – 67) 10 (6 – 15) 10 (3 – 14) 2 (2 – 4) 10 (3 – 28)
Medication <ul style="list-style-type: none"> <li>• Beta-blockers, n (%)</li> <li>• ACEi/ARB, n (%)</li> <li>• Statins, n (%)</li> <li>• Calcium channel blockers</li> <li>• Endothelin receptor blockers, n (%)</li> <li>• PDE5 inhibitor, n (%)</li> <li>• Soluble guanylate cyclase, n (%)</li> <li>• *Combination therapy, n (%)</li> </ul>	2 (20%) 2 (20%) 1 (10%) 2 (20%) 8 (80%) 5 (50%) 1 (10%) 5 (50%)

\* Combination therapy of a dual therapy comprising of either endothelin receptor blocker, PDE5 inhibitor or soluble guanylate cyclase

ACEi = angiotensin-converting enzyme inhibitors, ARB = angiotensin II receptor blockers,

PDE5 = phosphodiesterase type 5 inhibitor

### 7.3.2 Echocardiography Characteristics

Table 7.2 demonstrates the echocardiography characteristics of the participants at both rest and peak stress. There was good correlation between echocardiographic RVFWS and CMR-FT RVFWS ( $r=0.84$ ,  $p=0.004$ ). With dobutamine infusion there was a significant increase in mPAP (27.8 (21.8 – 54.9) to 35.4 (29.3 – 57.3),  $p=0.018$ ), heart rate (68 (58 – 82) to 102 (60 – 120),  $p=0.012$ ), CO (3.6 (2.9 – 5.1) to 5.5 (3.7 – 9.9),  $p=0.008$ ), LV ejection fraction (60 (51 – 73) to 69 (61 – 82),  $p=0.024$ ) and a significant reduction in E:E' (10.8 (5.6 – 17.4) to 10.4 (5.3 – 14.1),  $p=0.021$ ). No significant changes were demonstrated at low dose dobutamine.

**Table 7.2 Echocardiographic characteristics**

<b>Variable, median (range)</b>	<b>Rest</b>	<b>Peak stress</b>	<b>P value</b>
mPAP (mmHg)	27.8 (21.8 – 54.9)	35.4 (29.3 – 57.3)	<b>0.018</b>
TAPSE (cm)	1.8 (1.1 – 2.5)	1.5 (1.0 – 2.3)	0.201
FAC (%)	40 (25 – 61)	37 (22 – 47)	0.593
RA area (cm <sup>2</sup> )	22.5 (13.3 – 32.4)	19.9 (9.5 – 34.0)	0.374
RVFWS (%)	-18.3 (-10.7 - -32.0)	-16.9 (-12.3 - -24.1)	0.917
HR (bpm)	68 (58 – 82)	102 (60 – 120)	<b>0.012</b>
CO (mL/min)	3.6 (2.9 – 5.1)	5.5 (3.7 – 9.9)	<b>0.008</b>
RA reservoir strain (%)	32.0 (8.0 – 46.0)	24.5 (10.0 – 47.0)	0.362
LVEF (%)	60 (51 – 73)	69 (61 – 82)	<b>0.024</b>
LV GLS (%)	-16.6 (-12.8 - -21.5)	-18.5 (-14.8 - -22.6)	0.314
LA volume (mL)	52.5 (44.0 – 56.0)	48.0 (29.0 – 71.0)	0.588
LA reservoir strain (%)	25.5 (11.0 – 39.0)	32.0 (14.0 – 47.0)	0.052
E:E'	10.8 (5.6 – 17.4)	10.4 (5.3 – 14.1)	<b>0.021</b>
mPAP/CO	7.5 (4.5 – 15.3)	6.4 (4.5 – 14.8)	0.398

mPAP – mean pulmonary artery pressure, TAPSE – tricuspid annular plane systolic excursion, FAC – fractional area change, RA – right atrial, RVFWS – right ventricular free wall systolic strain, HR – heart rate, CO – cardiac output, LVEF – left ventricular ejection fraction, GLS – global longitudinal strain, LA – left atrial.

### **7.3.3 mPAP/CO vs echocardiographic parameters**

The flow-pressure relationship of mPAP/CO did not correlate with the echocardiographic derived TAPSE or FAC (Table 7.3). There was good between mPAP/CO and echocardiographic RVFWS at all stages of dobutamine infusion. The strongest mPAP/CO correlation to echocardiographic RVFWS was at rest (Spearman's  $\rho=0.96$ ,  $p<0.001$ ). There was good mPAP/CO correlation to echocardiographic RVFWS at low dose dobutamine (Spearman's  $\rho=0.77$ ,  $p=0.01$ ) and peak dose dobutamine (Spearman's  $\rho=0.85$ ,  $p=0.003$ ) (Figure 7.1).

#### **7.3.4 mPAP/CO vs CMR parameters**

The flow-pressure relationship of mPAP/CO did not correlate with the signal intensity (SI) change in the RV oxygen-sensitive (OS) CMR sequence, the RV native T1 signal or the CMR RV ejection fraction (Table 7.3). However, mPAP/CO did correlate with CMR feature tracking (CMR-FT) derived RVFWS at all stages of dobutamine infusion from rest (Spearman's  $\rho=0.96$ ,  $p<0.001$ ) to low dose dobutamine (Spearman's  $\rho=0.76$ ,  $p=0.015$ ) and at peak dose dobutamine (Spearman's  $\rho=0.87$ ,  $p=0.002$ ) (Figure 7.1).

**Table 7.3 Flow-pressure relationship correlated with imaging parameters**

<b>Variable correlated with mPAP/CO</b>	<b>Spearman's rho</b>	<b>P value</b>
RV OS-CMR SI	-0.18	0.702
CMR RV native T1	-0.66	0.156
CMR RVEF	-0.52	0.183
Echo TAPSE	0.193	0.647
Echo FAC	0.68	0.066

mPAP – mean pulmonary artery pressure, CO – cardiac output, RV – right ventricular, OS-CMR SI – oxygen sensitive cardiovascular magnetic resonance signal intensity, RVEF – right ventricular ejection fraction, CMR-FT – cardiovascular magnetic resonance feature tracking, RVFWS – right ventricular free wall systolic strain, Echo – echocardiography, TAPSE – tricuspid annular plane systolic excursion, FAC – fractional area change

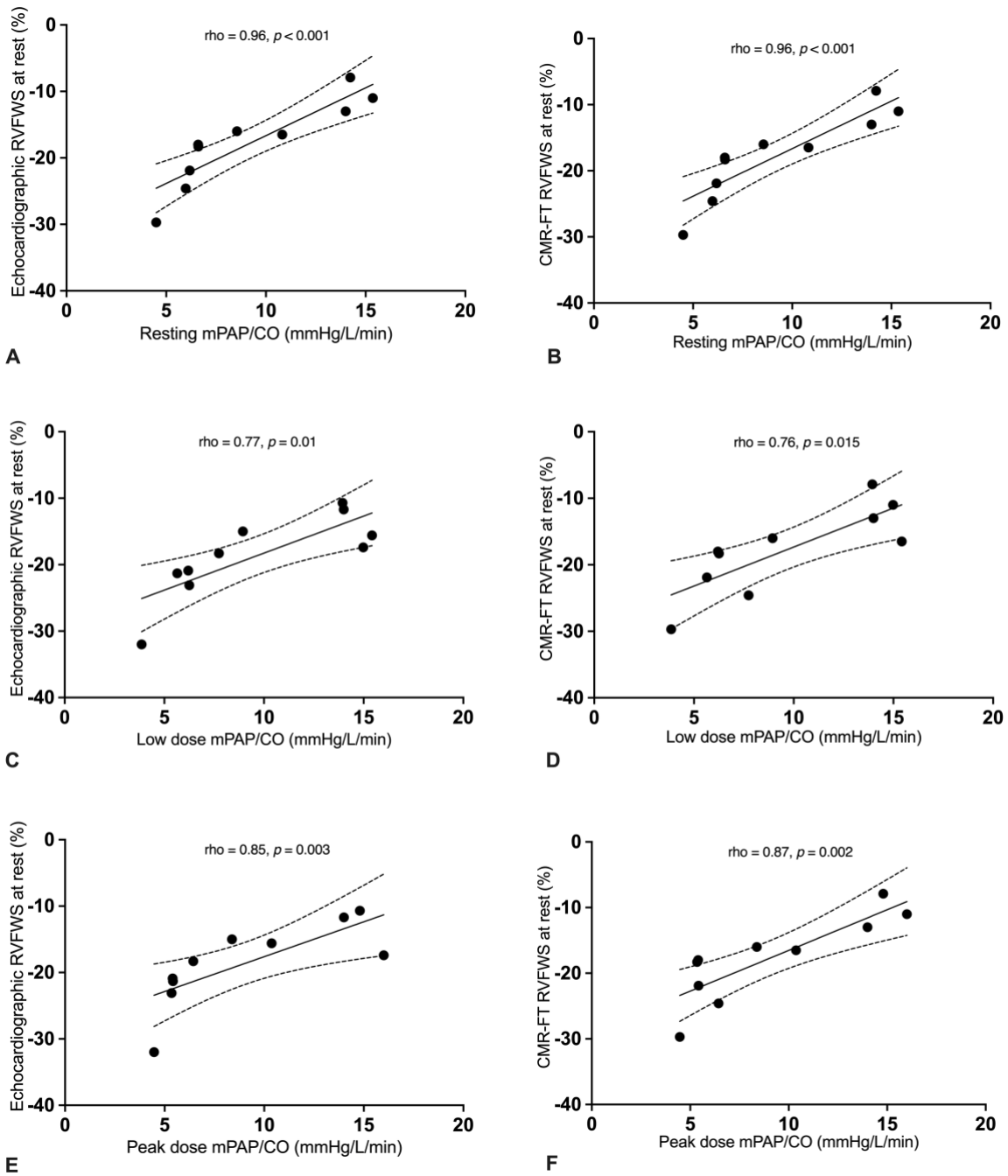


**Figure 7.1: Correlation between echocardiographic RVFWS and CMR-FT RVFWS to mPAP/CO at rest, low dose dobutamine and peak dose dobutamine.**

## 7.4 Discussion

Our study demonstrates that resting RVFWS either by CMR or echocardiography correlates with mPAP/CO. This simple, non-invasive measure is much quicker and easier to perform than calculation of the mPAP/CO using low dose DSE. Interestingly both the RV OS-CMR SI and the CMR RV native T1 signal did not correlate with mPAP/CO. This is likely because they are measuring different physiological responses to PAH. RV OS-CMR SI is measuring the oxygenation of the RV myocardium and the native T1 is measuring the degree of interstitial fibrosis, both important parameters but not directly linked to the pressure-flow relationship. RVFWS however, appears to be correlated with mPAP/CO during stress whereby worse RVFWS corresponds with abnormally elevated mPAP/CO during DSE.

The assessment of RV contractile function usually relies on load dependent measures such as tricuspid annular plane systolic excursion (TAPSE), tricuspid annular systolic velocity (S') or fractional area change (FAC). The measurement of RVFWS whilst still load dependent is much less so and may give a better representation of RV contractile function. A gold-standard measurement of RV contractility involves using invasive catheters to simultaneously measure pressure and volume, ideally over multiple loading conditions. The fact that RVFWS correlates to mPAP/CO whereas TAPSE and FAC do not reflects that it is less load dependent and may be considered for further investigation of RV contractile function.

Whilst our entire cohort had established and treated PAH, it is possible that this technique of resting RVFWS may be able to detect early abnormalities in patients at risk of PAH development. In fact, Hekimsoy et al. (164) found that the peak longitudinal systolic strain (PLSS) at the apical segment of the RV free wall was significantly lower in SSc patients with newly right heart catheter (RHC) confirmed PAH compared with patients without PAH on

RHC and correlated with mPAP. A cut-off value of 14.48% PLSS at the apical segment of the RV lateral wall was only 62% sensitive in identifying PAH but was 100% specific in ruling out PAH. After 12 months, PLSS of the RV free wall was lower in the non-PAH group compared to baseline suggesting that PLSS falls over time in patients with SSc, possibly in response to rising pulmonary vascular resistance, until PAH is clinically evident and treatment commences. The subsequent development of PAH was not determined in this cohort.

It is still unclear if a one off measurement or temporal changes in RVFWS can be used to predict the development of PAH. Hence studies of larger cohorts of patients at risk of PAH development with longer follow-up periods are needed to determine the clinical utility of RVFWS for detecting early PAH.

#### **7.4.1 Study limitations**

The major limitation to this study is the small sample size, limiting the conclusions that can be drawn from this study. However, despite this limitation a significant correlation was still observed between RVFWS and mPAP/CO which may indicate its strength in the prediction of the pressure-flow relationship. Furthermore, the lack of a 'gold standard' of invasive measurement of RV contractility limit the ability to directly determine what RVFWS is measuring.

## **7.5 Conclusion**

Right ventricular free wall systolic strain as measured by both feature tracking CMR and echocardiography correlate to measures of right ventricular pressure-flow relationship. Further investigation into the utility of RVFWS in the detection of subclinical PAH is warranted.

## **Chapter 8 : Conclusions**

This thesis has explored the utility of cardiovascular magnetic resonance (CMR) in assessing myocardial dysfunction in pulmonary arterial hypertension (PAH). By utilising novel cardiovascular magnetic resonance techniques, we have demonstrated subclinical myocardial dysfunction in PAH with relatively preserved cardiac function. Particularly, in the areas of myocardial oxygenation, myocardial extracellular matrix, coronary microvascular function and myocardial deformation. The key finding with this body of work is the presence of myocardial deoxygenation to stress in the right ventricle (RV) and left ventricle (LV) of PAH patients, at the early ‘adaptive’ phase.

### **8.1 Myocardial Oxygenation in PAH**

This thesis investigated the utility of oxygen-sensitive cardiovascular magnetic resonance (OS-CMR) in patients with PAH. OS-CMR technique has never been studied in the RV, and hence in Chapter 3, we had aimed to determine the feasibility of RV OS-CMR. We found that pharmacological induced OS-CMR was a feasible and safe technique to identify and study myocardial oxygenation in the RV of PAH patients. We followed this with a larger study to understand the prevalence of myocardial deoxygenation in the RV of patients with PAH.

Chapter 4 studied the extent of blunted myocardial oxygenation response to vasodilator stress in the RV PAH. Specifically, we demonstrated the presence of in-vivo myocardial deoxygenation in the ‘early’ adaptive stage of PAH. These findings also had a good correlation with the LV OS-CMR changes; an area of myocardium with established validation with the OS-CMR technique. Moreover, a moderate inverse correlation between RV OS-CMR and mean pulmonary artery pressure (mPAP) was observed. This was interesting as right heart

catheter (RHC) resting hemodynamic measures such as mPAP and cardiac output are associated with severity of symptoms. However, there are considerable inter-individual variability in symptoms that are not explained completely by RHC hemodynamic severity (124). Therefore, myocardial deoxygenation findings provide further mechanistic insights into the pathophysiology of RV dysfunction in PAH population.

## **8.2 Myocardial extracellular matrix (ECM) and coronary microvascular function in PAH**

In PAH the RV undergoes a compensatory process in response to increased haemodynamic pressures and other stressful stimuli. This compensatory process is in the form of RV hypertrophy (RVH) whereby there is an increase in cardiomyocyte size, which is reflected by increased wall thickness and cardiac mass (146). This increase of cardiomyocyte occurs in the form of myocardial collagen accumulation which changes the myocardial ECM. In Chapters 4 and 5, we utilised CMR T1-mapping techniques to demonstrate changes in the RV and LV myocardium ECM. Furthermore in the LV of PAH, by utilizing Stress/Rest T1-mapping technique, we demonstrated blunting of the myocardial blood flow (MBF) indicating the presence of coronary microvascular dysfunction (CMD) in the LV of PAH.

## **8.3 Myocardial Deformation in PAH**

Chapters 6 and 7 studied CMR and echocardiographic myocardial strain changes in PAH. While no significant changes were demonstrated, there were associations with RV free wall strain to either myocardial wall thickness and/or myocardial deoxygenation of the RV in ‘early’ adaptive PAH.

## **Chapter 9 : Future Directions**

Future studies would be essential to determine the utility of these novel cardiovascular magnetic resonance (CMR) techniques in predicting progressive cardiac dysfunction and mortality in pulmonary arterial hypertension (PAH). In particular in the right ventricle (RV) of PAH, where it has been well documented that these patients can experience silent progressive RV failure leading to death (13, 14). Currently, the pathophysiological drivers of the progressive transition from RV adaptation to maladaptation remain unclear. While the findings in this thesis provide novel insights into the mechanisms of myocardial dysfunction in PAH; it should also be considered as hypothesis-generating for future studies. More work is required to determine if these novel markers can predict early or impending RV failure and consequently guide therapy augmentation.

Furthermore, the characterisation of myocardial deoxygenation and coronary microvascular dysfunction could aid certain therapies such as ranolazine and trimetazidine that target myocardial ischemia and oxidative stress. Moreover, these novel CMR techniques could be studied to detect early changes in patients at risk of PAH development, such as systemic sclerosis. This could potentially open avenues for early therapeutic intervention before irreversible pulmonary arterial damage.

## Chapter 10 : References

1. McLaughlin VV, McGoon MD. Pulmonary arterial hypertension. *Circulation*. 2006;114(13):1417-31.
2. Hatano S, Strasser T, World Health O. Primary pulmonary hypertension : report on a WHO meeting, Geneva, 15-17 October 1973 / edited by Shuichi Hatano and Toma Strasser. Geneva: World Health Organization; 1975.
3. Simonneau G, Montani D, Celermajer DS, Denton CP, Gatzoulis MA, Krowka M, et al. Haemodynamic definitions and updated clinical classification of pulmonary hypertension. *European Respiratory Journal*. 2019;53(1):1801913.
4. Yuan JX, Rubin LJ. Pathogenesis of pulmonary arterial hypertension: the need for multiple hits. *Circulation*. 2005;111(5):534-8.
5. Machado Rajiv D, James V, Southwood M, Harrison Rachel E, Atkinson C, Stewart S, et al. Investigation of Second Genetic Hits at the BMPR2 Locus as a Modulator of Disease Progression in Familial Pulmonary Arterial Hypertension. *Circulation*. 2005;111(5):607-13.
6. Hoeper MM, Simon R, Gibbs J. The changing landscape of pulmonary arterial hypertension and implications for patient care. *European Respiratory Review*. 2014;23(134):450.
7. Pulido T, Adzerikho I, Channick RN, Delcroix M, Galiè N, Ghofrani H-A, et al. Macitentan and Morbidity and Mortality in Pulmonary Arterial Hypertension. *New England Journal of Medicine*. 2013;369(9):809-18.
8. Sitbon O, Channick R, Chin KM, Frey A, Gaine S, Galiè N, et al. Selexipag for the Treatment of Pulmonary Arterial Hypertension. *New England Journal of Medicine*. 2015;373(26):2522-33.
9. Galiè N, Barberà JA, Frost AE, Ghofrani H-A, Hoeper MM, McLaughlin VV, et al. Initial Use of Ambrisentan plus Tadalafil in Pulmonary Arterial Hypertension. *New England Journal of Medicine*. 2015;373(9):834-44.
10. Galiè N, Humbert M, Vachiery J-L, Gibbs S, Lang I, Torbicki A, et al. 2015 ESC/ERS Guidelines for the diagnosis and treatment of pulmonary hypertension: The Joint Task Force for the Diagnosis and Treatment of Pulmonary Hypertension of the European Society of Cardiology (ESC) and the European Respiratory Society (ERS): Endorsed by: Association for European Paediatric and Congenital Cardiology (AEPC), International Society for Heart and Lung Transplantation (ISHLT). *European Heart Journal*. 2015;37(1):67-119.
11. Farber HW, Miller DP, Poms AD, Badesch DB, Frost AE, Muros-Le Rouzic E, et al. Five-Year outcomes of patients enrolled in the REVEAL Registry. *Chest*. 2015;148(4):1043-54.
12. Humbert M, Sitbon O, Chaouat A, Bertocchi M, Habib G, Gressin V, et al. Survival in patients with idiopathic, familial, and anorexigen-associated pulmonary arterial hypertension in the modern management era. *Circulation*. 2010;122(2):156-63.
13. van de Veerdonk MC, Kind T, Marcus JT, Mauritz GJ, Heymans MW, Bogaard HJ, et al. Progressive right ventricular dysfunction in patients with pulmonary arterial hypertension responding to therapy. *J Am Coll Cardiol*. 2011;58(24):2511-9.
14. van de Veerdonk MC, Marcus JT, Westerhof N, de Man FS, Boonstra A, Heymans MW, et al. Signs of right ventricular deterioration in clinically stable patients with pulmonary arterial hypertension. *Chest*. 2015;147(4):1063-71.
15. Strange G, Stewart S, Celermajer DS, Prior D, Scalia GM, Marwick TH, et al. Threshold of Pulmonary Hypertension Associated With Increased Mortality. *Journal of the American College of Cardiology*. 2019;73(21):2660.

16. D'Alonzo GE, Barst RJ, Ayres SM, Bergofsky EH, Brundage BH, Detre KM, et al. Survival in patients with primary pulmonary hypertension. Results from a national prospective registry. *Annals of internal medicine*. 1991;115(5):343-9.
17. Tonelli AR, Arelli V, Minai OA, Newman J, Bair N, Heresi GA, et al. Causes and circumstances of death in pulmonary arterial hypertension. *American journal of respiratory and critical care medicine*. 2013;188(3):365-9.
18. Janicki JS, Brower GL. The role of myocardial fibrillar collagen in ventricular remodeling and function. *Journal of cardiac failure*. 2002;8(6 Suppl):S319-25.
19. Sutton MGSJ, Sharpe N. Left Ventricular Remodeling After Myocardial Infarction. *Circulation*. 2000;101(25):2981-8.
20. Mewton N, Liu Chia Y, Croisille P, Bluemke D, Lima João AC. Assessment of Myocardial Fibrosis With Cardiovascular Magnetic Resonance. *Journal of the American College of Cardiology*. 2011;57(8):891-903.
21. Anderson KR, Sutton MGSJ, Lie JT. Histopathological types of cardiac fibrosis in myocardial disease. *The Journal of Pathology*. 1979;128(2):79-85.
22. Polyakova V, Hein S, Kostin S, Ziegelhoeffer T, Schaper J. Matrix metalloproteinases and their tissue inhibitors in pressure-overloaded human myocardium during heart failure progression. *J Am Coll Cardiol*. 2004;44(8):1609-18.
23. Lopez B, Gonzalez A, Querejeta R, Larman M, Diez J. Alterations in the pattern of collagen deposition may contribute to the deterioration of systolic function in hypertensive patients with heart failure. *J Am Coll Cardiol*. 2006;48(1):89-96.
24. Zaffran S, Kelly Robert G, Meilhac Sigolène M, Buckingham Margaret E, Brown Nigel A. Right Ventricular Myocardium Derives From the Anterior Heart Field. *Circulation Research*. 2004;95(3):261-8.
25. Herpel E, Singer S, Flechtenmacher C, Pritsch M, Sack FU, Hagl S, et al. Extracellular matrix proteins and matrix metalloproteinases differ between various right and left ventricular sites in end-stage cardiomyopathies. *Virchows Archiv : an international journal of pathology*. 2005;446(4):369-78.
26. Caspari PG, Gibson K, Harris P. Changes in myocardial collagen in normal development and after beta blockade. *Recent advances in studies on cardiac structure and metabolism*. 1975;7:99-104.
27. Oken DE, Boucek RJ. Quantitation of collagen in human myocardium. *Circ Res*. 1957;5(4):357-61.
28. Chin KM, Coghlan G. Characterizing the Right Ventricle: Advancing Our Knowledge. *The American journal of cardiology*. 2012;110(6, Supplement):S3-S8.
29. Zong P, Sun W, Setty S, Tune JD, Downey HF. Alpha-adrenergic vasoconstrictor tone limits right coronary blood flow in exercising dogs. *Experimental biology and medicine* (Maywood, NJ). 2004;229(4):312-22.
30. Zong P, Tune JD, Setty S, Downey HF. Endogenous nitric oxide regulates right coronary blood flow during acute pulmonary hypertension in conscious dogs. *Basic research in cardiology*. 2002;97(5):392-8.
31. Andersen S, Nielsen-Kudsk JE, Vonk Noordegraaf A, de Man FS. Right Ventricular Fibrosis. *Circulation*. 2019;139(2):269-85.
32. Ryan JJ, Archer SL. Emerging concepts in the molecular basis of pulmonary arterial hypertension: part I: metabolic plasticity and mitochondrial dynamics in the pulmonary circulation and right ventricle in pulmonary arterial hypertension. *Circulation*. 2015;131(19):1691-702.
33. Bogaard HJ, Natarajan R, Henderson SC, Long CS, Kraskauskas D, Smithson L, et al. Chronic pulmonary artery pressure elevation is insufficient to explain right heart failure. *Circulation*. 2009;120(20):1951-60.

34. Piao L, Fang Y-H, Parikh K, Ryan JJ, Toth PT, Archer SL. Cardiac glutaminolysis: a maladaptive cancer metabolism pathway in the right ventricle in pulmonary hypertension. *Journal of Molecular Medicine*. 2013;91(10):1185-97.
35. Akasaka T, Yoshikawa J, Yoshida K, Hozumi T, Takagi T, Okura H. Comparison of relation of systolic flow of the right coronary artery to pulmonary artery pressure in patients with and without pulmonary hypertension. *The American journal of cardiology*. 1996;78(2):240-4.
36. Murray PA, Vatner SF. Reduction of maximal coronary vasodilator capacity in conscious dogs with severe right ventricular hypertrophy. *Circ Res*. 1981;48(1):25-33.
37. van Wolferen SA, Marcus JT, Westerhof N, Spreeuwenberg MD, Marques KM, Bronzwaer JG, et al. Right coronary artery flow impairment in patients with pulmonary hypertension. *Eur Heart J*. 2008;29(1):120-7.
38. Piao L, Fang YH, Parikh K, Ryan JJ, Toth PT, Archer SL. Cardiac glutaminolysis: a maladaptive cancer metabolism pathway in the right ventricle in pulmonary hypertension. *Journal of molecular medicine (Berlin, Germany)*. 2013;91(10):1185-97.
39. Piao L, Sidhu VK, Fang YH, Ryan JJ, Parikh KS, Hong Z, et al. FOXO1-mediated upregulation of pyruvate dehydrogenase kinase-4 (PDK4) decreases glucose oxidation and impairs right ventricular function in pulmonary hypertension: therapeutic benefits of dichloroacetate. *Journal of molecular medicine (Berlin, Germany)*. 2013;91(3):333-46.
40. Oikawa M, Kagaya Y, Otani H, Sakuma M, Demachi J, Suzuki J, et al. Increased [18F]fluorodeoxyglucose accumulation in right ventricular free wall in patients with pulmonary hypertension and the effect of epoprostenol. *J Am Coll Cardiol*. 2005;45(11):1849-55.
41. Piao L, Fang YH, Cadete VJ, Wietholt C, Urboniene D, Toth PT, et al. The inhibition of pyruvate dehydrogenase kinase improves impaired cardiac function and electrical remodeling in two models of right ventricular hypertrophy: resuscitating the hibernating right ventricle. *Journal of molecular medicine (Berlin, Germany)*. 2010;88(1):47-60.
42. Gan C, Lankhaar JW, Marcus JT, Westerhof N, Marques KM, Bronzwaer JG, et al. Impaired left ventricular filling due to right-to-left ventricular interaction in patients with pulmonary arterial hypertension. *Am J Physiol Heart Circ Physiol*. 2006;290(4):H1528-33.
43. Marcus JT, Vonk Noordegraaf A, Roeleveld RJ, Postmus PE, Heethaar RM, Van Rossum AC, et al. Impaired Left Ventricular Filling Due to Right Ventricular Pressure Overload in Primary Pulmonary Hypertension: Noninvasive Monitoring Using MRI. *Chest*. 2001;119(6):1761-5.
44. Hardegree Evan L, Sachdev A, Fenstad Eric R, Villarraga Hector R, Frantz Robert P, McGoon Michael D, et al. Impaired Left Ventricular Mechanics in Pulmonary Arterial Hypertension. *Circulation: Heart Failure*. 2013;6(4):748-55.
45. Tonelli AR, Plana JC, Heresi GA, Dweik RA. Prevalence and Prognostic Value of Left Ventricular Diastolic Dysfunction in Idiopathic and Heritable Pulmonary Arterial Hypertension. *Chest*. 2012;141(6):1457-65.
46. Hardziyenka M, Campian ME, Reesink HJ, Surie S, Bouma BJ, Groenink M, et al. Right Ventricular Failure Following Chronic Pressure Overload Is Associated With Reduction in Left Ventricular Mass: Evidence for Atrophic Remodeling. *Journal of the American College of Cardiology*. 2011;57(8):921-8.
47. Manders E, Bogaard H-J, Handoko ML, van de Veerdonk MC, Keogh A, Westerhof N, et al. Contractile Dysfunction of Left Ventricular Cardiomyocytes in Patients With Pulmonary Arterial Hypertension. *Journal of the American College of Cardiology*. 2014;64(1):28.
48. Nitenberg A, Foulst J-M, Kahan A, Perennec J, Devaux J-Y, Menkes C-J, et al. Reduced coronary flow and resistance reserve in primary scleroderma myocardial disease. *American Heart Journal*. 1986;112(2):309-15.

49. Kahan A, Allanore Y. Primary myocardial involvement in systemic sclerosis. *Rheumatology (Oxford, England)*. 2006;45 Suppl 4:iv14-7.
50. Galiè N, Saia F, Palazzini M, Manes A, Russo V, Bacchi Reggiani ML, et al. Left Main Coronary Artery Compression in Patients With Pulmonary Arterial Hypertension and Angina. *Journal of the American College of Cardiology*. 2017;69(23):2808-17.
51. Yeh DD, Ghoshhajra B, Inglessis-Azuaje I, MacGillivray T, Liberthson R, Bhatt AB. Massive Pulmonary Artery Aneurysm Causing Left Main Coronary Artery Compression in the Absence of Pulmonary Hypertension. *Texas Heart Institute Journal*. 2015;42(5):465-7.
52. Meloche J, Lampron M-C, Nadeau V, Maltais M, Potus F, Lambert C, et al. Implication of Inflammation and Epigenetic Readers in Coronary Artery Remodeling in Patients With Pulmonary Arterial Hypertension. *Arteriosclerosis, Thrombosis, and Vascular Biology*. 2017;37(8):1513-23.
53. Friedrich MG. The Future of Cardiovascular Magnetic Resonance Imaging. *European Heart Journal*. 2017;38(22):1698-701.
54. Caputo GR, Tscholakoff D, Sechtem U, Higgins CB. Measurement of canine left ventricular mass by using MR imaging. *AJR American journal of roentgenology*. 1987;148(1):33-8.
55. Moon JC, Lorenz CH, Francis JM, Smith GC, Pennell DJ. Breath-hold FLASH and FISP cardiovascular MR imaging: left ventricular volume differences and reproducibility. *Radiology*. 2002;223(3):789-97.
56. Koch JA, Poll LW, Godehardt E, Korbmacher B, Mödder U. Right and left ventricular volume measurements in an animal heart model in vitro: first experiences with cardiac MRI at 1.0 T. *Eur Radiol*. 2000;10(3):455-8.
57. Beygui F, Furber A, Delépine S, Helft G, Metzger J-P, Geslin P, et al. Routine breath-hold gradient echo MRI-derived right ventricular mass, volumes and function: accuracy, reproducibility and coherence study. *The international journal of cardiovascular imaging*. 2004;20(6):509-16.
58. Alfakih K, Plein S, Thiele H, Jones T, Ridgway JP, Sivananthan MU. Normal human left and right ventricular dimensions for MRI as assessed by turbo gradient echo and steady-state free precession imaging sequences. *Journal of Magnetic Resonance Imaging*. 2003;17(3):323-9.
59. Hudsmith LE, Petersen SE, Francis JM, Robson MD, Neubauer S. Normal human left and right ventricular and left atrial dimensions using steady state free precession magnetic resonance imaging. *Journal of cardiovascular magnetic resonance : official journal of the Society for Cardiovascular Magnetic Resonance*. 2005;7(5):775-82.
60. Mooij CF, de Wit CJ, Graham DA, Powell AJ, Geva T. Reproducibility of MRI measurements of right ventricular size and function in patients with normal and dilated ventricles. *J Magn Reson Imaging*. 2008;28(1):67-73.
61. Clarke CJ, Gurka MJ, Norton PT, Kramer CM, Hoyer AW. Assessment of the Accuracy and Reproducibility of RV Volume Measurements by CMR in Congenital Heart Disease. *JACC: Cardiovascular Imaging*. 2012;5(1):28-37.
62. Blalock SE, Banka P, Geva T, Powell AJ, Zhou J, Prakash A. Interstudy variability in cardiac magnetic resonance imaging measurements of ventricular volume, mass, and ejection fraction in repaired tetralogy of fallot: A prospective observational study. *Journal of Magnetic Resonance Imaging*. 2013;38(4):829-35.
63. Swift AJ, Capener D, Johns C, Hamilton N, Rothman A, Elliot C, et al. Magnetic Resonance Imaging in the Prognostic Evaluation of Patients with Pulmonary Arterial Hypertension. *American journal of respiratory and critical care medicine*. 2017;196(2):228-39.

64. Roeleveld RJ, Vonk-Noordegraaf A, Marcus JT, Bronzwaer JGF, Marques KMJ, Postmus PE, et al. Effects of Epoprostenol on Right Ventricular Hypertrophy and Dilatation in Pulmonary Hypertension. *CHEST*. 2004;125(2):572-9.
65. Wilkins MR, Paul GA, Strange JW, Tunariu N, Gin-Sing W, Banya WA, et al. Sildenafil versus Endothelin Receptor Antagonist for Pulmonary Hypertension (SERAPH) study. *American journal of respiratory and critical care medicine*. 2005;171(11):1292-7.
66. Chin KM, Kingman M, de Lemos JA, Warner JJ, Reimold S, Peshock R, et al. Changes in Right Ventricular Structure and Function Assessed Using Cardiac Magnetic Resonance Imaging in Bosentan-Treated Patients With Pulmonary Arterial Hypertension. *The American journal of cardiology*. 2008;101(11):1669-72.
67. Peacock AJ, Crawley S, McLure L, Blyth KG, Vizza CD, Poscia R, et al. Changes in Right Ventricular Function Measured by Cardiac Magnetic Resonance Imaging in Patients Receiving Pulmonary Arterial Hypertension-Targeted Therapy. *Circulation: Cardiovascular Imaging*. 2014;7(1):107-14.
68. Mehta BB, Auger DA, Gonzalez JA, Workman V, Chen X, Chow K, et al. Detection of elevated right ventricular extracellular volume in pulmonary hypertension using Accelerated and Navigator-Gated Look-Locker Imaging for Cardiac T1 Estimation (ANGIE) cardiovascular magnetic resonance. *Journal of Cardiovascular Magnetic Resonance*. 2015;17(1):110.
69. Spruijt OA, Vissers L, Bogaard H-J, Hofman MBM, Vonk-Noordegraaf A, Marcus JT. Increased native T1-values at the interventricular insertion regions in precapillary pulmonary hypertension. *The international journal of cardiovascular imaging*. 2016;32(3):451-9.
70. Pauling L, Coryell CD. The magnetic properties and structure of hemoglobin, oxyhemoglobin and carbonmonoxyhemoglobin. *Proceedings of the National Academy of Sciences*. 1936;22(4):210-6.
71. Thulborn KR, Waterton JC, Matthews PM, Radda GK. Oxygenation dependence of the transverse relaxation time of water protons in whole blood at high field. *Biochimica et Biophysica Acta (BBA)-General Subjects*. 1982;714(2):265-70.
72. Li D, Dhawale P, Rubin PJ, Haacke EM, Gropler RJ. Myocardial signal response to dipyridamole and dobutamine: Demonstration of the BOLD effect using a double-echo gradient-echo sequence. *Magnetic resonance in medicine*. 1996;36(1):16-20.
73. Wacker CM, Hartlep AW, Pflieger S, Schad LR, Ertl G, Bauer WR. Susceptibility-sensitive magnetic resonance imaging detects human myocardium supplied by a stenotic coronary artery without a contrast agent. *Journal of the American College of Cardiology*. 2003;41(5):834-40.
74. Dharmakumar R, Arumana JM, Tang R, Harris K, Zhang Z, Li D. Assessment of regional myocardial oxygenation changes in the presence of coronary artery stenosis with balanced SSFP imaging at 3.0 T: theory and experimental evaluation in canines. *Journal of Magnetic Resonance Imaging*. 2008;27(5):1037-45.
75. Reeder SB, Faranesh AZ, Boxerman JL, McVeigh ER. In vivo measurement of T\* 2 and field inhomogeneity maps in the human heart at 1.5 T. *Magnetic resonance in medicine*. 1998;39(6):988-98.
76. Foltz WD, Al-Kwif O, Sussman MS, Stainsby JA, Wright GA. Optimized spiral imaging for measurement of myocardial T2 relaxation. *Magnetic resonance in medicine*. 2003;49(6):1089-97.
77. Dharmakumar R, Hong J, Brittain JH, Plewes DB, Wright GA. Oxygen-sensitive contrast in blood for steady-state free precession imaging. *Magnetic resonance in medicine*. 2005;53(3):574-83.

78. Dharmakumar R, Arumana JM, Larson AC, Chung Y, Wright GA, Li D. Cardiac phase-resolved blood oxygen-sensitive steady-state free precession MRI for evaluating the functional significance of coronary artery stenosis. *Investigative radiology*. 2007;42(3):180-8.
79. Sree Raman K, Nucifora G, Selvanayagam JB. Novel cardiovascular magnetic resonance oxygenation approaches in understanding pathophysiology of cardiac diseases. *Clinical and experimental pharmacology & physiology*. 2018.
80. Look DC, Locker DR. Time saving in measurement of NMR and EPR relaxation times. *Review of Scientific Instruments*. 1970;41(2):250-1.
81. Messroghli DR, Radjenovic A, Kozerke S, Higgins DM, Sivananthan MU, Ridgway JP. Modified Look-Locker inversion recovery (MOLLI) for high-resolution T1 mapping of the heart. *Magnetic resonance in medicine*. 2004;52(1):141-6.
82. Piechnik SK, Ferreira VM, Dall'Armellina E, Cochlin LE, Greiser A, Neubauer S, et al. Shortened Modified Look-Locker Inversion recovery (ShMOLLI) for clinical myocardial T1-mapping at 1.5 and 3 T within a 9 heartbeat breathhold. *Journal of cardiovascular magnetic resonance*. 2010;12(1):69.
83. Chow K, Flewitt JA, Green JD, Pagano JJ, Friedrich MG, Thompson RB. Saturation recovery single-shot acquisition (SASHA) for myocardial T1 mapping. *Magnetic resonance in medicine*. 2014;71(6):2082-95.
84. Parsai C, O'Hanlon R, Prasad SK, Mohiaddin RH. Diagnostic and prognostic value of cardiovascular magnetic resonance in non-ischaemic cardiomyopathies. *Journal of Cardiovascular Magnetic Resonance*. 2012;14(1):54.
85. Kehr E, Sono M, Chugh SS, Jerosch-Herold M. Gadolinium-enhanced magnetic resonance imaging for detection and quantification of fibrosis in human myocardium in vitro. *The international journal of cardiovascular imaging*. 2008;24(1):61-8.
86. Kellman P, Wilson JR, Xue H, Ugander M, Arai AE. Extracellular volume fraction mapping in the myocardium, part 1: evaluation of an automated method. *Journal of Cardiovascular Magnetic Resonance*. 2012;14(1):63.
87. Kellman P, Wilson JR, Xue H, Bandettini WP, Shanbhag SM, Druey KM, et al. Extracellular volume fraction mapping in the myocardium, part 2: initial clinical experience. *Journal of Cardiovascular Magnetic Resonance*. 2012;14(1):64.
88. Dass S, Suttie JJ, Piechnik SK, Ferreira VM, Holloway CJ, Banerjee R, et al. Myocardial tissue characterization using magnetic resonance noncontrast t1 mapping in hypertrophic and dilated cardiomyopathy. *Circulation: Cardiovascular Imaging*. 2012;5(6):726-33.
89. Liu A, Wijesurendra RS, Francis JM, Robson MD, Neubauer S, Piechnik SK, et al. Adenosine Stress and Rest T1 Mapping Can Differentiate Between Ischemic, Infarcted, Remote, and Normal Myocardium Without the Need for Gadolinium Contrast Agents. *JACC Cardiovascular imaging*. 2016;9(1):27-36.
90. Piechnik SK, Ferreira VM, Lewandowski AJ, Ntusi NAB, Banerjee R, Holloway C, et al. Normal variation of magnetic resonance T1 relaxation times in the human population at 1.5 T using ShMOLLI. *Journal of Cardiovascular Magnetic Resonance*. 2013;15(1):13.
91. McCommis KS, Zhang H, Goldstein TA, Misselwitz B, Abendschein DR, Gropler RJ, et al. Myocardial Blood Volume Is Associated With Myocardial Oxygen Consumption: An Experimental Study With Cardiac Magnetic Resonance in a Canine Model. *JACC: Cardiovascular Imaging*. 2009;2(11):1313-20.
92. McCommis KS, Goldstein TA, Abendschein DR, Misselwitz B, Pilgram T, Gropler RJ, et al. Roles of myocardial blood volume and flow in coronary artery disease: an experimental MRI study at rest and during hyperemia. *European Radiology*. 2010;20(8):2005-12.
93. Wacker CM, Bauer WR. Myocardial microcirculation in humans--new approaches using MRI. *Herz*. 2003;28(2):74-81.

94. Mahmud M, Piechnik SK, Levelt E, Ferreira VM, Francis JM, Lewis A, et al. Adenosine stress native T1 mapping in severe aortic stenosis: evidence for a role of the intravascular compartment on myocardial T1 values. *Journal of Cardiovascular Magnetic Resonance*. 2014;16(1):92.
95. Levelt E, Piechnik SK, Liu A, Wijesurendra RS, Mahmud M, Ariga R, et al. Adenosine stress CMR T1-mapping detects early microvascular dysfunction in patients with type 2 diabetes mellitus without obstructive coronary artery disease. *Journal of Cardiovascular Magnetic Resonance*. 2017;19(1):81.
96. Shah R, Sree Raman K, Walls A, Woodman RJ, Faull R, Gleadle JM, et al. Gadolinium-Free Cardiovascular Magnetic Resonance Stress T1 Mapping in Patients With Chronic Kidney Disease. *JACC: Cardiovascular Imaging*. 2019:3064.
97. Burrage MK, Shanmuganathan M, Masi A, Hann E, Zhang Q, Popescu IA, et al. Cardiovascular magnetic resonance stress and rest T1-mapping using regadenoson for detection of ischemic heart disease compared to healthy controls. *Int J Cardiol*. 2021;333:239-45.
98. Schuster A, Hor Kan N, Kowallick Johannes T, Beerbaum P, Kutty S. Cardiovascular Magnetic Resonance Myocardial Feature Tracking. *Circulation: Cardiovascular Imaging*. 2016;9(4):e004077.
99. Eitel I, Stiermaier T, Lange T, Rommel K-P, Koschalka A, Kowallick JT, et al. Cardiac Magnetic Resonance Myocardial Feature Tracking for Optimized Prediction of Cardiovascular Events Following Myocardial Infarction. *JACC: Cardiovascular Imaging*. 2018;11(10):1433.
100. Claus P, Omar AMS, Pedrizzetti G, Sengupta PP, Nagel E. Tissue Tracking Technology for Assessing Cardiac Mechanics. *JACC: Cardiovascular Imaging*. 2015;8(12):1444.
101. Padervinskienė L, Krivickienė A, Hoppenot D, Miliauskas S, Basevičius A, Nedzelskienė I, et al. Prognostic Value of Left Ventricular Function and Mechanics in Pulmonary Hypertension: A Pilot Cardiovascular Magnetic Resonance Feature Tracking Study. *Medicina (Kaunas)*. 2019;55(3):73.
102. Karamitsos TD, Hudsmith LE, Selvanayagam JB, Neubauer S, Francis JM. Operator induced variability in left ventricular measurements with cardiovascular magnetic resonance is improved after training. *Journal of cardiovascular magnetic resonance : official journal of the Society for Cardiovascular Magnetic Resonance*. 2007;9(5):777-83.
103. Cerqueira MD, Weissman NJ, Dilsizian V, Jacobs AK, Kaul S, Laskey WK, et al. Standardized myocardial segmentation and nomenclature for tomographic imaging of the heart. A statement for healthcare professionals from the Cardiac Imaging Committee of the Council on Clinical Cardiology of the American Heart Association. *Circulation*. 2002;105(4):539-42.
104. Sharma P, Socolow J, Patel S, Pettigrew RI, Oshinski JN. Effect of Gd-DTPA-BMA on blood and myocardial T1 at 1.5T and 3T in humans. *J Magn Reson Imaging*. 2006;23(3):323-30.
105. Karamitsos TD, Leccisotti L, Arnold JR, Recio-Mayoral A, Bhamra-Ariza P, Howells RK, et al. Relationship Between Regional Myocardial Oxygenation and Perfusion in Patients With Coronary Artery Disease. *Circulation: Cardiovascular Imaging*. 2010;3(1):32-40.
106. Gomez A, Bialostozky D, Zajarias A, Santos E, Palomar A, Martinez ML, et al. Right ventricular ischemia in patients with primary pulmonary hypertension. *J Am Coll Cardiol*. 2001;38(4):1137-42.
107. Grover S, Lloyd R, Perry R, Lou PW, Haan E, Yeates L, et al. Assessment of myocardial oxygenation, strain, and diastology in MYBPC3-related hypertrophic cardiomyopathy: a cardiovascular magnetic resonance and echocardiography study. *European heart journal cardiovascular Imaging*. 2019.
108. Shah R, Parnham S, Liang Z, Perry R, Bradbrook C, Smith E, et al. Prognostic Utility of Oxygen-Sensitive Cardiac Magnetic Resonance Imaging in Diabetic and Nondiabetic

- Chronic Kidney Disease Patients With No Known Coronary Artery Disease. *JACC: Cardiovascular Imaging*. 2019;2900.
109. Karamitsos TD, Arnold JR, Pegg TJ, Francis JM, Birks J, Jerosch-Herold M, et al. Patients With Syndrome X Have Normal Transmural Myocardial Perfusion and Oxygenation. *Circulation: Cardiovascular Imaging*. 2012;5(2):194-200.
110. Parnham S, Gleadle JM, Bangalore S, Grover S, Perry R, Woodman RJ, et al. Impaired myocardial oxygenation response to stress in patients with chronic kidney disease. *Journal of the American Heart Association*. 2015;4(8):e002249.
111. Arnold JR, Karamitsos TD, Bhamra-Ariza P, Francis JM, Searle N, Robson MD, et al. Myocardial oxygenation in coronary artery disease: insights from blood oxygen level-dependent magnetic resonance imaging at 3 Tesla. *Journal of the American College of Cardiology*. 2012;59(22):1954-64.
112. Bogaard HJ, Abe K, Vonk Noordegraaf A, Voelkel NF. The right ventricle under pressure: cellular and molecular mechanisms of right-heart failure in pulmonary hypertension. *Chest*. 2009;135(3):794-804.
113. Piao L, Marsboom G, Archer SL. Mitochondrial metabolic adaptation in right ventricular hypertrophy and failure. *Journal of molecular medicine (Berlin, Germany)*. 2010;88(10):1011-20.
114. Fischer K, Yamaji K, Luescher S, Ueki Y, Jung B, von Tengg-Kobligk H, et al. Feasibility of cardiovascular magnetic resonance to detect oxygenation deficits in patients with multi-vessel coronary artery disease triggered by breathing maneuvers. *Journal of cardiovascular magnetic resonance : official journal of the Society for Cardiovascular Magnetic Resonance*. 2018;20(1):31.
115. Taylor AJ, Salerno M, Dharmakumar R, Jerosch-Herold M. T1 Mapping: Basic Techniques and Clinical Applications. *JACC: Cardiovascular Imaging*. 2016;9(1):67-81.
116. Messroghli DR, Moon JC, Ferreira VM, Grosse-Wortmann L, He T, Kellman P, et al. Clinical recommendations for cardiovascular magnetic resonance mapping of T1, T2, T2\* and extracellular volume: A consensus statement by the Society for Cardiovascular Magnetic Resonance (SCMR) endorsed by the European Association for Cardiovascular Imaging (EACVI). *Journal of Cardiovascular Magnetic Resonance*. 2017;19(1):75.
117. Patel RB, Li E, Benefield BC, Swat SA, Polsinelli VB, Carr JC, et al. Diffuse right ventricular fibrosis in heart failure with preserved ejection fraction and pulmonary hypertension. *ESC Heart Failure*. 2020;7(1):254-64.
118. Sree Raman K, Stokes M, Walls A, Perry R, Steele PM, Burdeniuk C, et al. Feasibility of oxygen sensitive cardiac magnetic resonance of the right ventricle in pulmonary artery hypertension. *Cardiovascular diagnosis and therapy*. 2019;9(5):502-12.
119. Vogel-Claussen J, Skrok J, Shehata ML, Singh S, Sibley CT, Boyce DM, et al. Right and Left Ventricular Myocardial Perfusion Reserves Correlate with Right Ventricular Function and Pulmonary Hemodynamics in Patients with Pulmonary Arterial Hypertension. *Radiology*. 2011;258(1):119-27.
120. Dass S, Holloway CJ, Cochlin LE, Rider OJ, Mahmood M, Robson M, et al. No evidence of myocardial oxygen deprivation in nonischemic heart failure. *Circulation: Heart Failure*. 2015;8(6):1088-93.
121. Attard MI, Dawes TJW, de Marvao A, Biffi C, Shi W, Wharton J, et al. Metabolic pathways associated with right ventricular adaptation to pulmonary hypertension: 3D analysis of cardiac magnetic resonance imaging. *European Heart Journal - Cardiovascular Imaging*. 2018;20(6):668-76.
122. Ong P, Camici PG, Beltrame JF, Crea F, Shimokawa H, Sechtem U, et al. International standardization of diagnostic criteria for microvascular angina. *International Journal of Cardiology*. 2018;250:16-20.

123. Dumitrescu D, Sitbon O, Weatherald J, Howard LS. Exertional dyspnoea in pulmonary arterial hypertension. *European Respiratory Review*. 2017;26(145):170039.
124. Sun X-G, Hansen James E, Oudiz Ronald J, Wasserman K. Exercise Pathophysiology in Patients With Primary Pulmonary Hypertension. *Circulation*. 2001;104(4):429-35.
125. Saunders LC, Johns CS, Stewart NJ, Oram CJE, Capener DA, Puntmann VO, et al. Diagnostic and prognostic significance of cardiovascular magnetic resonance native myocardial T1 mapping in patients with pulmonary hypertension. *Journal of Cardiovascular Magnetic Resonance*. 2018;20(1):78.
126. Piechnik SK, Neubauer S, Ferreira VM. State-of-the-art review: stress T1 mapping—technical considerations, pitfalls and emerging clinical applications. *Magnetic Resonance Materials in Physics, Biology and Medicine*. 2018;31(1):131-41.
127. Ntusi NAB, Piechnik SK, Francis JM, Ferreira VM, Rai ABS, Matthews PM, et al. Subclinical myocardial inflammation and diffuse fibrosis are common in systemic sclerosis – a clinical study using myocardial T1-mapping and extracellular volume quantification. *Journal of Cardiovascular Magnetic Resonance*. 2014;16(1):21.
128. Liu A, Wijesurendra RS, Liu JM, Greiser A, Jerosch-Herold M, Forfar JC, et al. Gadolinium-Free Cardiac MR Stress T1-Mapping to Distinguish Epicardial From Microvascular Coronary Disease. *Journal of the American College of Cardiology*. 2018;71(9):957.
129. Jespersen L, Hvelplund A, Abildstrøm SZ, Pedersen F, Galatius S, Madsen JK, et al. Stable angina pectoris with no obstructive coronary artery disease is associated with increased risks of major adverse cardiovascular events. *European Heart Journal*. 2011;33(6):734-44.
130. Petersen JW, Pepine CJ. Microvascular coronary dysfunction and ischemic heart disease: Where are we in 2014? *Trends in Cardiovascular Medicine*. 2015;25(2):98-103.
131. Marcus JT, Gan CT-J, Zwanenburg JJM, Boonstra A, Allaart CP, Götte MJW, et al. Interventricular Mechanical Asynchrony in Pulmonary Arterial Hypertension: Left-to-Right Delay in Peak Shortening Is Related to Right Ventricular Overload and Left Ventricular Underfilling. *Journal of the American College of Cardiology*. 2008;51(7):750-7.
132. Raman B, Ariga R, Mahmud M, Piechnik S, Borlotti A, Jerosch-Herold M, et al. 011 Adenosine stress T1 mapping: a novel contrast free method to assess myocardial perfusion and ischaemia in hypertrophic cardiomyopathy. *Heart (British Cardiac Society)*. 2017;103(Suppl 1):A8.
133. Tsoumani Z, Miller C, Schmitt M, Nucifora G. 28 Adenosine stress native T1 mapping demonstrates impaired myocardial perfusion reserve in non-ischemic dilated cardiomyopathy. *European Heart Journal - Cardiovascular Imaging*. 2019;20(Supplement\_2).
134. McCann GP, Gan CT, Beek AM, Niessen HWM, Noordegraaf AV, van Rossum AC. Extent of MRI Delayed Enhancement of Myocardial Mass Is Related to Right Ventricular Dysfunction in Pulmonary Artery Hypertension. *American Journal of Roentgenology*. 2007;188(2):349-55.
135. Manders E, Rain S, Bogaard H-J, Handoko ML, Stienen GJM, Vonk-Noordegraaf A, et al. The striated muscles in pulmonary arterial hypertension: adaptations beyond the right ventricle. *European Respiratory Journal*. 2015;46(3):832.
136. Homsí R, Luetkens JA, Skowasch D, Pizarro C, Sprinkart AM, Gieseke J, et al. Left Ventricular Myocardial Fibrosis, Atrophy, and Impaired Contractility in Patients With Pulmonary Arterial Hypertension and a Preserved Left Ventricular Function: A Cardiac Magnetic Resonance Study. *Journal of thoracic imaging*. 2017;32(1):36-42.
137. Karamitsos TD, Dass S, Suttie J, Sever E, Birks J, Holloway CJ, et al. Blunted myocardial oxygenation response during vasodilator stress in patients with hypertrophic cardiomyopathy. *Journal of the American College of Cardiology*. 2013;61(11):1169-76.

138. Beache GM, Herzka DA, Boxerman JL, Post WS, Gupta SN, Faranesh AZ, et al. Attenuated myocardial vasodilator response in patients with hypertensive hypertrophy revealed by oxygenation-dependent magnetic resonance imaging. *Circulation*. 2001;104(11):1214-7.
139. Levelt E, Rodgers CT, Clarke WT, Mahmood M, Ariga R, Francis JM, et al. Cardiac energetics, oxygenation, and perfusion during increased workload in patients with type 2 diabetes mellitus. *European heart journal*. 2015;37(46):3461-9.
140. Sitbon O, Gomberg-Maitland M, Granton J, Lewis MI, Mathai SC, Rainisio M, et al. Clinical trial design and new therapies for pulmonary arterial hypertension. *European Respiratory Journal*. 2019;53(1):1801908.
141. de Siqueira ME, Pozo E, Fernandes VR, Sengupta PP, Modesto K, Gupta SS, et al. Characterization and clinical significance of right ventricular mechanics in pulmonary hypertension evaluated with cardiovascular magnetic resonance feature tracking. *Journal of cardiovascular magnetic resonance : official journal of the Society for Cardiovascular Magnetic Resonance*. 2016;18(1):39.
142. Kallianos K, Brooks GC, Mukai K, Seguro de Carvalho F, Liu J, Naeger DM, et al. Cardiac Magnetic Resonance Evaluation of Left Ventricular Myocardial Strain in Pulmonary Hypertension. *Academic radiology*. 2018;25(1):129-35.
143. Padervinskienė L, Krivickienė A, Hoppenot D, Miliauskas S, Basevičius A, Nedzelskienė I, et al. Prognostic Value of Left Ventricular Function and Mechanics in Pulmonary Hypertension: A Pilot Cardiovascular Magnetic Resonance Feature Tracking Study. *Medicina (Kaunas)*. 2019;55(3).
144. Sree Raman K, Shah R, Stokes M, Walls A, Woodman RJ, Ananthakrishna R, et al. Left ventricular ischemia in pre-capillary pulmonary hypertension: a cardiovascular magnetic resonance study. *Cardiovasc Diagn Ther*. 2020;10(5):1280-92.
145. de Man FS, Handoko ML, Vonk-Noordegraaf A. The unknown pathophysiological relevance of right ventricular hypertrophy in pulmonary arterial hypertension. *European Respiratory Journal*. 2019;53(4):1900255.
146. Hill JA, Olson EN. Cardiac Plasticity. *New England Journal of Medicine*. 2008;358(13):1370-80.
147. Trip P, Rain S, Handoko ML, van der Bruggen C, Bogaard HJ, Marcus JT, et al. Clinical relevance of right ventricular diastolic stiffness in pulmonary hypertension. *European Respiratory Journal*. 2015;45(6):1603.
148. Wong Yeun Y, Ruiter G, Lubberink M, Raijmakers Pieter G, Knaapen P, Marcus JT, et al. Right Ventricular Failure in Idiopathic Pulmonary Arterial Hypertension Is Associated With Inefficient Myocardial Oxygen Utilization. *Circulation: Heart Failure*. 2011;4(6):700-6.
149. Rain S, Handoko ML, Trip P, Gan CT-J, Westerhof N, Stienen Ger J, et al. Right Ventricular Diastolic Impairment in Patients With Pulmonary Arterial Hypertension. *Circulation*. 2013;128(18):2016-25.
150. Kolb TM, Peabody J, Baddoura P, Fallica J, Mock JR, Singer BD, et al. Right Ventricular Angiogenesis is an Early Adaptive Response to Chronic Hypoxia-Induced Pulmonary Hypertension. *Microcirculation*. 2015;22(8):724-36.
151. Simpson CE, Damico RL, Kolb TM, Mathai SC, Khair RM, Sato T, et al. Ventricular mass as a prognostic imaging biomarker in incident pulmonary arterial hypertension. *European Respiratory Journal*. 2019;53(4):1802067.
152. Kovacs G, Berghold A, Scheidl S, Olschewski H. Pulmonary arterial pressure during rest and exercise in healthy subjects: a systematic review. *Eur Respir J*. 2009;34(4):888-94.
153. Lonsdorfer-Wolf E, Richard R, Doutreleau S, Billat VL, Oswald-Mammosser M, Lonsdorfer J. Pulmonary hemodynamics during a strenuous intermittent exercise in healthy subjects. *Med Sci Sports Exerc*. 2003;35(11):1866-74.

154. Reeves JT, Linehan JH, Stenmark KR. Distensibility of the normal human lung circulation during exercise. *Am J Physiol Lung Cell Mol Physiol*. 2005;288(3):L419-25.
155. Lau EM, Manes A, Celermajer DS, Galie N. Early detection of pulmonary vascular disease in pulmonary arterial hypertension: time to move forward. *Eur Heart J*. 2011;32(20):2489-98.
156. Lewis GD, Bossone E, Naeije R, Grunig E, Saggar R, Lancellotti P, et al. Pulmonary vascular hemodynamic response to exercise in cardiopulmonary diseases. *Circulation*. 2013;128(13):1470-9.
157. Kovacs G, Maier R, Aberer E, Brodmann M, Scheidl S, Troster N, et al. Borderline pulmonary arterial pressure is associated with decreased exercise capacity in scleroderma. *American journal of respiratory and critical care medicine*. 2009;180(9):881-6.
158. Lau EMT, Vanderpool RR, Choudhary P, Simmons LR, Corte TJ, Argiento P, et al. Dobutamine stress echocardiography for the assessment of pressure-flow relationships of the pulmonary circulation. *Chest*. 2014;146(4):959-66.
159. Hardegree EL, Sachdev A, Villarraga HR, Frantz RP, McGoon MD, Kushwaha SS, et al. Role of serial quantitative assessment of right ventricular function by strain in pulmonary arterial hypertension. *The American journal of cardiology*. 2013;111(1):143-8.
160. Saito M, Wright L, Negishi K, Dwyer N, Marwick TH. Mechanics and prognostic value of left and right ventricular dysfunction in patients with systemic sclerosis. *European heart journal cardiovascular Imaging*. 2018;19(6):660-7.
161. Fine NM, Chen L, Bastiansen PM, Frantz RP, Pellikka PA, Oh JK, et al. Outcome prediction by quantitative right ventricular function assessment in 575 subjects evaluated for pulmonary hypertension. *Circ Cardiovasc Imaging*. 2013;6(5):711-21.
162. Lang RM, Badano LP, Mor-Avi V, Afilalo J, Armstrong A, Ernande L, et al. Recommendations for cardiac chamber quantification by echocardiography in adults: an update from the American Society of Echocardiography and the European Association of Cardiovascular Imaging. *J Am Soc Echocardiogr*. 2015;28(1):1-39 e14.
163. Chemla D, Castelain V, Humbert M, Hebert JL, Simonneau G, Lecarpentier Y, et al. New formula for predicting mean pulmonary artery pressure using systolic pulmonary artery pressure. *Chest*. 2004;126(4):1313-7.
164. Hekimsoy V, Kaya EB, Akdogan A, Sahiner L, Evranos B, Canpolat U, et al. Echocardiographic assessment of regional right ventricular systolic function using two-dimensional strain echocardiography and evaluation of the predictive ability of longitudinal 2D-strain imaging for pulmonary arterial hypertension in systemic sclerosis patients. *The international journal of cardiovascular imaging*. 2018;34(6):883-92.